EXPERIMENTAL AND UPSCALING NUMERICAL SIMULATION STUDY ON THE EFFECT OF SURFACTANT ADDITIVES IN COMPLETION FLUIDS ON EAGLE FORD SHALE OIL RESERVOIR

A Thesis

by

I WAYAN RAKANANDA SAPUTRA

Submitted to the Office of Graduate and Professional Studies of
Texas A&M University
in partial fulfillment of the requirements for the degree of

MASTER OF SCIENCE

Chair of Committee,	David S. Schechter
Committee Members,	Maria A. Barrufet
	Jenn-Tai Liang
Head of Department,	Duane A. McVay

May 2018

Major Subject: Petroleum Engineering

ABSTRACT

The addition of surfactant to the completion fluid of a shale oil well has been widely believed to improve well performance. Previous laboratory studies showed that the method is based on enhanced capillary-driven spontaneous imbibition as a result of surfactant interaction with the oil/water/rock system. However, published work on this subject is highly limited on the result in laboratory-scale work. The purpose of this study is to fill this gap by providing a field-scale impact of SASI as derived by numerical model-based upscaling workflow.

This study provides a complete workflow on assessing the effectivity of SASI which consists of three big parts: laboratory experiments, lab-scale modelling, and field-scale modelling. On the laboratory experiment, interfacial tension, contact angle, zeta potential, surfactant adsorption isotherm, and ultimately, spontaneous imbibition were done as part of data gathering process. Lab-scale modelling was done to model the spontaneous imbibition of the previous step to construct the relative permeability and capillary pressure data for upscaling purpose. In order to incorporate the heterogeneity commonly found on shale rock samples, a CT-based rock digitalization method was implemented to build the lab-scale model. Utilizing all data obtained from lab-scale model and laboratory experiments, the field-scale model was then constructed and the effect of SASI on the field-scale was calculated.

Four fluid systems were tested in this work consisting of one case of water without surfactant component as the base case and three cases with different surfactants. Reduction of IFT, alteration of wettability to water-wet region, and stable zeta potential were observed for the three surfactants tested. Adsorption isotherm measurement also showed a positive correlation between the wettability alteration performance and the amount of surfactant adsorbed. Oil production from

spontaneous imbibition was increased seven-fold on the best surfactant tested when compared to the base case. Through numerical upscaling, field-scale effect of SASI was also approximated. With the result of 22.7% increase of initial oil production rate and 18.4% improvement of cumulative oil from the best surfactant tested. In addition, a rigorous sensitivity analysis incorporating seven different reservoir properties was also done and the effectivity of SASI was found to be a function of some of the tested reservoir properties.

DEDICATION

This thesis is dedicated to my mother, my father, my sister, my friends, and my keyboards as without any of their support, the completion of this work would not be possible.

ACKNOWLEDGEMENTS

I would like to thank my advisor, Dr. David Schechter, for trusting me to become a member of a top-shelf, cutting-edge research group, for all the learning process and experience through my two-and-a-half years journey of finishing a master degree program, and lastly for assigning

I would like to thank my committee members, Dr. Maria Barrufet and Dr. Jenn Tai-Liang for their guidance and support throughout the course of this research.

I would also like to thank Johannes Alvarez for all the invaluable guidance, idea, and suggestions throughout my master program.

I would also like to acknowledge my fellow research group colleague in 815 and 801, especially Kang Han Park for the support and assistance.

Finally, I would like to thank all the undergraduate student worker of Lab 802 and 803 and also John Maldonado for all his help during my master.

CONTRIBUTORS AND FUNDING SOURCES

Contributors

This work was supervised by a thesis committee consisting of Professor David S. Schechter and Professor Jenn-Tai Liang of the Department of Petroleum Engineering and Professor Maria A. Barrufet of Chemical Engineering.

All work for the thesis was completed independently by the student.

Funding Sources

This work was made possible in part by Crisman Institute for Petroleum Research under Project Number 2.14.16.

Its contents are solely the responsibility of the authors and do not necessarily represent the official views of the Crisman Institute for Petroleum Research.

TABLE OF CONTENTS

Page

LIST OF FIGURES

Page

LIST OF TABLES

Page

1. INTRODUCTION

Since its rise during the early 2000s, oil production from shale oil well has been increasing steadily and now considered as the main driver for U.S. crude oil production, which accounts for 65% of the total onshore US oil production as shown by Fig. 1 (EIA 2017). Tremendous production volume from the shale reservoir allows US to return as a significant figure in the world petroleum market, providing sufficient supply of gas to meet the domestic demand and are able to shift the balance of oil price as shown by the oil price drop in 2015. Although that the price drop was caused by the overproduction from OPEC countries as driven by Saudi Arabia, US booming shale oil production is the root of the overflow where OPEC was trying to minimize supply from the unconventional reservoir by making the production from shale economically unfeasible in the lower oil price condition. However, with some decline in the production during the price drop, shale oil industry survived and continues to grow.

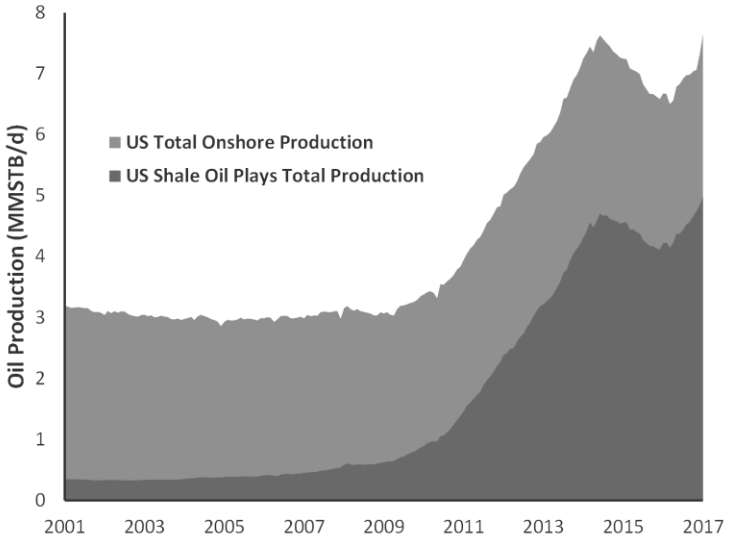

Fig. 1 - Comparison of oil production from shale to total US onshore oil production

The presence of shale oil reservoir has been known since the early time of conventional reservoir petroleum industry since shale is essentially the source rock of hydrocarbon found in the conventional reservoir. Producing from this reservoir deemed to be unreasonable since it is located below the commonly-produced reservoir at the time and that the rock has a unique ultra-tight nature. Deeper target zone would result in a higher expenditure to drill, but it was the ultra-tight property of the rock that really made producing from shale to be extremely challenging. The average pore size of matrix in shale reservoirs are in the nanometer range, spanning from 10-100nm on different shale plays (Nelson 2009). As a comparison, the size of methane molecule is 0.414 nm. Nanometer-order pore size would directly cause the porosity and permeability of shale to be ultra-low as well. Porosity of shale usually falls close to 10% while the permeability is on the order of hundreds nanodarcy. To provide a comparison, conventional sandstone reservoirs whose pore size is in the order of micrometer, usually comes with porosity around 20% and permeability in the order of hundreds microdarcy, three order of magnitudes larger than shale. As a result, shale reservoirs were not considered to be exploited. It was not until the early 1990s when George P. Mitchell started implementing the combination of massive multi-stage hydraulic fracturing and horizontal well to enable gas production from Barnett shale in a significant productivity that the production of hydrocarbon from shale reservoir became economically appealing (Steward 2013).

Both horizontal well and multi-stage hydraulic fracturing improves the well productivity by allowing more contact area from the well to the reservoir, a necessity to economically produce a low porosity and ultra-low permeability reservoir. Horizontal well improves production by improving area of contact to the reservoir as more reservoir volume is accessed by penetrating the shale formation horizontally than vertically. Hydraulic fracturing also improves production by

increasing contact area, with the addition of creating a better, if not the only, flow path from matrix to the well. By pumping a large volume of fluid in high pressure into the reservoir, an artificial fracture network is created around the well. These fractures will provide more access to the reservoir, in addition of the increase from drilling the well horizontally, with also improvement of the flow geometry around the well as generated fractures will have permeability in 3 orders of magnitude improvement from the matrix (Advani et al. 1985).

The development of the two mentioned technology, horizontal drilling and multi-stage hydraulic fracture, during the shale boom allowed capital cost of making a shale oil well to be reduced while still able to increase the productivity of the well. However, it is widely known that despite of all the effort that has been done to improve horizontal drilling and hydraulic fracturing technology, recovery factor of each shale oil well is still relatively low. Different methods have been proposed on how to recover more oil that is left downhole. Longer lateral and larger hydraulic fracture operation has been the chosen path in developing the production method to increase recovery. Infill drilling naturally comes as another first option to access more part of the reservoir, however on a study done in 10 different unconventional basins shows that the productivity of infill well is considerably lower than the parent well with also a faster decline of production observed (Lindsay et al. 2018). Although that the total field production would increase, the option of drilling infill well could be uneconomical. Addition of surfactant into the hydraulic fracturing fluid is currently an uprising technique as it is believed to improve both initial production and EUR of a shale oil well.

Surfactant addition into fracturing fluid is not an entirely novel method, it has been used as one of the component of fracturing fluid to reduce the effect of water block that could form as water moves into the matrix during the high pressure injection of fracturing fluid (Liang et al.

2016). It is not until recently that it was realized that a bigger potential on what the surfactant molecule is capable of doing in the reservoir exists. Surfactant molecules possess the ability to be soluble in both water and oil as it contains both hydrophobic and hydrophilic group in their molecule. This unique property results in the change of interaction between oil and water as surfactant molecules are able to bridge the two immiscible fluid with its two different groups, with the most notable change observed when surfactant presents in a system of oil, water, and rock are the decrement of interfacial tension between oil and water and also the alteration of wettability (Alvarez and Schechter 2016). In a shale oil reservoir, these two effects is believed to translate into higher well productivity through a mechanism of surfactant-assisted spontaneous imbibition (SASI).

Imbibition occurs as oil moves out of the rock pore as water moves into the pore, replacing the oil. The word spontaneous expresses that the fluid movement takes place without any pressure difference applied on the system, meaning that the cause of the fluid exchange is not caused by viscous force. It is capillary force that drives the movement of oil out of the pore and water in to the pore. The presence of surfactant accelerates and enhances this phenomenon as it causes the two effects mentioned before, IFT and wettability alteration. Young and Laplace defines the capillary pressure as a function of both wettability, as represented by contact angle, IFT, and pore radius. By altering wettability to be more in the water-wet region, surfactant modifies the direction of the capillary force that cause SASI to occur to be more favorable, hence increasing the amount of oil expelled as well as the rate of the oil expulsion. However, the effect of IFT decrement as caused by surfactant can also translates to lower capillary force as the strength of the force is controlled by the IFT of the oil and water. Unaltered IFT is also undesirable as it could reduce the

penetration of surfactant into the matrix, reducing the surfactant performance in enhancing the imbibition.

Several lab studies of surfactant performance in enhancing the imbibition phenomenon have been done in the past five years and continues to be a rising topic. Tests done on three most prolific oil-bearing shale reservoir, Bakken, Eagle Ford, and Wolfcamp, showed that addition of surfactant lead to increase of oil production from spontaneous imbibition when compared to base case of fluid without surfactant (AlvarezSaputra et al. 2017a; Alvarez and Schechter 2016, 2017). Most studies consist of IFT, contact angle, and zeta potential measurements, giving an understanding on the effect of different surfactant on different oil and rock combination. And in order to gauge the surfactant performance to improve the oil production, spontaneous imbibition experiment was done by submerging core plugs in surfactant solution in an Amott cell set up. Results of those tests show that surfactant reduced the IFT to different degrees as a function of the surfactant, oil, and rock composition. Wettability alteration was also observed with the general trend of increasing water-wetness for experiments ran with surfactant solution. Imbibition also showed ranges of production improvement with also various degree of enhancement on different surfactant, oil, and rock combination. In the end, all studies suggested that the concept of surfactant-assisted spontaneous imbibition to improve oil recovery works, at least for lab-scale studies.

The field application of this surfactant-assisted spontaneous imbibition is to add the appropriate surfactant chemical during the fracturing process in the fracturing fluid as it will allow the most reservoir contact for the surfactant molecule. It is really unfortunate that most studies of surfactant-assisted spontaneous imbibition that have been published is limited to laboratory-scale observation. Field-scale performance study has a great significance, since it would provide a new

perspective on the significance of the concept to well production. Especially when most of the lab studies are limited to observing the imbibition without any pressure difference applied which is not essentially true when it comes to the field where pressure drawdown does exist. Therefore, this particular study is aimed to fill that gap of the procedure in assessing the method of surfactant-assisted spontaneous imbibition.

The final goal of this work is to provide a complete workflow in evaluating surfactant performance in improving well productivity which includes upscaling the lab-scale result to field-scale, filling the gap in the current widely-used workflow. On that note, this work is divided into three parts, experimental, lab-scale modeling, and field-scale modelling. On the experimental part of the work, every possible and necessary data regarding the interaction of oil, water, surfactant, and rock is gathered which includes rock and fluid characterization, interfacial-tension, contact angle, zeta potential, adsorption isotherm, CT-Scan images, and ultimately, spontaneous imbibition experiment. All collected data then will be used on the second part of the work which models the spontaneous imbibition experiment to obtain the capillary pressure and relative permeability curves of each fluid system tested. In order to accurately obtain the curves, rock digitalization method utilizing CT-Scan technology is carried out to include the heterogeneity of the rock sample used in the imbibition experiment in the numerical model. Using the curves obtained from the lab-scale modelling part, a field model is generated with the surfactant-assisted spontaneous imbibition mechanism included to provide a view of the field-scale impact of the method. In addition, on the field-scale model, sensitivity analysis is also done to understand which reservoir properties affect the success of SASI implementation on the field-scale.

1.1 Research Objectives and Overview

This research is aimed to provide a complete workflow in evaluating surfactant-assisted spontaneous imbibition from the laboratory measurements up to field-scale result by upscaling the lab-scale experiments and under the assumption that the field implementation of SASI is assumed to be by adding the surfactant into the hydraulic fracturing fluids. In detail, the objectives of the research are as follows:

1. To investigate the method of adding surfactant in the hydraulic fracturing fluid to improve oil recovery.
2. To upscale the surfactant-assisted spontaneous imbibition observed in laboratory experiment to a field-scale dimension through the use of numerical simulation.
3. To evaluate the dominant aspect of the surfactant-assisted spontaneous imbibition process on the field-scale simulation.
4. Provide a comprehensive workflow to assess the effect of surfactant addition on completion fluid from laboratory experiments to the field-scale modelling.

The thesis is divided into four parts. Started by literature review, giving a brief summary of the previous study and information available on the surfactant-assisted spontaneous imbibition, methods commonly used on measuring different surfactant-related properties, and finally concepts that the modelling work grounded on. The next part is the display of all the laboratory measurement result of surfactant-related properties, interfacial tension, contact angle, zeta potential, adsorption isotherm, and spontaneous imbibition. In addition, all characterization of fluids and rocks used in this work is also presented. Following the experimental part is the lab-scale modelling section

which provides the detail information on how the CT-based rock digitalization method is done in this work and the history matching process to obtain the capillary pressure and relative permeability curves as well as several points observed from the result. The last part of this work is the field-scale work, consisting of the description of field model used in the study, followed by the result of upscaling work, and sensitivity analysis with different reservoir properties that would affect the effectivity of SASI field implementation.

2. LITERATURE REVIEW

Summary of most major work done related to spontaneous imbibition and how surfactant could affect the spontaneous imbibition process will be covered first in the literature review to provide some essential understanding that is critical for the model construction part. The next part of the review summarizes the concept and methods of different experimental procedure that is related to spontaneous imbibition and also to the interaction of surfactant in oil-water-rock system. For the last part, previous efforts on modelling and upscaling the imbibition or the surfactant activity in imbibition

2.1 Surfactant-Assisted Spontaneous Imbibition

Surfactant-Assisted Spontaneous Imbibition (SASI), a method of improving oil recovery of a shale oil well by addition of specific surfactant blend that has been emerging in the past three years. The basic concept of the method exploits the unique amphiphilic characteristic, meaning that it has affinity to both water and oil molecule, of surfactant molecule. Surfactant molecule's amphiphilic nature causes reduction of IFT and alteration of wettability to occur in an oil-water-rock system, the combination of the two phenomena resulting in increment of oil production from a process of spontaneous imbibition, more detail on the mechanism of how surfactant improves oil production will be covered later. Up until this manuscript is written, scientific publication on the impact of SASI on a field-scale case is extremely difficult to find. One brief review on the field-scale performance of SASI which based on interviews done with operator states that 15-20%

improvement of well performance is the number that is correlated to the field-scale effect of SASI (Rassenfoss 2017). On the laboratory work side, an ample number of lab-scale published study on this method can be found with all studies came up with an accord that higher and faster oil recovery is observed on imbibition cases that involve surfactant in the aqueous-phase as compared to those that do not (AlvarezSaputra et al. 2017a, 2017b; Alvarez and Schechter 2016, 2017; AlvarezTovar et al. 2017; Kim et al. 2016; Morsy et al. 2014; Neog and Schechter 2016; Nguyen et al. 2017; Nguyen et al. 2014; Teklu et al. 2018; Wang et al. 2014; Xu and Fu 2012). A range of oil production enhancement from 100% improvement up to 400% improvement is observed on the studies previously listed, indicating that the effectivity of the methods varies with different reservoir, surfactant type, and tested.

Alvarez and Schechter tested the surfactant-assisted spontaneous imbibition method in improving oil recovery on rock and oil sample collected from the Wolfcamp shale oil play (Alvarez and Schechter 2017). Four different surfactant types were tested, nonionic, nonionic/cationic, anionic, and nonionic/anionic. Charge carried by the hydrophilic head of the surfactant molecule is the key difference of the four surfactants. Nonionic means the head is neutral, anionic means the head is negatively-charge, cationic means the head is positively-charged, and mixed surfactant means that two type of surfactant molecule is present. Spontaneous imbibition experiments done on the quartz-rich Wolfcamp rocks showed that production from SASI is ranging from 29-34% OOIP while for experiments ran on solutions not mixed with surfactant produce oil in the range of 7-10% of OOIP. Wettability test done on the study indicated that the anionic surfactant altered wettability to the water-wet region the most and it is also important to note that the same surfactant showed the best oil production, indicating a correlation of wettability and oil production.

Wolfcamp shale oil formation consists of two type of rock lithology, quartz-rich and carbonate-rich. While on the quartz-rich sample, anionic surfactant was found to work the best as shown before, different result was observed for carbonate-rich rock sample. Cationic surfactant modified wettability to water-wet region the most and also produced the largest amount of oil compared to the anionic surfactant used in the testing (AlvarezSaputra et al. 2017a). Contrast between the two lithology's gives an indication that each rock type reacts differently to different kind of surfactant.

Performance of SASI on Bakken shale oil plays provided by Alvarez et al. gives an overview to the intricate relationship between the effectivity of each surfactant and the type of rock (AlvarezSaputra et al. 2017b). Five surfactants were tested, two anionics, one nonionic, one nonionic/cationic mixture, and one "nano" surfactant on rocks with two different lithology, quartz-rich and carbonate-rich. Recovery improvement due to SASI resulted in increment of oil production from 15.9% to 40.6% on the quartz-rich rock and 8.4% to 33.9% on the carbonate-rich rock. Another interesting finding on this study is that the anionic surfactant performed the highest production improvement on quartz-rich rock as well as strongest wettability alteration and highest adsorption, while for the carbonaceous lithology, the nano surfactant performed the best production improvement on the SASI as well as strongest wettability alteration and highest adsorption. Two conclusions can be drawn from this study, a correlation of SASI performance, wettability alteration, and surfactant adsorption is observed and that each lithology has their own specific type of surfactant that is compatible for SASI application on them.

Some other works on the Bakken shale oil plays can also be found with similar conclusion. Nguyen et al. studied the effect of surfactant addition on the formation and observed an increment of oil production from 40% to 85% on imbibition experiment utilizing preserved core and from

10% to 50% on cleaned and aged core (Nguyen et al. 2017). Two other studies were also found, examining the effect of surfactant on Bakken samples with all resulted in positive result of production improvement for rock samples submerged in surfactant solution (Teklu et al. 2018; Wang et al. 2014).

On the Eagle Ford side of shale oil reservoir, several studies have also been done with similar result observed. Xu and Fu tested the effect of weakly emulsifying surfactants on spontaneous imbibition mechanism and observed an increment of oil production (Xu and Fu 2012). Outcrop of Eagle Ford shale was also tested with enhanced oil production on the imbibition process from 30% to 48% and 10% to up to 30% are observed (Kim et al. 2016; Nguyen et al. 2014). Alvarez et al. compared the performance of four surfactants on Eagle Ford samples and observed that cationic surfactant performed the strongest wettability alteration, highest zeta potential number, largest adsorption isotherm, and best oil recovery improvement with increment of production from 2.1% to 9%.

In summary, on laboratory-scale observations, it can be safely concluded that surfactant improve oil recovery based on the imbibition process. Contact angle, IFT, zeta potential, and adsorption isotherm can be used as an indication on the methods and mechanism that drives the production enhancement. However, it also can be concluded that each combination of rock sample and oil sample would have its own well-suited surfactant that would give the highest oil recovery.

It is highly important to understand the mechanism of surfactant-assisted spontaneous imbibition in order to design the most optimum surfactant and also in order to accurately model the process. Although that imbibition in shale is a relatively new technology, the method of producing oil through imbibition has been around in the conventional reservoir side of the

petroleum industry with the earliest application of spontaneous imbibition can be traced back to early 1950s on Spraberry Trend formation (Weiss and Xie 2007; Xie et al. 2005). Imbibition is the process of aqueous-phase movement into the rock replacing the oleic-phase that previously present in the pore space of the rock with three known different driving forces, viscous, gravity, and capillary (Menouar and Knapp 1980). Specifically on this study, viscous force can be easily eliminated from the driving mechanism since viscous force is created by pressure difference applied on the tested sample. Although that pressure difference does exist in the field in the form of pressure drawdown, laboratory studies of spontaneous imbibition do not have pressure applied on the sample due to, among other reason, the objective of analyzing specifically capillary forces on the oil recovery. Therefore, viscous force can be removed from the possible driving force of imbibition, leaving the driving mechanism of spontaneous imbibition to capillary and/or gravity forces.

The debate of whether gravity or capillary action that dominates the exchange of oil and water has been going on since the rise of spontaneous imbibition as an oil recovery improvement method itself. Imbibition as caused by gravity occurs due to the density difference of the oleic- and aqueous-phase, being oleic is the lighter of the two. Gravity pulls the heavier aqueous-phase to the bottom while oleic-phase will move to the top causing imbibition to be dominating the bottom part of core sample in the usual imbibition experiments. Such pattern of oil recovery is observed in several literatures, especially those that incorporates direct visual inspection of the core after imbibition which requires cutting the core plug into half or those studies that incorporate CT-Scan technology to observe the fluid distribution inside the core plug without the need of destroying the sample.

One good example of the imbibition study with direct visual inspection can be seen on Fig. 2. Imbibition experiment was done utilizing oil-saturated chalk core and a low IFT (0.1mN/m) surfactant solution, resulting in the fluid distribution as shown where imbibition of water occurred primarily in the bottom part of the sample shown by the lighter color around the area. While for the CT-Scan incorporated study, Alvarez et al. shows that the same trend is observed on the imbibition case that did not utilize surfactant in the solution. CT-Scan images are a distribution map of density around the scanned sample, water being the heavier fluid compared to oil will be displayed as higher number or brighter color. Fig. 3 shows the CT images in time of the corresponding core and it can be seen that water was imbibing into the bottom part of the core plug as brighter color gradually became more dominant from time to time. The movement of water imbibing into the bottom part of the rock sample while oil is moving out from the top part can also be regarded as a co-current movement (Schechter et al. 1991). Both examples show that gravity-driven imbibition does exist within specific system properties and conditions.

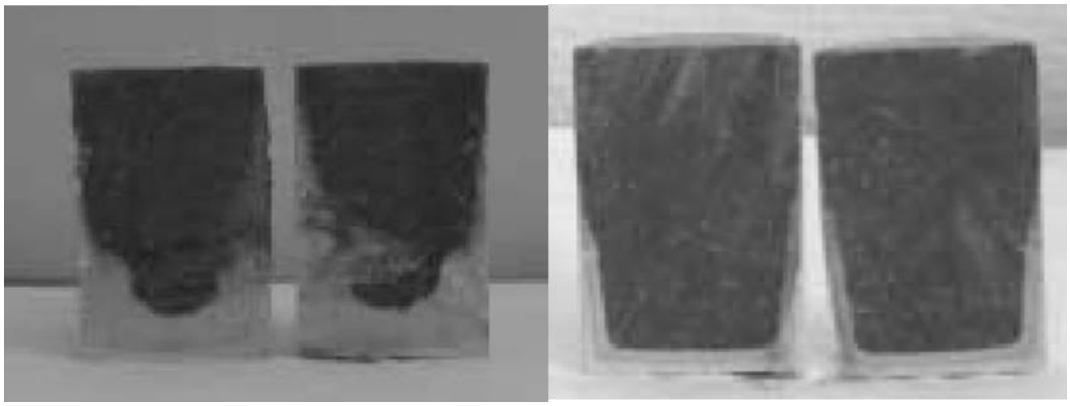

Fig. 2 - Recovery of oil around the bottom part of core plug due to gravity-driven imbibition. Reprinted from (Standnes and Austad 2003).

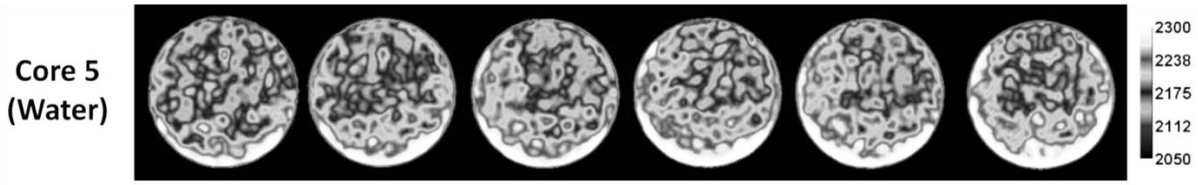

Fig. 3 - CT-Scan image showing gravity-driven imbibition. Reprinted with permission from (AlvarezSaputra et al. 2017a)

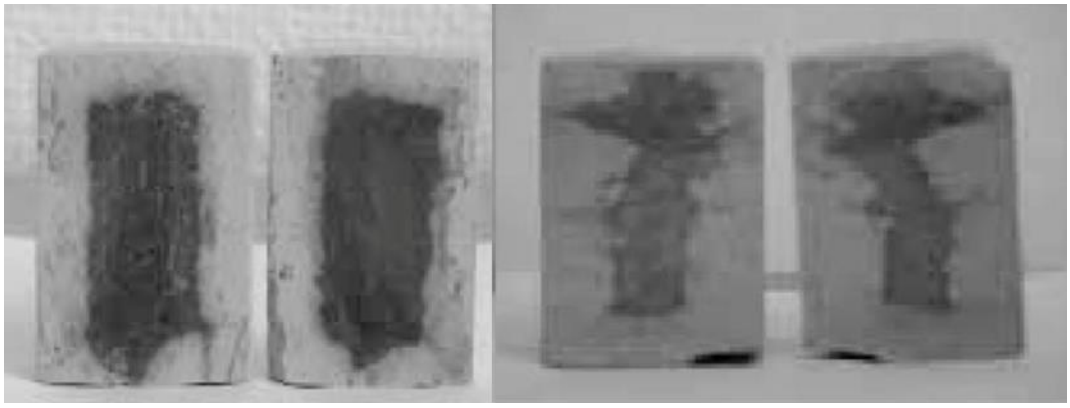

Fig. 4 - Recovery of oil uniformly around the core plug due to capillary-driven imbibition. Reprinted from (Standnes and Austad 2003)

On the other side of the table, capillary-driven imbibition is the exchange process of aqueous- and oleic-phase as caused by the adhesion and cohesion force between the oil, water, and rock. Since the action is not a function of the difference in density between the two phases, fluid pattern from capillary-dominated imbibition is different from the gravity-driven condition. On another imbibition experiments ran by Austad and Standnes (2003), a radial fluid production pattern was observed in capillary-driven imbibition as oil is expulsed out of the core plug while water is imbibing in as can be seen in Fig. 4. Study done by Mattax and Kyte (1962), Parsons and Chaney (1965), Xie et al. (2005), although did not include observation of final fluid distribution after imbibition experiment, also believed that capillary was the driving force of the imbibition process they observed in their experiment (Mattax and Kyte 1962; Parsons and Chaney 1966; Xie

et al. 2005). The movement of water into the rock sample in a radial manner indicated that a counter-current movement was involved as there was only one pathway for oil and water to move in and out of the rock sample. Several other studies stating capillary as the driving force of the imbibition they observed also mentioned this counter-current movement as the mechanism of oil-water flow during capillary-driven spontaneous imbibition (Babadagli et al. 1999; Cuiec et al. 1994).

Schechter et al. (1994) in their work concluded that both gravity and capillary can be present as the driving force of spontaneous imbibition while also defining the transition between the domination of one force to another. Inversed Bond Number (N_B), as defined by Eq. 1, can be used as an indicator of whether capillary or gravity dominates the imbibition process (Schechter et al. 1994). In this equation, C is a representation of pore geometry, σ is the interfacial tension of oil and water, ϕ is the porosity, k is the permeability, $\Delta\rho$ is the difference of density between the aqueous- and oleic-phase, g is gravity, and h is the vertical length of the rock sample. For a condition which results in the Inversed Bond Number to be smaller than one, gravitational force is the dominant force in the imbibition process. Inversed Bond Number larger than five means capillary is the driving force of the oil and water movement in the core plug. Value between one and five indicates that the two forces contribute to the imbibition process. Looking at the equation, reducing the value of interfacial tension will result in gravity taking control of the imbibition mechanism while low permeability value of the rock sample will result in reversed effect of capillary dominating the driving force of imbibition. This observation has high importance in the later part where surfactant and shale rock sample are included in the imbibition process.

$$N_B^{-1} = C\frac{\sigma\sqrt{\frac{\phi}{k}}}{\Delta\rho g h} \ldots\ldots \text{Eq. 1}$$

It is important to note that the equation above was derived under the assumption of rock sample having an ultra-water-wet condition. Under this assumption, reduction of IFT value by addition of surfactant can shift the dominant force of imbibition from capillary to gravity. Schechter et al. (1991) showed that lower IFT will cause gravitational force to overtake capillary in driving the imbibition process, in agreement to the equation of Inversed Bond Number. Although that water-wet rock sample does exist in the form of sandstone reservoir, since the focus of this study is in the shale oil rock which generally has wettability that falls in the oil-wet region, it is important to take wettability into consideration while reviewing the driving force of spontaneous imbibition.

Rock systems categorized as possessing oil-wet wettability exhibit limited imbibition as the volume of oil produced from these rocks is unsubstantial (Austad and Standnes 2003; Salehi et al. 2008). Surface displaying oil-wetness restricts the flow of oil more while also traps oil in the pore under capillary force hence the lower oil productivity. Therefore, it is important to be able to alter the wettability of oil-wet surface to water-wet in order to produce oil through spontaneous imbibition in a substantial amount.

Zhang et al. (2009) added surfactant into imbibition system and reviewed the effect of wettability alteration on the imbibition process with shifting wettability to water-wetness was mentioned as one way of increasing recovery from imbibition (Zhang et al. 2009). This statement was also confirmed by several other works (Morrow 1990; Morrow and Mason 2001; Standnes and Austad 2003). Surfactant is an exceptionally unique molecule due to its amphiphilic nature,

allowing it to bond with both polar and non-polar molecule or in this case, both oil and water molecule. Wettability alteration and IFT reduction are two of the most common reverberation from surfactant addition into an oil-water-rock system. Both also have high importance in the sense of spontaneous imbibition since IFT is an important parameter in determining whether capillary or gravity dominates an imbibition process and wettability and also IFT determine the strength of the capillary force that would drive the movement of oil and water.

In the earlier section, the understanding of all forces that could cause imbibition has been developed. Capillary as one of the force listed is proven to dominate the imbibition when the imbibition is occurring in a low permeability rock as literature showed and also as shown by the equation of inversed bond number where lower permeability will shift the number to be greater than one, indicating capillary-dominated imbibition (Alvarez and Schechter 2016). The strength of capillary force can be defined by the Young-Laplace equation as shown by Eq. 2. Wettability as represented by contact angle (θ), interfacial tension (γ), and pore radius (r) are variables that determine the capillary pressure. Water-wet surface is represented by having contact angle less than 90^o, making the capillary positive or favorable to oil expulsion. Higher IFT value will result in stronger capillary force which also will result in more oil production from capillary-driven spontaneous imbibition, the same implication can also be obtained on smaller pore radius. The presence of surfactant as both wettability alteration and IFT reduction agent will definitely affect the capillary pressure in causing the spontaneous imbibition, therefore an understanding of how surfactant impact both properties must be developed to be able to design and accurately model surfactant effect on spontaneous imbibition method.

$$P_c = \frac{2\gamma \cos\theta}{r} \text{……Eq. 2}$$

The molecular activity of which enabling surfactant to alter the wettability of a solid surface is a very interesting subject to examine. Different kind of surfactant molecule will have their own unique mechanism, which also could variate when interacting with oil having different properties. However, in order to carefully review the mechanism of wettability alteration by surfactant molecule, the concept of wettability as caused by hydrocarbon molecule must be understood beforehand.

Wettability is defined as the tendency of one fluid to spread on or adhere to a solid surface in the presence of other immiscible fluids (Craig 1993). In context of petroleum industry, there are two types of wettability, water-wet and oil-wet. Rocks with water-wet properties will allow water to have the largest contact area with its surface while minimalizing the contact with oil and vice versa. In its original state, most reservoir rock is water-wet. As oil starts moving into the rock pores, either during secondary migration into conventional reservoir or during hydrocarbon generation in the source rock, the wettability of reservoir rock is subject to shift to oil-wet region (Austad and Standnes 2003; Salehi et al. 2008; Standnes and Austad 2000a, 2000b). The process of wettability shift to oil-wet has been a subject of interest and through the development of Atomic Force Microscopy (AFM), more light had been shed into this matter. Adsorption of different hydrocarbon molecule in oil, especially on the heavier molecule side of the oil, on to the rock surface is the basic concept of oil-based wettability alteration. Lord and Buckley (2002), Kumar et al. (2008), and Seiedi et al. (2010) ran AFM on mineral surfaces before and after contact with oil and found asphaltene molecule adsorbed on the surface of the mineral as accompanied with

wettability shift to oil-wet region (Kumar et al. 2005; Lord and Buckley 2002; Seiedi et al. 2011). Fig. 5 is the AFM image gathered in their work which shows change in surface configuration after contact with oil. Considerable surface configuration change can be observed as asphaltene adsorbed to the surface of the mineral, contact angle as an indication of wettability is also observed to shift to oil-wet. Thomas et al. (1993) and Standnes and Austad (2002) also supported the theory and said that fatty acid and carboxylate polymer from the crude oil are the most adsorbed material, specifically on carbonate surfaces, and their adsorption causes the surface to turn oil-wet since the presence of oil molecule on the surface of the rock would attract oil more than water (Standnes and Austad 2003; Thomas et al. 1993). Based on all previously-listed studies, it can be safely assumed that wettability is highly dominated by adsorption of molecules on the surface of the rock.

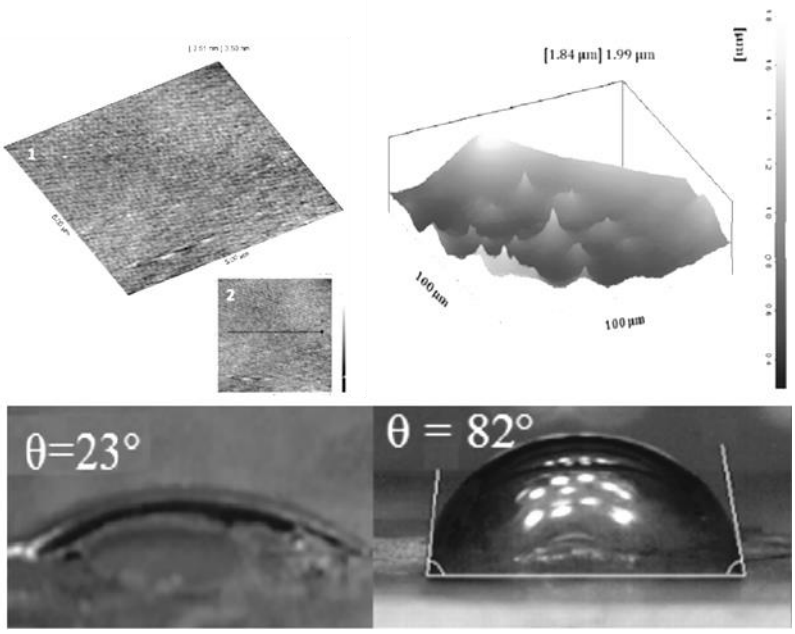

Fig. 5 - AFM and water drop image before (left) and after (right) contact with oil. Reprinted with permission from (Seiedi et al. 2011).

Now that the basic of wettability and its two extreme ends are defined, the mechanism of surfactant's wettability alteration properties can be reviewed. As mentioned before, there are different types of surfactant molecules and the mechanism that it incorporates also depends on its type. Basically, there are four classifications of surfactant molecules based on the charge carried on the head part of the molecule. Anionic surfactant is those surfactants with negatively-charged head, cationic surfactant bears positive charge in its head, nonionic surfactant has neutral head, and zwitterionic surfactant possesses both negatively- and positively-charged head. An oil-wet surface will have oil molecules adsorbed on its surface and depends on the charge that the surface carries, the adsorbed oil molecule will display different charge as well. Negatively-charged surface will cause the adsorbed oil molecule to display positive charge and vice versa.

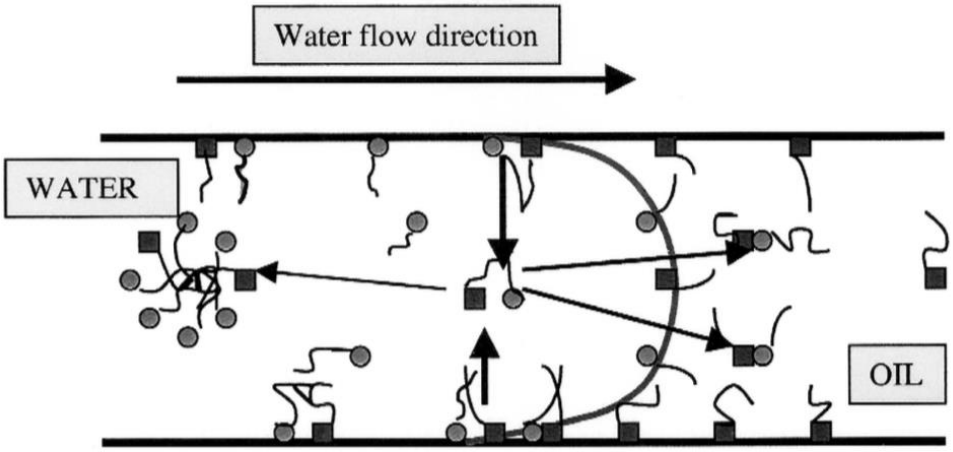

Fig. 6 - Ion-pair surfactant-induced wettability alteration. Reprinted with permission from (Standnes and Austad 2000b).

For explanation purpose, consider a positive-charged rock surface. In line with previous explanation, adsorbed oil molecule on this surface will display negative charge. Cationic surfactant alters the wettability on this system by the bonding of the head of the surfactant molecule to the

positively-charged adsorbed oil molecule, forming an ion-pair (Salehi et al. 2008; Standnes and Austad 2000b, 2003). Then due to the hydrophilicity nature of the surfactant molecule, the formed pair detaches from the rock surface, restoring the water-wetness of the surface. On a negatively-charged surface, the opposite occurs. Positive charged will be exhibited by the adsorbed oil molecule and anionic surfactant will form the ion-pair configuration. Ion-pair mechanism is believed to cause the strongest wettability alteration as a permanent removal of oil molecule is involved in the mechanism. A simple diagram explaining this process can be seen in Fig. 6.

Nonionic surfactant works in different mechanism where due to the absence of dominant charge on its head, the ability of ion-pair formation is also lacking. In this system, hydrophobic tail of surfactant bonds with the adsorbed oil molecule, hence creating a double layer of molecule on the surface of the rock (Salehi et al. 2008; Standnes and Austad 2000b). The hydrophilic part of the surfactant molecule will face the pore space in this oil-surfactant double layer configuration, hence causing the surface to be water-wet as shown in Fig. 7. Double-layer mechanism is also the mechanism of wettability alteration when similar charge of surfactant and adsorbed oil molecule is found. Temporary alteration is often related to the double layer mechanism as the bond between adsorbed oil molecule and surfactant hydrophobic tail is relatively weak (Standnes and Austad 2000a).

Once again, adsorption is proven to be the dominant aspect in the properties of wettability in an oil-water-surfactant-rock system. Study by Somasundaran and Zhang (2006) and Zhang and Somasundaran (2006) supported the theory of surfactant adsorption in altering the wettability of rock surface by providing an important graph which correlates adsorption, contact angle, and zeta potential or in other words, correlating surfactant adsorption to wettability of a rock surface as seen in Fig. 8 (Somasundaran and Zhang 2006; Zhang and Somasundaran 2006). A positive trend

between the amount of surfactant adsorbed and wettability can be perceived from the graph. Higher amount of surfactant adsorbed on the rock surface results in a more water-wet wettability state of the rock surface.

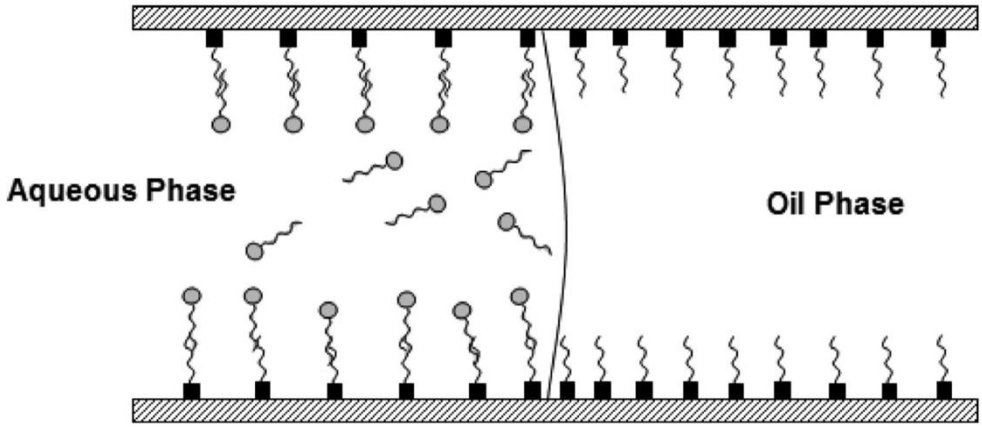

Fig. 7 - Double layer adsorption surfactant-induced wettability alteration. Reprinted from (Salehi et al. 2008).

In its interaction with oil and water molecule, surfactant also exhibits another important modification characteristic of diminishing the interfacial tension between oil and water. The interfacial tension of two immiscible fluids is defined as the energy required to create a new interface between the two phases. This energy is defined by the combination of surface energy of the two different fluid phases subtracted by the interaction energy. Interaction energy is the energy possessed by molecules located at the interface of two immiscible fluids, with the energy defined by the resultant of the interaction energy to the molecule in the bulk phase of its phase and the interaction energy to the molecule of the other phase (Rosen 2004). The molecule of surfactant with its unique amphiphilic nature positions itself on the surface, replacing molecules on the interface, with the hydrophilic head facing the aqueous-phase and hydrophobic head facing the oleic-phase as shown by Fig. 9. This configuration will cause an increment on the interaction

energy as surfactant molecule has higher affinity to both fluid phases compared to the original molecule available on the surface. Since interfacial tension is inversely related to the interaction energy, this will result a decreasing interfacial tension as surfactant molecules present in the system.

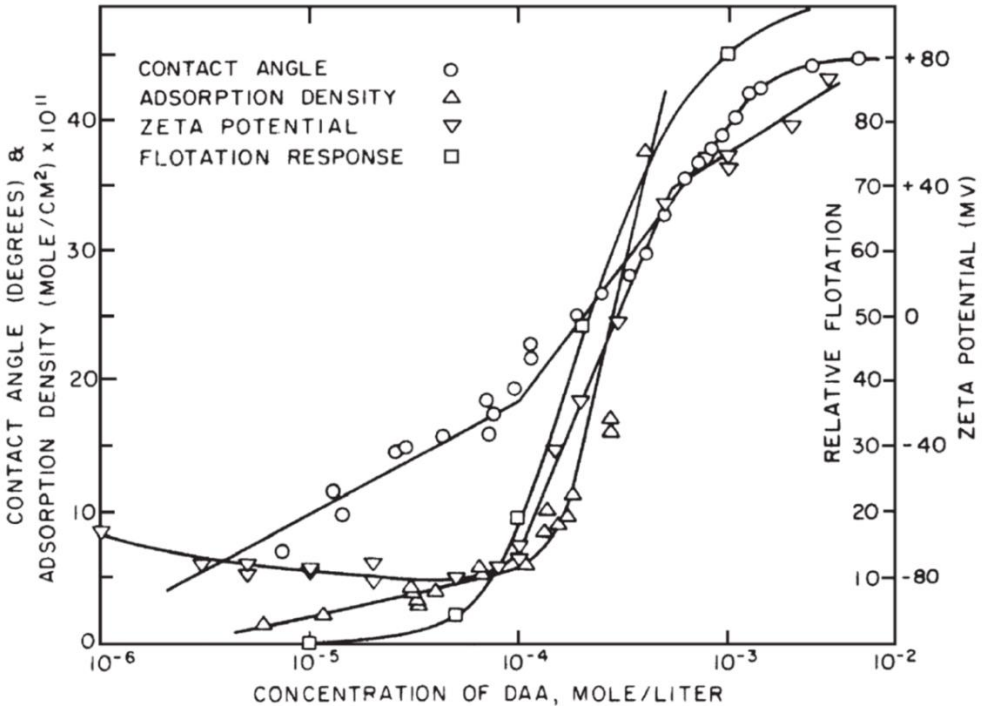

Fig. 8 - Correlation of adsorption, contact angle, and zeta potential. Reprinted with permission from (Somasundaran and Zhang 2006).

That being said, interfacial tension is probably one of the most commonly measured properties that is tightly related to surfactant. The reason being it gives a direct indication on surfactant effectivity on altering the interfacial equilibrium between oil molecule and water molecule. In correlation to the work of surfactant-assisted spontaneous imbibition, IFT also proven to be important as well. As shown before, the exchange of oil and water in this method is driven

by capillary force, whereas as defined by Young-Laplace equation, the magnitude of capillary force occurring in the system is a function of IFT.

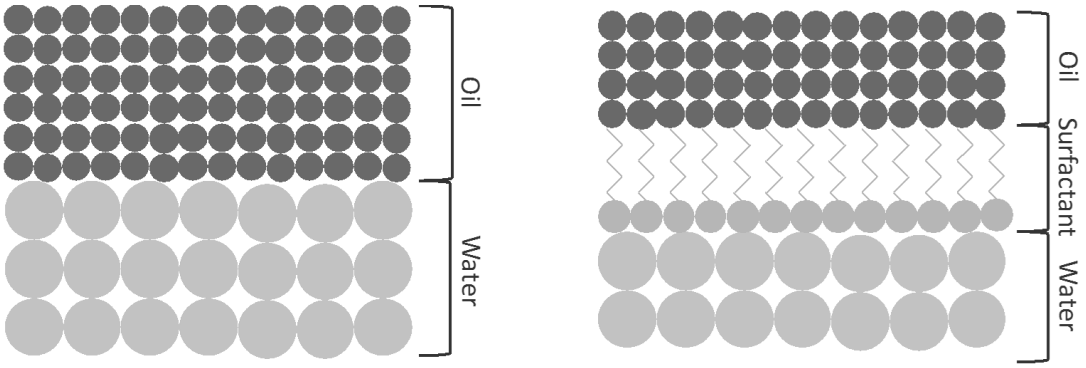

Fig. 9 - Interface configuration of oil and water with and without the presence of surfactant

In conclusion, different studies had shown that oil production through the mean of capillary-driven spontaneous imbibition can be highly beneficial when proper combination of wettability and interfacial tension properties is present. Oil-wet condition would shrink the production of oil from this method. However, addition of surfactant molecule into the system enables the wettability alteration of the rock to water-wet, encouraging the production of oil from spontaneous imbibition (Seiedi et al. 2011).

2.2 Laboratory Measurements of Surfactant-Related Properties

As previously explained, the amphiphilic nature of the surfactant molecule shifts the interfacial equilibrium on an oil-water-rock system. Change of interfacial tension and contact angle as some of the consequence of surfactant molecule addition to the oil-water-rock system has already been heavily explored in the previous section. However, in order to wholly analyze the mechanism of Surfactant-Assisted Spontaneous Imbibition and also in order to provide a complete workflow to assess different surfactant-oil-rock combination for this method, more-surfactant-related parameters must be observed and taken into consideration.

This section provides the theoretical background of experimental procedures in the first step of the work, laboratory data gathering. There are a total of five different experiments that is included in the experimental part of this work, the following section will only describe the literature study and theoretical background of those experiments that measure parameters directly related to surfactant molecule which includes measurement of interfacial tension, contact angle, zeta potential, adsorption isotherm, and CT-Scan assisted spontaneous imbibition.

2.3.1 Interfacial Tension

Due to its high importance, currently there are more than five methods that have been developed in order to measure fluid/fluid interfacial tension or in this case the IFT of oil and water. Drelich et al. published a complete study on the methods, providing a complete comparison study as well as groupings in order to be able to select which method to be used when measuring IFT on

different constraint or condition (Drelich et al. 2002). There are five groups based on the concept used to measure the interfacial tension.

a. Direct measurement using a microbalance

IFT is calculated directly by relying on the fundamental nature of an interface to minimize the interfacial area, with the energy exerted to achieve the smallest surface area is directly related to the interfacial tension. A solid surface with complete wetness to one of the liquid phase is put in contact with the interface with the other end of the surface connected to a balance. As the solid surface is pulled away from the interface, the force exerted on the surface by the fluid is recorded by the balance and converted into interfacial tension. There are two methods that utilizes this concept, Wilhelmy plate and the ring method with the difference in the two is the different shape of solid surface used as the name suggests, Fig. 10 provides a simple diagram on the experimental set-up of the two methods.

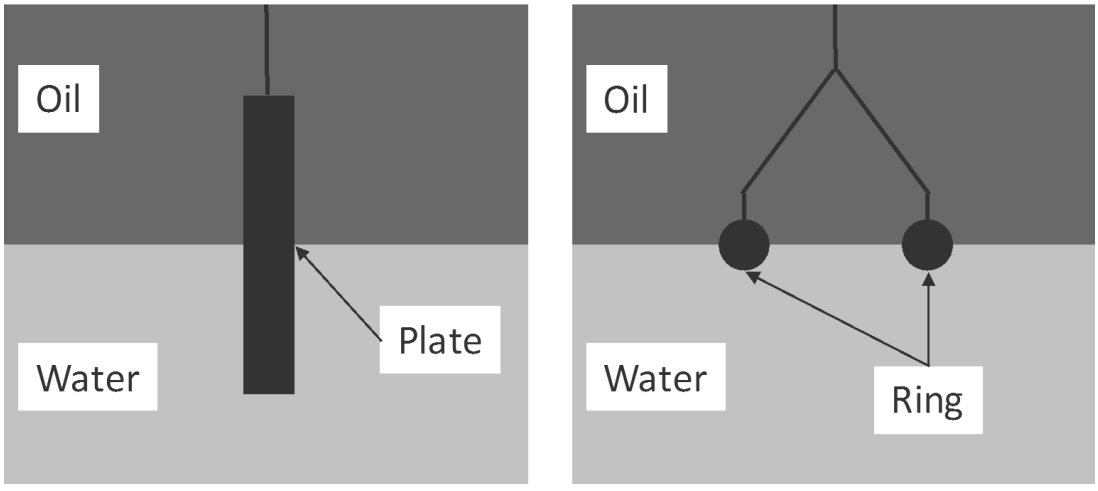

Fig. 10 - Wilhelmy plate and du Nouya ring method. Adapted from (Drelich et al. 2002).

b. Measurement of capillary pressure

In the second group, IFT is measured by utilizing the pressure difference across a curved interface as derived by Young and Laplace shown below.

$$\Delta P = \gamma \left(\frac{1}{R_1} + \frac{1}{R_2} \right) \ldots\ldots \text{Eq. 3}$$

By knowing both the pressure difference between the inside and outside and the radii of the bubble, IFT can be derived by reconstructing the equation. The maximum bubble pressure method is based on this concept. Gas bubble is created on the tip of a capillary tube surrounded by another fluid phase with the pressure of both the gas and the fluid phase is monitored.

c. Analysis of capillary-gravity

Methods categorized in this group are based on the concept of equilibrium between two forces acting on a fluid phase, gravity and capillary. By utilizing the capillary pressure equation as defined on Eq. 3 and the gravity force in the form of hydrostatic pressure, the IFT can be extracted from the equation as the rest of the variable in the equation is obtained from the experiment. One example of this method is the earliest capillary action demonstration of the rising of fluid level in a capillary tube or capillary rise method. By measuring the height of the capillary column formed by the fluid, IFT can be calculated.

d. Gravity-distorted drops

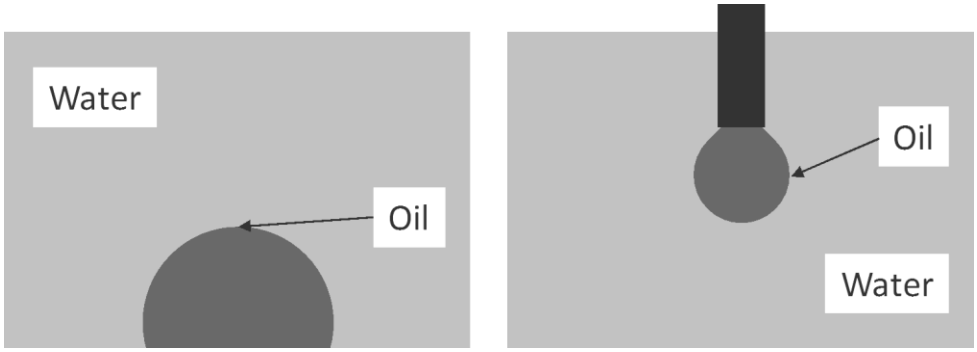

Fig. 11 - Sessile drop and pendant drop method. Adapted from (Andreas et al. 1937; Bashfort and Adams 1883; Stauffer 1965).

The fourth group was developed based on the previous method of capillary and gravity equilibrium. Interfacial tension causes the interface to form the smallest interfacial area as possible which would be in the form of spherical shapes. The spherical shape formed by a drop of a fluid surrounded by another fluid phases could give the interfacial tension between the two phases, however a perfect spherical shape is impossible to be produced as the drop will be distorted by the gravitational field. Therefore, IFT measurement methods in this group are based on a shape-fitting equation combined with Young-Laplace equation shown on Eq. 3. Pendant drop and sessile drop are the two methods that utilize this concept. Bashfort-Adams equation solve the shape-fitting problem for the sessile drop method (Bashfort and Adams 1883). Stauffer and Andreas et al. published the drop shape-fitting equation for the pendant drop method which requires trial and error of several constants to match the drop shape perfectly (Andreas et al. 1937; Stauffer 1965). Consequently, the drop must be recorded for the trial and error process to

be possible. Therefore, a camera and computer system is a necessary for IFT measuring methods based on the Stauffer and Andreas et al.

e. Reinforced distortion of drop

IFT measurement methods categorized in this group are those which developed due to the limitation of previously covered methods in measuring interfacial tension of two fluids with extreme condition. One example of this method is the spinning drop method which works by applying centrifugal force to distort the drop shape of a fluid surrounded by other fluid phases with the IFT is measured by correlating the extent of distortion to the centrifugal force applied (Vonnegut 1942). It is found that the spinning drop method is highly practical in measuring ultra-low IFT value commonly found in surfactant system used in conventional surfactant flooding EOR.

2.3.2 Contact Angle

Wettability alteration of a surface from oil-wet to water-wet is another effect that is observed when surfactant molecule is added into a system of oil-water-rock as has been explored in the previous section. This behavior is believed to play a crucial role in the surfactant-assisted spontaneous imbibition as a shift from oil-wet to water-wet alters the direction of capillary force to be in our favor. Therefore, an assessment to gauge the ability of a surfactant to alter the wettability of an oil-wet surface is highly important.

Wettability measurement in the oil industry has been developed since 1970s marked by the development of experimental procedure based on oil and water volume produced from imbibition and drainage process (Amott 1959). Currently there are three quantitative wettability measurement method that is widely used, the previously mentioned Amott method, USBM method, and contact angle method (Anderson 1986). Both Amott method and USBM method require force displacement of fluid into the rock sample, an impossible task to be done considering the ultra-tight nature of the rock of shale oil reservoir. Therefore, contact angle measurement method is used in this work and the concept and method on the experimental process is covered in the following part.

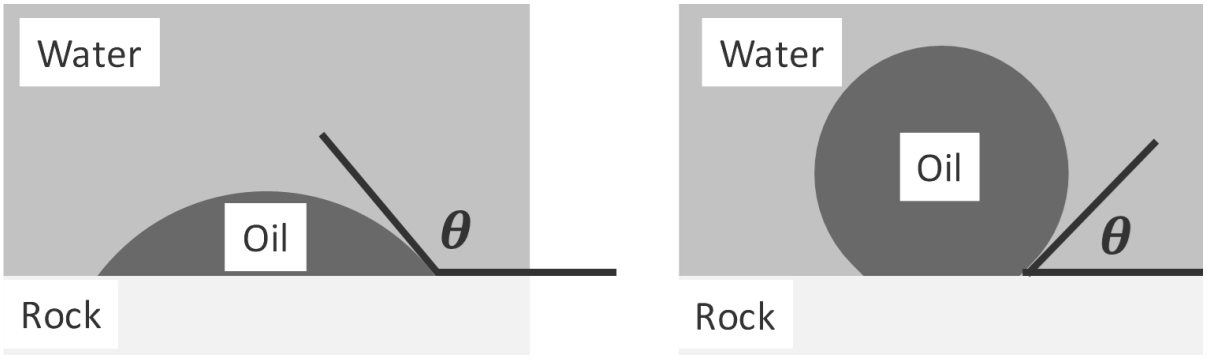

Fig. 12 - Contact angle of an oil-wet (left) and water-wet (right) surface

Contact angle is defined as the angle formed through the water phase as a drop of either oil or water is dispensed on to a solid surface, which in this case is a rock surface. Measurement of contact angle is essential in studying surfactant performance as contact angle can function not only as an assessment of wettability as explained previously, but also can be used to calculate capillary pressure through the use of the Young-Laplace equation. Another advantage of wettability assessment from contact angle measurement is the relatively low cost of running contact angle

compared to the Amott and USBM method since the two methods require recovery of core-plug sample while contact angle measurement can be executed from any form of rock debris. The simplicity of the measurement also allows for more test to be done, highly essential in the process of surfactant selection.

The measurement of contact angle requires rock sample to be submerged in either water- or oil-phase and the contact angle is measured on a drop, of either oil for rock submerged in water or a drop of water for oil submersion, positioned to contact the surface of the rock (Treiber and Owens 1972). The shape of the bubble or the angle formed by the outline of the bubble is a function of the amount of molecule from the drop that is adsorbed on the solid surface. A higher adsorption would cause the drop to be more spread out on the surface of the rock, indicating wettability to the fluid that forms the drop. On the other hand, less adsorption would cause the drop to form a more spherical shape, indicating that the rock surface's wettability is more to the ambient fluid. Fig. 12 illustrates the two conditions with the set-up of water as the ambient phase and oil as the drop phase. In order to classify the contact angle reading into either water-, intermediate-, or oil-wet, a convention is put together by Reed and Healy as shown in Table 1.

Table 1 - Contact angle wettability category. Adapted from (Reed and Healy 1984).

Contact Angle	**Wettability**
$0^o - 75^o$	Water-Wet
$75^o - 115^o$	Intermediate-Wet
$115^o - 180^o$	Oil-Wet

2.3.3 Zeta Potential

Solid particle suspended in fluid phase will cause layers of ion from the fluid phase to form around the particle with the surface charge of the solid particle controlling the distribution and thickness of the layer. Such layer can be explained by double layer model as shown by Fig. 13. Zeta potential is the measurement of the potential difference between the fluids as a dispersion medium and the slipping plane, which is located at a distance from the particle where no ion is found affected by the surface charge of the solid particle.

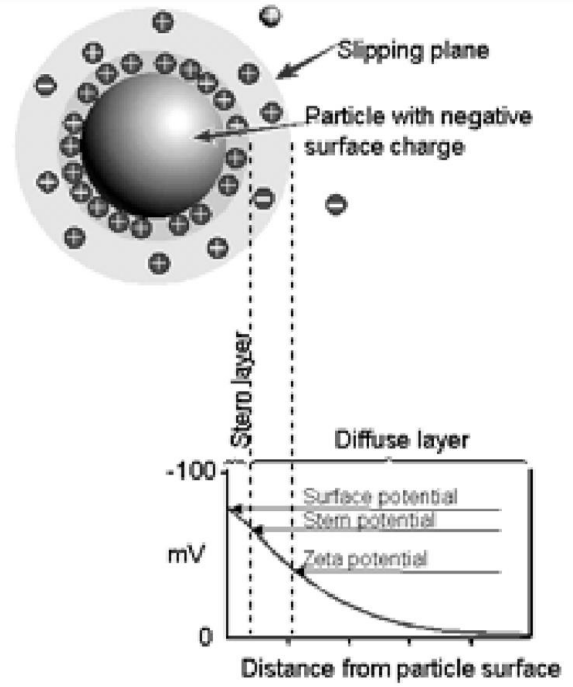

Fig. 13 - Double layer model of a solid particle dispersed in fluid phase. Reprinted from (Instruments 2011).

In the study of surfactant in its performance to enhance oil production, measurement zeta potential can be used as an additional measure of wettability (Alvarez and Schechter 2016). Zeta

potential reading is highly dependent on the charge of oil, water, rock, and surfactant as their charge controls the thickness of the ion layer formed around the rock particle (Hirasaki and Zhang 2004). Therefore, zeta potential measurement of rock particle suspended in water can be used as a test to determine the water-wetness of the rock particle.

Zeta potential cannot be measured directly and must be calculate from electrophoretic mobility, which the data can be acquired by two different experimental approach. The first approach is electrokinetic phenomena, where a potential difference is applied to the suspension using two electrodes and will cause the particle to move toward the electrodes with the opposite charge (Salopek et al. 1992). The velocity of the particle movement is proportional to the value of zeta potential. The second approach is electroacoustic phenomena were instead of potential difference, an ultrasonic wave is transmitted into the suspension that will cause the particle to move accordingly (O'Brien et al. 1995). The movement of the particle will generate electric signal due to their electric charge and zeta potential can be measured by measuring the signal.

2.3.4 Adsorption Isotherm

Adsorption is defined as the adhesion of atoms, molecules, or ions on to a solid surface. The word “on” is important here since an adsorbed phase is strictly attached and located on the surface of the solid phase, a completely different phenomenon from absorption where the absorbed molecule is located in the bulk volume of the solid phase. Adsorption occurs as molecules accumulate in the interfacial layer which occurs due to the process of reaching equilibrium due to

unbalanced force that occurs at the surface of a bulk material where certain type of molecules is attracted to cancel out the unbalanced force (Dąbrowski 2001).

Surfactant adsorption on rock surface is often correlated to the degree of wettability alteration with positive correlation of the amount of adsorption to the water-wetness of the sample is observed, while also correlated to the amount of loss that would be observed when injecting the surfactant into the reservoir (Curbelo et al. 2013). Therefore, surfactant adsorption data has high importance in assessing the surfactant performance in performing SASI. Surfactant adsorption quantity is usually presented in the form of adsorption isotherm graph which provides the amount of surfactant adsorbed onto rock surface on the function of the surfactant concentration in the solution. In order to construct this graph, multiple data points of the amount of surfactant adsorbed when put in contact with a rock is needed.

The measurement of adsorption of surfactant on a rock surface can be done in two ways, dynamic and static method. In the dynamic method, surfactant solution will be injected through a core plug and the difference of surfactant concentration pre- and post-injection will determine the adsorption quantity (Wang et al. 2015). While in static method, rock sample is crushed first then mixed with surfactant solution with different concentration and the change of surfactant on a rock surface is usually determined through this method (AlvarezSaputra et al. 2017b). Either static or dynamic condition would require the measurement of surfactant concentration in the fluid phase before and after the contact period. Direct measurement of the amount of surfactant molecule present in the fluid phase is impossible to be done practically, however there are two methods that have been widely used to gauge the surfactant concentration in a fluid sample.

a. Electrical conductivity method

Ionic charge presents on the head of a surfactant molecule could change the electrical conductance of a liquid-phase when surfactant is added due to the different degree of surfactant ionization (Dominguez et al. 1997). Water molecule by itself is relatively nonionic compared to surfactant, causing the conductance of water molecule to be lower than water that is mixed with surfactant. Therefore, a direct relation of the conductance of a solution and surfactant concentration in the solution should exist. Such relation does exist and conveniently in a linear nature with a deflection can be observed when surfactant concentration passes the CMC as shown in Fig. 14 (Ahmadi and Shadizadeh 2013).

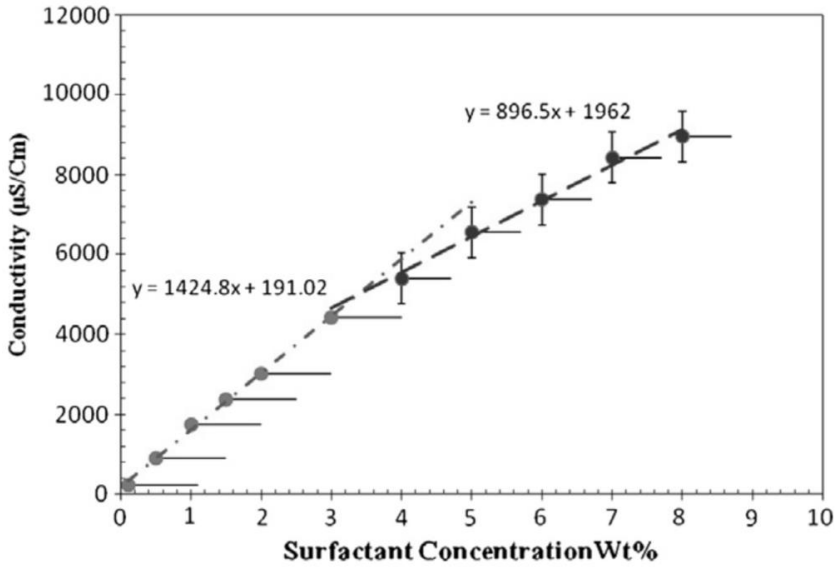

Fig. 14 - Correlation of conductance and surfactant concentration. Reprinted with permission from (Ahmadi and Shadizadeh 2013).

As an indirect measurement, a calibration curve to convert conductance reading to surfactant concentration must be constructed beforehand. Calibration curve is constructed

by measuring and plotting the conductance of surfactant solution with different surfactant concentration. This curve is unique for each surfactant system and therefore new calibration curve should be constructed for each surfactant tested.

b. UV-absorption Spectroscopy method

Shine a light into solution containing any molecule, certain wavelength of the light will be adsorbed by the molecule. According to Beer-Lambert Law, the amount of light adsorbed is linearly related to the amount of the molecule in the solution (Ingle and Crouch 1988). The same concept is also applicable to surfactant solution where surfactant molecule will adsorb light on different wavelength depending on the amount of the molecule, or in other words, the concentration of surfactant in the solution.

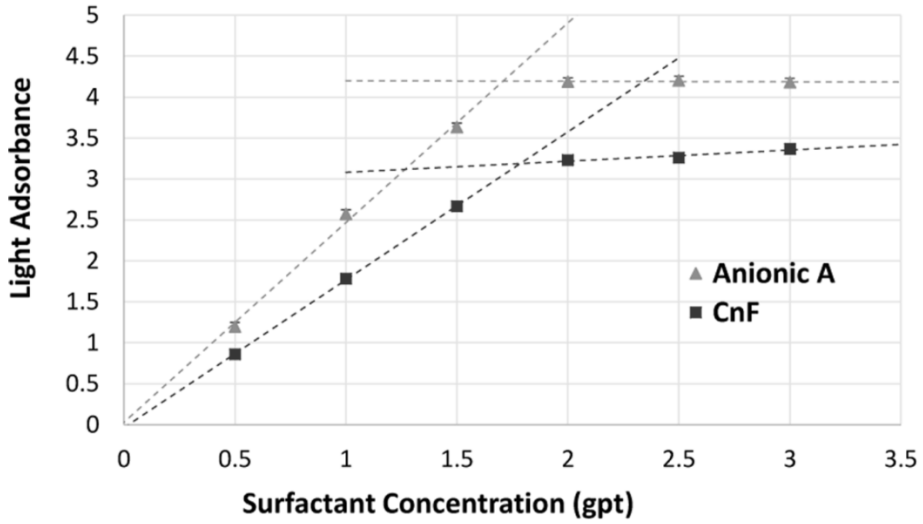

Fig. 15 - Calibration curve of light adsorbance and surfactant concentration. Reprinted with permission from (AlvarezSaputra et al. 2017b).

UV-absorption spectroscopy method is based on the Beer-Lambert concept, providing an indirect measurement of surfactant concentration based on the amount of light adsorbed. This method is also the most used procedure to measure surfactant concentration due to its accuracy and simplicity (AlvarezSaputra et al. 2017b; Mirchi et al. 2015; Zhang and Somasundaran 2006; Ziegler and Handy 1981). Alvarez et al. provides the detail procedure for measuring adsorption using the UV-Vis, which starts by detecting the wavelength that represents the surfactant molecule present in the solution. Wavelength scan done on multiple surfactant concentration using 190-300nm of wavelength range and by comparing the result, both characteristic wavelength of the corresponding surfactant as well as the calibration curve to convert the amount of light adsorbed on the characteristic wavelength to the surfactant concentration. An example to the calibration curve for this method can be seen on Fig. 15.

2.3.5 CT-Scan Assisted Spontaneous Imbibition

Surfactant performance in improving oil production through SASI can be directly observed by running the spontaneous imbibition experiment, submerging core plug in a surfactant solution in an Amott cell and observe the volume of oil production directly as it accumulates at the top of the cell. Multiple studies have implemented this method (AlvarezSaputra et al. 2017a, 2017b; AlvarezTovar et al. 2017; Kim et al. 2016; Morsy et al. 2014; Nguyen et al. 2017; Nguyen et al. 2014; Teklu et al. 2018; Wang et al. 2016; Xu and Fu 2012) due to its simplicity and straightforward result in giving the measurement of oil recovery. The only drawback of this

measurement is the requirement of having core plug sample of the tested reservoir, a luxury which sometimes is not available.

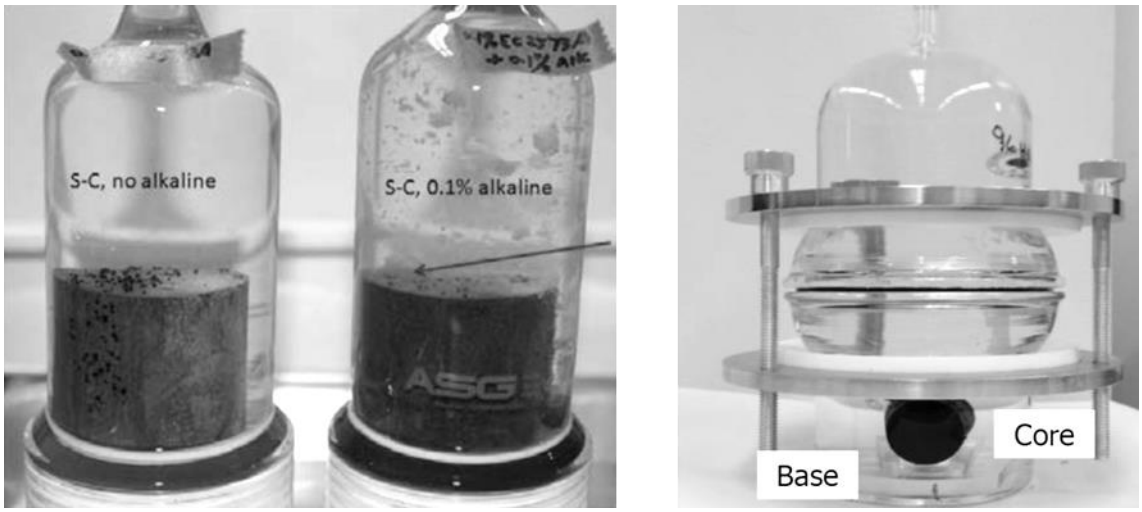

Fig. 16 - Vertical and horizontal core-plug orientation for spontaneous imbibition experiment. Reprinted from (Alvarez and Schechter 2016; Nguyen et al. 2014).

There is also different core plug orientation that is employed in the previously listed works that ran spontaneous imbibition in an Amott cell, vertical and horizontal core plug orientation shown in Fig. 16. Vertical orientation is more commonly used, however setting up core plug in this orientation could cause the gravity force to take a larger part in oil production on the imbibition process. Schechter et al. (1994) introduce the use of inverse Bond number, defined by Eq. 1, to determine the primary force in the imbibition process categorized as capillary-dominant when the inverse Bond number is larger than 5 and gravity-dominant when the number is smaller than 1 (Schechter et al. 1994). Vertical configuration will reduce the inverse bond number as variable h as the denominator will be larger compared to horizontal orientation, hence increasing the contribution of gravity force in the imbibition process.

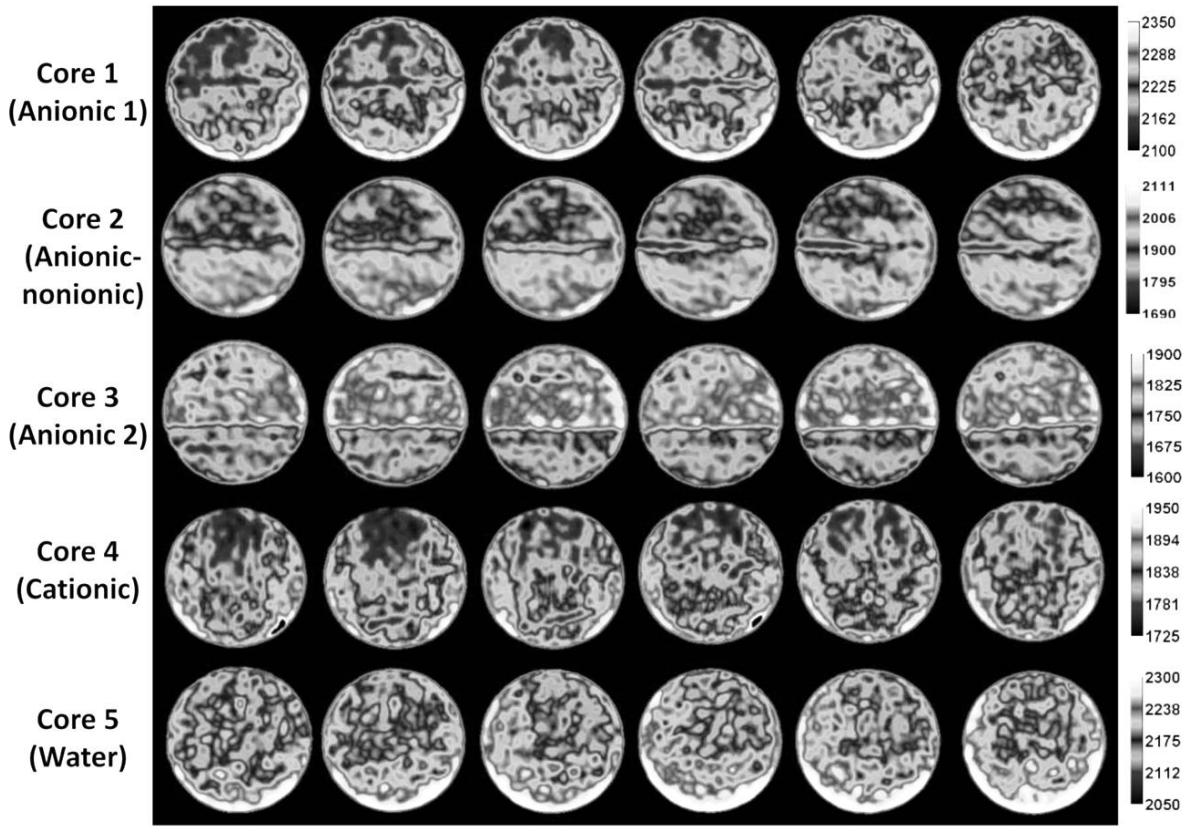

Fig. 17 - CT analysis of core plug under imbibition experiment with different solution. Reprinted with permission from (AlvarezSaputra et al. 2017a).

CT-scan technology is also incorporated in some of the study listed before. Alvarez et al. (2015) utilized the CT-scan to visualize the fluid exchange that occurs inside the core plug as oil moves outside the core and water moves in to the core in a non-destructive manner, providing a qualitative assessment on the imbibition process. As CT works by providing a density map of the scanned object, doping agent is added into the aqueous-phase to improve the contrast of aqueous- and oleic-phase by increasing the density of the aqueous-phase. Potassium Iodide in the concentration of 4wt% is used as doping agent as it was found to be inert to the IFT and contact angle measured using the solution (Alvarez and Schechter 2016). An example of CT images

compilation of different imbibition test condition in different experiment time can be seen in Fig. 17.

2.3 Numerical Modelling of Surfactant-Assisted Spontaneous Imbibition

For almost any method or phenomenon observed on the field of petroleum engineering, it is an absolute for the next step of the study regarding the matter to build its model, either analytical or numerical. The same goes for imbibition or surfactant-induced imbibition. There has been numerous attempts to model the imbibition mechanism for both analytical and numerical simulation method. Each of the modelling work has its own specific agenda, however, there are basically two main objectives, to provide a sensitivity analysis on different properties related to the imbibition process and to be able to provide a field-scale implication of imbibition by upscaling the laboratory data. On the following section, numerous works done on modelling and upscaling the imbibition, surfactant activity, and surfactant-assisted spontaneous imbibition will be reviewed. Although that this manuscript is focused on the Eagle Ford shale reservoir, most of the publication that will be reviewed will also include researches done on conventional reservoir due to the limited number of published work on modelling imbibition on shale rock.

As previously explained, multiple flow-related processes occur and exist during the process of imbibition as induced by surfactant molecule. Imbibition, counter-current flow of oil and water, concurrent flow of oil and water, and surfactant-induced alteration of relative permeability and capillary pressure happen simultaneously during the surfactant-assisted spontaneous imbibition. It

is essential to understand the modelling or upscaling process of each phenomenon in order to accurately model the process of SASI.

The first and the simplest, but also the most fundamental, model that is related to SASI is the analytical dimensionless scaling group method of imbibition. Different recovery factor and rate resulted from different imbibition test ran on different rock properties and also fluid properties prompted a discussion of grouping procedure that could eliminate the difference of imbibition condition on every test, merging every imbibition production curve to fall into one general curve. The grouping procedure is basically based on converting the time into a dimensionless variable that takes into account different properties, such as porosity, permeability, viscosity, relative permeability, capillary pressure, etc. Having a universal dimensionless grouping would enable an approximation of recovery from imbibition on different properties, minimizing experimental work, upscaling to field-scale, and also providing better understanding on the effect of each parameter to the performance of imbibition without the need for heavy computational power. But of course, the success of a dimensionless analysis is determined by its ability to merge any production curve regardless of its testing condition which apparently an extremely hard task to do.

There have been multiple works done on the scaling group analysis of imbibition on both co- or counter-current flow (Li and Horne 2002; Ma et al. 1997; Mattax and Kyte 1962; Parsons and Chaney 1966; Patel et al. 2013). Since scaling group analysis is not the main focus in this research, only the three most-widely-used scaling model will be explored next.

$$t_D = t\sqrt{\frac{k}{\phi}}\frac{\sigma}{\mu_w L^2} \ldots\ldots \text{Eq. 4}$$

Scaling group analysis from the work of Mattax and Kyte (1962) is the pioneer of scaling group in the context of oil recovery from imbibition process. Dimensionless time is defined as Eq. 4, where k is the permeability, ϕ is the porosity, σ is the interfacial tension between oleic- and aqueous-phase, μ_w is the water viscosity, and L is the length of rock sample used in the imbibition experiment. The derivation of this dimensionless time definition was based on the Leverett J-function and was also based on multiple assumption which would also become the limitation of conditions where the scaling group can be applied. Similar sample size, similar oil and water viscosity ratio, similar initial water saturation, exclusion of gravity effect, and also constant capillary pressure and relative permeability are the list of conditions where the scaling definition applies (Mattax and Kyte 1962).

$$t_D = t\sqrt{\frac{k}{\phi}}\frac{\sigma}{\sqrt{\mu_o\mu_w}}\frac{1}{L_C^2} \quad \text{.....Eq. 5}$$

The next dimensionless analysis came from the work of Ma et al. (1997) which can be safely claimed as a direct update of the previously mentioned work. Ma et al. took the similar basic form of the equation but also introduced a couple of new variable, specifically added to broaden the applicability of Mattax and Kyte's dimensionless analysis (Ma et al. 1997). As seen on Eq. 5, viscosity term was changed to a $\sqrt{\mu_o\mu_w}$ term to accommodate different viscosity of fluid present in imbibition test. The term L was also modified into L_C which defined as characteristic length, modification done in attempt to group imbibition recovery curves from rock sample of different sizes.

$$t_D = tc^2 \frac{kk_{re}^*}{\phi} \frac{P_C^*}{\mu_e} \frac{S_{wf}-S_{wi}}{L_a^2} \ldots\ldots \text{Eq. 6}$$

Although that the work of Ma et al. (1997) was already an update of previous scaling analysis, it was found out that there are several condition of which Eq. 5 does not function perfectly. Ultra-water-wet wettability condition and removal of gravity effect were taken as assumptions, making the applicability of the dimensionless analysis limited to the corresponding condition (Li and Horne 2002). Therefore to cope with every possible imbibition condition, IFT, wettability, gravity, etc, Li and Horne (2006) derived a more general dimensionless time definition, shown by Eq. 6. Different wettability and IFT are reflected on the addition of relative permeability (kk_{re}^*) and capillary pressure (P_C^*) term. Both co- and counter-current flow are included in the scaling analysis in the form of different mobility factor, represented as $\left({kk_{re}^*}/{\mu_e}\right)$. Scaling group analysis from Li and Horne (2006) works really well in numerous imbibition condition as imbibition production curve from different rock and fluid properties group nicely into one general curve.

The simplicity of scaling group analysis is really helpful in quickly approximating the impact of lab-scale imbibition on the field-scale. However, there are several weakness of utilizing scaling group analysis. Alteration of flow properties as caused by surfactant happens gradually as more and more surfactant imbibes into the pore, this feature is impossible to be modelled by the scaling group analysis as one single flow property is used. Scaling group analysis also usually only includes the spontaneous imbibition part where pressure difference or pressure drawdown is absent, while in a real life field case, production of oil is a combination of production from pressure

drawdown and also spontaneous imbibition. Numerical simulation is the answer to these drawbacks of scaling group analysis.

Numerical modelling of imbibition process as driven by capillary pressure can be traced back to the 1950s with the work done by Aronofsky and Natanson (1958). Reservoir modelling done before their work did not include capillary function in the flow equation which resulted in the mismatch of history-matching on fractured reservoir where capillary action plays a significant role to the production of oil. Aronofsky and Natanson added the capillary function into the model equation as another driving force for oil production which gave them better history-match result (Aronofsky et al. 1958). Kazemi and Merril (1979) later tested the ability of numerical model to model spontaneous imbibition on a core-scale experiment and confirmed that capillary-driven imbibition is properly modeled (Kazemi and Jr. 1979). Imbibition was also modeled through an unorthodox approach where the transfer of oil and water is represented by diffusion mechanism (Bech et al. 1991).However, this method is rarely used since it does not accurately represent the physical mechanism of capillary-driven spontaneous imbibition.

Previously-listed work provided the ability of numerical simulation to model the capillary-driven imbibition, solving one piece of the puzzle for numerical modelling of SASI, however the discussion on whether co- or counter-current flow was not yet to be started. Two different publication discussed the application of counter-current flow imbibition to numerical model (Behbahani and Blunt 2005; Pooladi-Darvish and Firoozabadi 2000). Behbahani et al. utilized a commercial reservoir numerical simulator while Darvish and Firoozabadi investigated their own model to evaluate the counter-current flow modelling in a fractured reservoir on a numerical simulator and both work indicated that numerical model is able to model counter-current spontaneous imbibition. Andersen et al. (2013) further confirmed the finding, providing another

important aspect of SASI modelling, which is the counter-current imbibition flow (Andersen et al. 2014).

Six imbibition modelling works mentioned before(Andersen et al. 2014; Aronofsky et al. 1958; Bech et al. 1991; Behbahani and Blunt 2005; Kazemi and Jr. 1979; Pooladi-Darvish and Firoozabadi 2000) were all done on unaltered reservoir's flow condition, without any surfactant-induced flow properties alteration. Single set of capillary pressure and relative permeability curves is applied on the model where movement of oil and water during spontaneous imbibition is driven by the pressure difference between the two phases as defined by the single capillary pressure curve supplied. On each timestep and in each gridblock, saturation and pressure are solved through this method, a relatively simple procedure as only one iteration procedure is needed. Addition of surfactant will undeniably complicate this process since the presence of surfactant will alter the flow-related properties as explained in earlier section. An ideal model of SASI will start with intake of surfactant solution into the grid by the exact procedure of water imbibition in surfactant-free imbibition model. After getting into the grid, surfactant will alter the relative permeability curves and capillary pressure curve of the corresponding grid which will either increase or reduce the capillary driving force or flow capacity as determined by relative permeability. Then, another iteration procedure must be done to retrieve the updated fluid saturation and pressure of the grid to accommodate the change of flow properties. As the extend of capillary and relative permeability curves modification is a function of surfactant in the grid, the two curves will undergo continuous change through the whole simulation runtime which also includes recalculation of pressure and fluid saturation as explained before. In summary, inclusion of surfactant into numerical simulation adds another level of complexity to the model. However, due to the high importance of this

surfactant-assisted spontaneous imbibition, several publications have been published in the past with different approach and simplification to tackle this complex procedure.

Modelling of surfactant-assisted spontaneous imbibition on a core-scale laboratory experiment was done by Adibhatla et al. (2005) utilizing an in-house numerical reservoir simulation, UTCHEM (Adibhatia et al. 2005). Carbonate rock samples were used for the imbibition experiments along with different surfactants. Alteration of flow properties due to the presence of surfactant was modeled by applying modification on capillary pressure, relative permeability, and end-points of each. The presence of surfactant molecule is correlated to change of interfacial-tension of oil and water. IFT then will be used to calculate a coefficient called trapping number which then used to calculate the endpoint of relative permeability curves. Since trapping number does not include wettability alteration variable, another correlation is used to modify the calculated endpoint according to the contact angle value. After the endpoints have been calculated, the curve then is constructed based on Brooks-Corey relative permeability model. Meanwhile, capillary pressure is modified from the base-case capillary pressure from Leverett's J-function with the original base-case capillary pressure obtained from history-matching.

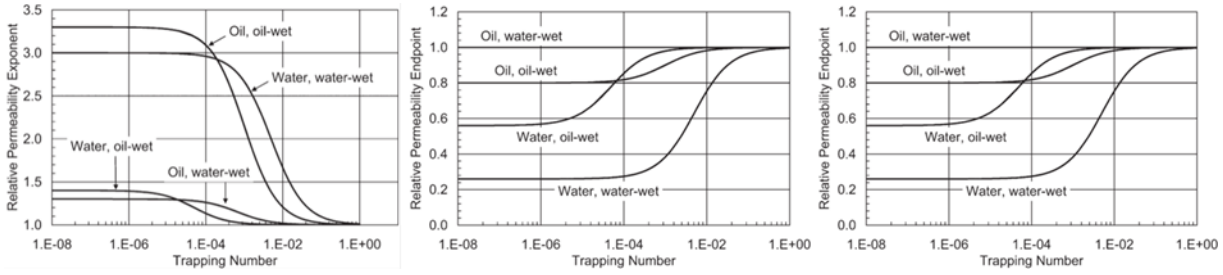

Fig. 18 - Graphs of difference CDC on different wettability condition. Reprinted from (Delshad et al. 2009).

Delshad et al. (2009) published another modelling effort utilizing the UTCHEM simulator with a more straightforward approach on the modelling of wettability alteration (Delshad et al. 2009). Graphs of Capillary Desaturation Curves (CDC) shown in Fig. 18 correlating trapping number to endpoints are used. Different CDC graphs are needed for applying this method on different rock type.

The work done on UTCHEM previously were mostly done under ultra-low IFT surfactant where residual saturation will be affected. Kathel and Mohanty (2013) later proposed another approach that is applicable on certain surfactant where the reduction of IFT is not as significant. An assumption was taken under the development of the approach where residual saturation or endpoints of both relative permeability and capillary pressure curve are not affected and the effect of surfactant is limited only on the maximum value and the shape of the curve (Kathel and Mohanty 2013).

Kalaei et al. (2012) built a numerical model on imbibition with changing capillary pressure and relative permeabilities (Kalaei et al. 2012). However, instead of surfactant concentration in each grid controlling the amount of alteration, a time dependent function of wettability variable was introduced. Where the wettability variable will be used to calculate the capillary pressure curves and relative permeability endpoints and exponents. Kalaei et al. also showed that counter-current flow was modeled in their numerical simulation as well. Chahardowli and Bruining (2013, 2014) used similar modelling mechanism of time-dependent alteration in their work (Chahardowli and Bruining 2014; Chahardowli et al. 2013).

Comparing the characteristic of surfactant used in this study and all previous modelling efforts of SASI, it can be concluded that the concept of trapping number will not work in the modelling effort of this study since as explained by Kathel and Mohanty (2013). The time-dependent ramp function from Kalaei et al. (2012) and Chahardowli and Bruining (2013, 2014) are also going to be hard to implement due to the intricacy in measuring the time-dependent capillary and relative permeability alteration variables. Another method should be developed to model the flow properties modification as caused by surfactant on numerical simulation basis.

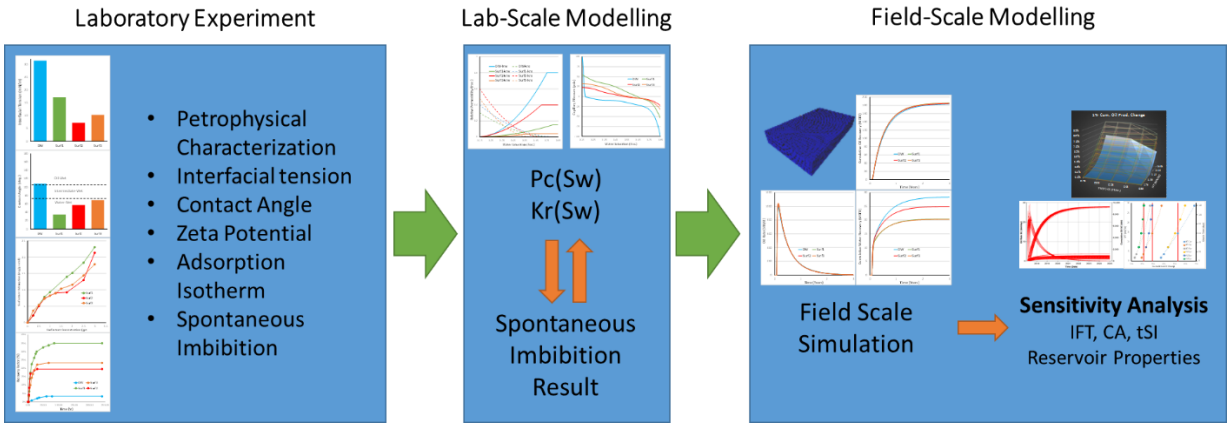

Fig. 19 - Workflow of complete surfactant-assisted spontaneous imbibition (SASI) assessment

Based on previous efforts done by different author, a new workflow to model and to upscale the lab-scale result of Surfactant-Assisted Spontaneous Imbibition to field-scale is proposed, shown in Fig. 19. Modelling of surfactant interaction in oil/water/rock system is modeled through the change of capillary pressure and relative permeability curves. In each grid block, two capillary pressure curves, two water relative permeability curves, and two oil relative permeability curves are given. Where one curve of each properties represents the original unaltered condition and the one represents the surfactant-affected condition. More detail on the technique to obtain all relative permeability and capillary pressure curves will be explained in later section. Then, utilizing the amount of surfactant adsorbed in each grid block as the weighting factor, a new curve is calculated by averaging the two given curves. Surfactant adsorption is modeled by plugging in different surfactant adsorption isotherm of different surfactant system. This method allows the modelling of continuously-changing flow properties during the imbibition process as fluid saturation and surfactant concentration changes. Upscaling is done by plugging the previously used capillary

pressure and relative permeability curves, which are unique to each fluid system, to a field model. Aside from the size difference, the field-scale model also incorporates pressure drawdown in addition of the capillary action that is modeled in the laboratory-scale model, giving a representative model of what a field implementation of SASI would result to oil recovery.

This workflow incorporates a complete set of experimental procedure to measure any possible surfactant-related properties that is useful for building the numerical model. Done as the first step in the workflow, laboratory experiment part of the workflow consists of petrophysical characterization, interfacial tension, contact angle, zeta potential, surfactant adsorption isotherm, and spontaneous imbibition experiment.

After all experimental data are acquired, the next step is to build the lab-scale model which models the spontaneous imbibition experiment that was done in the previous step. Core-scale imbibition simulation is done to acquire the capillary pressure and relative permeability curves of each fluid system. An extensive measure will be included in building the core model, where core plug grid model is constructed from the CT-Scan images of the exact core plug used for each corresponding spontaneous imbibition experiment. Shale oil reservoir is widely-known as a highly heterogeneous sample, even to the core-scale dimension. By constructing the grid model by "digitalizing" the rock, it would enable the elimination of rock sample heterogeneity from the capillary pressure and relative permeability curves obtained from the lab-scale model.

Field-scale simulation is the last part of the workflow, where flow properties acquired from the lab-scale model is applied to a field-scale model. Sensitivity analysis by varying reservoir and surfactant properties can also be done to provide a more complete assessment on the impact of SASI on the field-scale.

More detail on the concept, procedure, and results of each step will be covered in the following sections.

4. LABORATORY EXPERIMENTS

As the numerical model is only as good and accurate as the data fed into it, a complete understanding of all the rock, oil, and surfactant incorporated in the model must be possessed. One way to fulfil this requirement is by gathering information as much as possible regarding all sample and chemicals used from laboratory measurement. In this part of the work, all experiments and measurements that were done are covered with each of their method as well as their result. Analysis of rock and oil sample is the first data gathering that was done, comprising of geological information regarding the reservoir where the samples were taken from, rock sample preparation, X-Ray diffraction result, oil density measurement, and oil Total Acid Number (TAN) and Total Basic Number (TBN) measurement. The next part discusses the fluid systems used in this work, which consists the description of surfactant and its concentration. Interfacial tension measurement as measured by inversed pendant drop method will be covered next, followed by contact angle measurement through captive bubble method. Zeta potential measurement will be the second last experimental data gathering with ultimately CT-Scan assisted spontaneous imbibition experiments as the final data gathering process. Due to the high number of experimental procedure and the low permeability nature of the sample, data gathering process from laboratory experiments could take at least 4 months to finish. However, this time frame is highly irrelevant when complete and accurate description of rock, oil, and surfactant will be obtained.

4.1 Rock and Oil Sample Analysis

Sidewall core plugs from an Eagle Ford shale oil well in the Dewitt county area were retrieved and used for any experiments incorporating rock sample; contact angle, zeta potential, surfactant adsorption, and spontaneous imbibition. The expensive price tag of a sidewall core retrieval job makes sidewall core plug a highly limited material, however, the use of sidewall core is essential as it is probably the closest representation of reservoir rock. Matching oil is also retrieved from the well in the surrounding area, ensuring the compatibility of rock and oil. Acquiring oil from the same reservoir is also critical as interaction of oil, water, and rock is a condition of the composition of each phase. Fig. 20 shows the core plugs and oil used in this study.

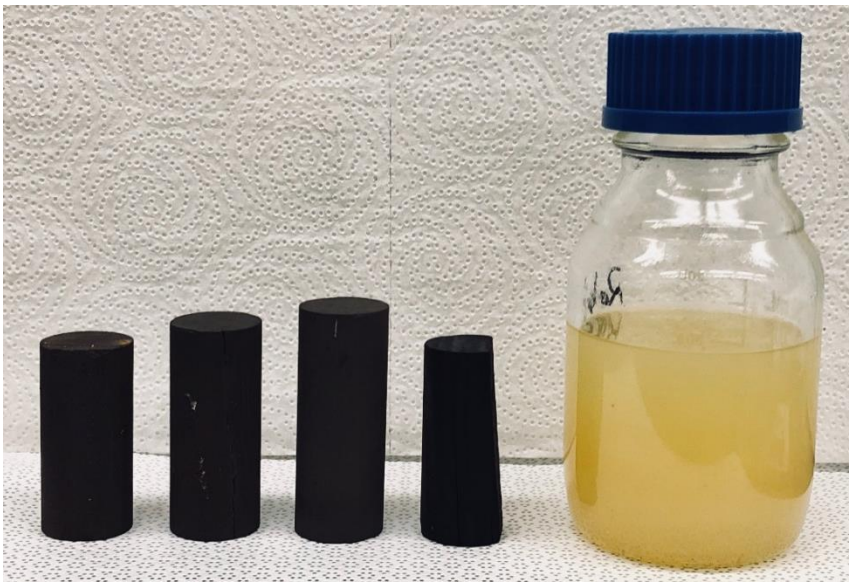

Fig. 20 - Sidewall core plugs and oil

4.1.1 Rock Description

In addition to the four sidewall core plugs shown previously, several broken plugs were also received and processed differently for another experiments. Intact cores were used for spontaneous imbibition, while broken plugs and end-trims were crushed for zeta potential and surfactant adsorption measurement with some was cut into smaller pieces for contact angle measurement. Core samples did not come from same depth but were chosen carefully to be as close as possible.

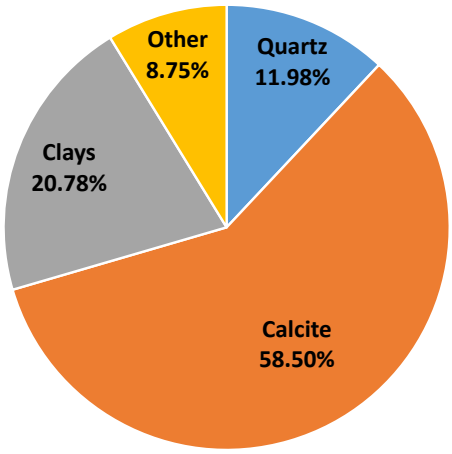

Fig. 21 - Average mineral composition of Eagle Ford rock sample from XRD

Mineral composition was measured by using XRD with the summary of the building blocks can be seen in Fig. 21. As can be seen, the rock sample falls into carbonaceous category as calcite content is almost five times the composition of quartz mineral. It can also be observed that clay content is considerably high with the clay mineral smectite dominates the composition of the clay. Some dolomite mineral was also detected but in a small percentage. Knowing the composition of

the rock sample is important as it could give an approximation on the properties of the rock system. For example, wettability, mechanical strength, and porosity, although not exactly can be determined from rock composition alone, can be approximated by comparing the trend from other studies.

Table 2 contains more detailed information of the intact sidewall core plugs for the spontaneous imbibition experiment. Porosity and permeability data were given by the company that supplied the core plugs. Porosity was measured using helium porosimeter and permeability was given as air permeability.

Table 2 - Core plug dimension, porosity, and permeability data

Rock ID	**L (cm)**	**D1 (cm)**	**D2 (cm)**	**Φ (frac.)**	**k (nd)**
Plug1	6.57	2.53	2.53	.0867	200
Plug2	5.47	2.52	2.52		
Plug3	5.51	2.54	2.3		
Plug4	6.08	2.54	2.54		

4.1.2 Aging and Cleaning Process

Although that sidewall coring process allows the retrieval of real reservoir rock for laboratory experiment, there is a high chance that the condition of the sample when it finally arrives in the lab is no longer similar to reservoir condition. Contact with atmosphere and/or different system during the retrieval job, packing, and transportation could definitely alter the properties of the rock sample. Fluid saturation and wettability state are two essential properties on this study that could have changed during the time it takes for the rock sample to get to the lab.

Fig. 22 - Core plug and rock chip aging oven

In order to restore the rock sample to reservoir condition, rock samples were "aged" for an extended period of time. Aging process to restore reservoir state has been utilized extensively in different studies with the main objective of reinstating original reservoir wettability to the sample (Alvarez and Schechter 2016; Jadhunandan and Morrow 1995; Standnes and Austad 2000a). Rock sample was submerged in its corresponding crude oil under high temperature for an extended period of time. As explained before in the literature review portion of this work, wettability of a rock surface is prone to shift to oil-wet under contact with oil molecule due to the adsorption of the hydrocarbon molecule on the surface of the rock. The oil-wetness original wettability of the reservoir rock then should be able to be restored by the aging process.

Another objective of the aging process on this study was to restore the fluid saturation of the sample before the spontaneous imbibition experiment. Due to its ultra-low permeability, the commonly used saturating procedure by means of fluid displacement is not possible to be applied

on shale rock sample. High-temperature extended-aging process was implemented for the resaturation process where instead of displacement force, oleic-phase would encroach into the pore through capillary action. However, the disadvantage of this process is the time allocation needed which in this work was 3-4 months.

Fig. 23 - Dean-Stark apparatus for core plug cleaning

Another important aspect on the rock handling side of this work is the cleaning process. As mentioned before, lab-scale model was constructed from the 3D CT-Scan image of the corresponding rock. Rock core plug cleaning utilizing Dean-Stark apparatus was done to ensure

the removal of any material other than the rock material from the exterior and the pore of the core plug. In this cleaning process, the core plugs were boiled for 2 weeks in toluene and for 1 week in toluene in the Dean-Stark apparatus shown in Fig. 23. Then the samples were taken out of the apparatus and dried in the vacuum oven for 1 week and eventually scanned in the CT-Scan to be used in the rock digitalization process.

4.1.3 Oil Density

Fig. 24 - Anton-Paar DMA 4100M for density measurement

Measurement of oil density was the first oil sample characterization done in this work. Density was measured on the Anton-Paar DMA 4100M, shown in Fig. 24, which has the capability of density data acquisition on high temperature. Density of the oil used in this study measured 0.7077 $^{g}/_{cc}$ on $180^{o}\ F$, a considerably light oil which is expected as the oil is recovered from

well in the wet gas/condensate area and the light colored of the oil sample as shown in Fig. 20. The density data is important as it is needed to calculate the interfacial tension of oil and water on the IFT measurement experiment which will be covered later.

4.1.4 Oil Total Acid Number and Total Basic Number

The next oil characterization method is the measurement of Total Acid Number (TAN) and Total Basic Number (TBN). TAN and TBN gives out the strength of acidic and basic content in the crude oil which could be correlated to the interaction of the oil with rock and surfactant. Carboxylic acid is believed as one of the strongest oil-wet wettability inducer and could be gauged by measuring the acidic content of the crude oil. The value of TAN and TBN can also be used to determine the amount of positive and negative ion in the oil, the amount of H^+ which bears positive charge is directly measured by TAN number and the amount of OH^- which bears negative charge is directly measured by the TBN number.

Measurement of TAN and TBN is based on the concept of titration, crude oil is first diluted with a solvent containing toluene, isopropanol, and water in 500:499:5 volume ratio. The dilution is done by mixing 2-3 grams of oil sample with the solvent until the volume reaches 60mL. Then the mixture is placed in a Metrohm 905 Titrando, where the titration with either 0.1M KOH solution for TAN measurement or 0.1M HCl solution for TBN measurement is done. However, the instrument must be calibrated first with the solvent to determine the blank number by running the titration with 0.1M KOH on 60mL of solvent. The result of TAN and TBN number will be in

the unit of $^{mg-KOH}/_{g-sample}$ which for TAN roughly translates to the amount of KOH needed to neutralize the acidic content of the sample.

Table 3 - TAN and TBN of crude oil (in $^{\boldsymbol{mg-KOH}}/_{\boldsymbol{g-sample}}$)

Sample	TAN	TBN
Eagle Ford	0.1989	0.6100
Wolfcamp	0.2972	0.1200
Bakken	0.5628	0.2300

Eagle Ford oil used in this study was measured having TAN of 0.1989 $^{mg-KOH}/_{g-sample}$ and TBN of 0.61 $^{mg-KOH}/_{g-sample}$. Having only one TAN and TBN data really limits the analysis of the result, Table 3 contains TAN and TBN data of crude oil sample from other shale oil play in the US. Compared to crude oil recovered from Bakken and Wolfcamp shale plays, Eagle Ford oil has the strongest basic content as well as the weakest acid content.

4.2 Fluid System Description

There are a total of four different fluid system tested in this study, with the main difference on the type and amount of surfactant in each fluid system. Table 4 contains all data regarding content and composition of each fluid system. Fluid system DW was used as base case for every result where no surfactant is added into the system. Other three fluid systems have different surfactant mixed with different concentration as listed in Table 4. All three surfactants tested are

anionic surfactant, bearing negative charge, as shown by the presence of sulfonate compound. Surf2 is different from the other two surfactants as it contain nano-sized solvent in the form of citrus terpenes. All of the surfactants used in this study are also commercially available for direct field application.

Table 4 - Fluid system composition and concentration

Fluid System	Surfactant Content	Composition	Surfactant Concentration
DW	-	-	-
Surf1	Methanol	10-30	2gpt
	Alkylbenzene sulfonate cmpd. w/ 2-propanamine	10-30	
	Slylbenzene sulfonate	5-10	
	Ethoxylated alcohols	5-10	
Surf2	Isopropyl alcohol	7-13	1gpt
	Citrus terpenes	10-30	
	Sulfonated surfactant	10-30	
Surf3	Methanol	10-30	1gpt
	Alkylbenzene sulfonate cmpd. w/ 2-propanamine	10-30	
	Slylbenzene sulfonate	5-10	
	Ethoxylated alcohols	5-10	

Concentration of surfactant in this study is defined in the unit of gallon per thousand gallon, gpt, which is a widely-used unit in the field due to its simplicity. Making a surfactant solution of 1gpt concentration is done by mixing 1 gallon of surfactant with 1000 gallon of water. In a more research-friendly concentration unit, gpt can also be converted to vol% unit where 1gpt is equal to 0.1vol%.

All four fluid systems were also color-coded in order to be able to easily distinguish different fluid used throughout the experiments. In the following section containing the experimental result of each fluid system, all data that is measured with DW will be colored blue, for Surf1 are green, for Surf2 are red, and for Surf3 are orange.

4.3 Interfacial Tension

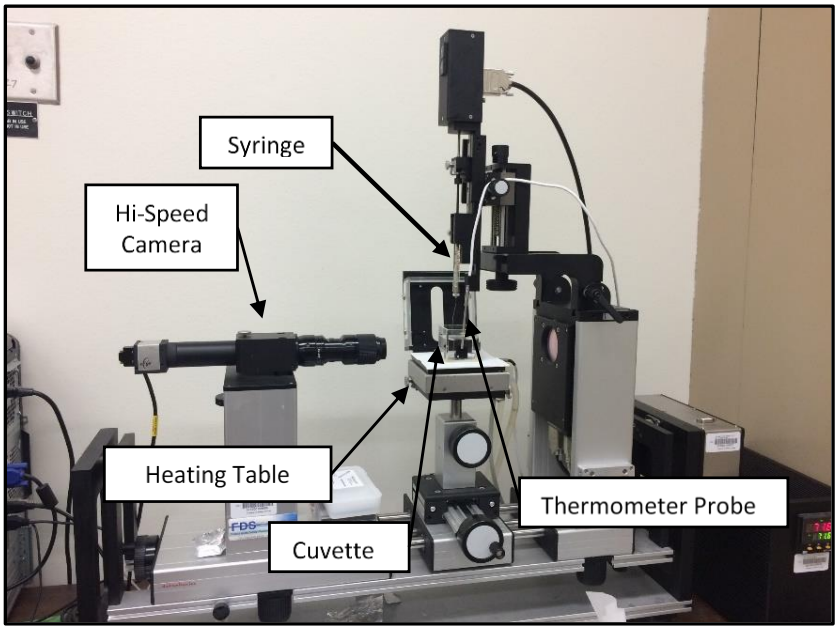

Fig. 25 - Dataphysics OCA15Pro for IFT and contact angle measurement

Measurement of IFT was done utilizing the pendant drop method on Dataphysics OCA15Pro shown in Fig. 25. IFT measurement through pendant drop method is done by dispensing either one of the fluid phase in the ambient of another fluid phase where then based on the maximum volume of oil bubble and also density of each fluids, the IFT between the two fluid phases can be calculated. The normal pendant drop method is done by dispensing fluid downwards.

Applying this configuration to this work would mean to dispense water bubble into a pool of oil. However, the turbidity of the oil sample would restrict the visibility of the water bubble dispensed inside the oil. Therefore, a modified version of pendant drop method named inversed-pendant drop method was used in measuring the IFT. A J-shaped needle was used in order to be able to dispense oleic-phase upward in the ambient phase of a clear aqueous-phase. The J-shaped needle is essential as the oil is lighter than water, which is the base component of the aqueous-phase, which means that dispensing downward is not possible. Fig. 26 shows a more detailed view on the inversed-pendant drop method configuration.

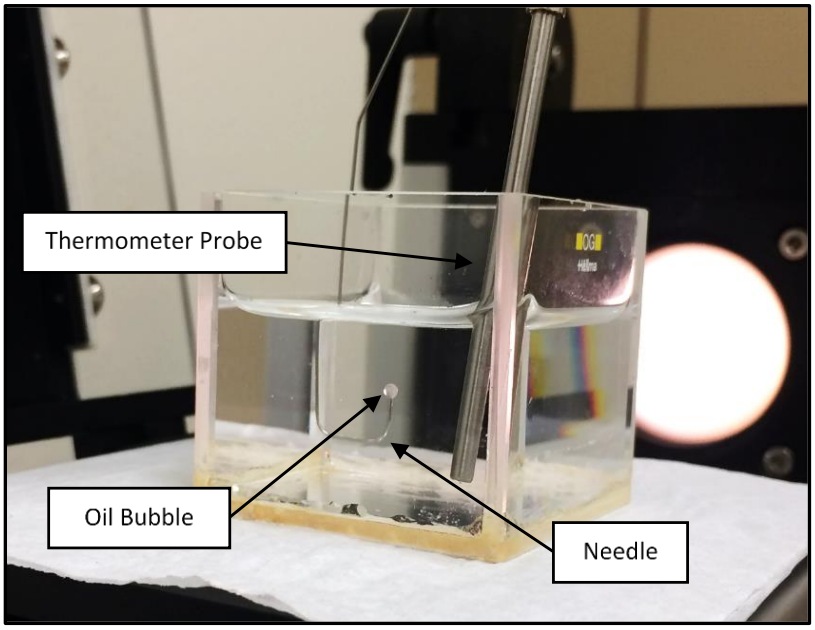

Fig. 26 - Inversed pendant drop method schematic for IFT measurement

Measurement was done on $180^o\ F$ by heating up the tested fluid system in a cuvette that was positioned on top of a heating table. Temperature probe was used to check the temperature of the system intermittently during the heating to make sure the temperature of $180^o\ F$ is reached.

Oil sample was placed inside a motorized syringe with the J-shaped needle attached. After reaching the desired temperature, oil bubble was slowly dispensed inside the aqueous-phase until the bubble detached from the tip of the needle. With the resolution of 0.001μL, a very fine and smooth increment of oil bubble size is possible to be done with the motorized syringe, eliminating the possibility of error due to fluid inertia during dispensing. A high-speed camera system captured the image of the bubble and a built-in software calculates the IFT based on the density data given.

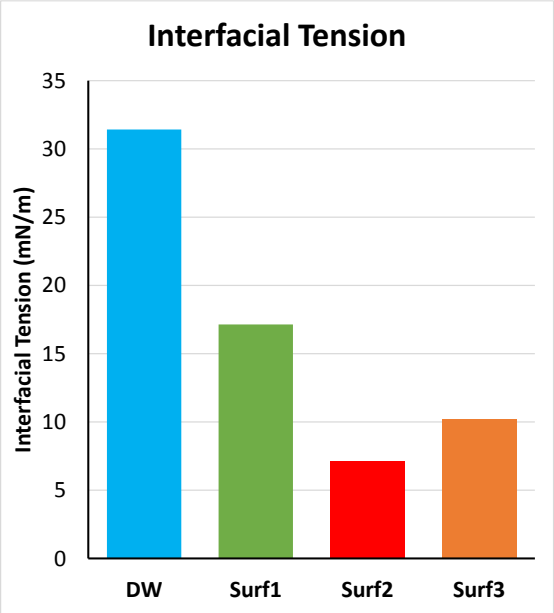

Fig. 27 - Interfacial tension of the four tested fluid system

Comparison of interfacial tension between oil and all four fluid systems is given in Fig. 27. Original IFT of Eagle Ford oil was measured 31.4 mN/m, relatively high compared to base case of oil from another shale oil play 31.4 mN/m where IFT measurement done using crude oil from Wolfcamp and Canyon Lime gave IFT value of 21.2 mN/m and 25.9 mN/m respectively. Density difference between Eagle Ford, Wolfcamp, and Canyon Lime could be the explanation

behind this finding. Eagle Ford oil is significantly lighter compared to the other two oil, making the density difference between the oleic-phase and aqueous-phase more pronounce, increasing the interfacial tension between the two phases. Another explanation is the high level of xylene found in the Eagle Ford oil, often used as non-polar solvent, xylene in oil increases the interfacial tension of oil and water.

All surfactants were able to reduce the interfacial tension of oil and water but with different extent on each surfactant. Surf2 reduced IFT the most to 7.17 mN/m followed by Surf3 with 10.25 mN/m and Surf1 with 17.14 mN/m. Surf2 behaved in an unorthodox way as its higher surfactant concentration content reduced IFT the least compared to the other two surfactants. This unorthodox behavior could be beneficial as higher IFT correlates to larger capillary driving force capacity, in the other hand, high IFT value could also lead to blocking as represented by lower relative permeability curve compared to those oil and water system with lower IFT.

4.4 Contact Angle

Measurement of contact angle was done on the same Dataphysics OCA 15Pro device previously used to measure the IFT with different configuration and method. Procedure for measuring the contact angle was based on captive bubble method where oil bubble is dispensed and put in contact against the bottom-facing surface of a rock sample with the whole process done in the aqueous-phase. Fig. 28 shows the configuration of the device for contact angle measurement. The camera system integrated to the device captured the image of oil bubble interacting on the rock surface and the built-in software calculated the angle formed between the

bubble and the surface. Contact angle was calculated by the software as angle of the surface and bubble through the oleic-phase. However, as shown by Fig. 12, the convention used for contact angle data is as the angle measured through the aqueous-phase. Therefore, a conversion must be done to the contact angle data given by the software as shown by Eq. 7 where CA_m is the measured contact angle calculated by the software.

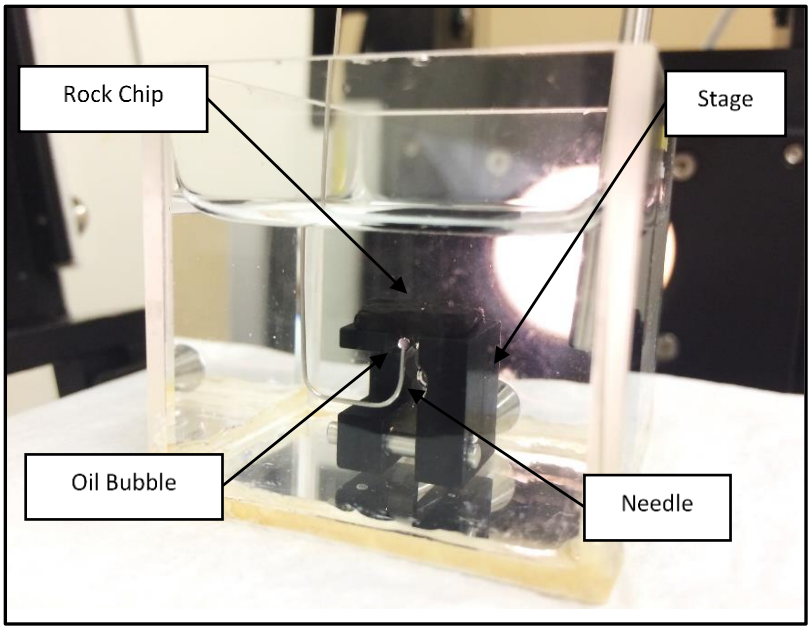

Fig. 28 - Captive bubble method schematic for contact angle measurement

Rock chip for the contact angle measurement was prepared by cutting rock chips in the dimension of approximately 1cm x 1cm from broken core plugs or end-trims retrieved from the well. Rock chips then were aged in the corresponding oil in the same oven used for the core plug aging process for two weeks to restore the original wettability of the sample. Several rock chips were prepared for the contact angle measurement where reported contact angle data is the average of all measurement done on different rock chips.

$$CA = 180 - CA_m \text{.....Eq. 7}$$

Each fluid system was poured into the cuvette which then was heated on the heating table until the desired temperature. After reaching the temperature, aged rock chip was cleaned from excess oil and positioned on the stage. Oil bubble was formed at the tip of the J-shaped needle and carefully put in contact with the bottom-facing surface of the chip. To ensure the repeatability and the consistency of the contact angle measurement, each contact angle measurement was done by dispensing 0.15µL of oil bubble.

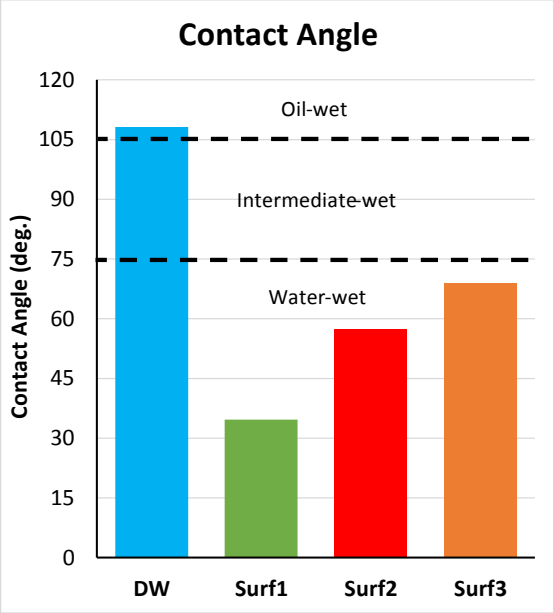

Fig. 29 - Contact angle of the four tested fluid systems

The original wettability of Eagle Ford system was found to be in the oil-wet region with contact angle of 108.2°. Every fluid systems containing surfactant were able to alter the wettability of the rock surface from the initially oil-wet condition to water-wet region as shown by Fig. 29. Contact angle of under Surf1 was 34.7°, for Surf2 it was 57.3°, and lastly for Surf3 it was 69.1°.

The ability of altering wettability to water-wet region is highly essential as it would modify the capillary pressure force to be in our favor. As shown previously, oil-wet wettability gives out negative capillary pressure, reducing the imbibition performance and hindering the flow of oil by trapping the oil in the pore space. While water-wet wettability would make a positive capillary pressure, enhancing the imbibition process and also the production of oil out of the pore space.

For presentation purpose, a compilation of different oil bubble from different fluid systems are shown in Fig. 30. The wettability alteration performance of surfactant can be easily observed as oil bubble was moving towards a more spherical shape for test done using surfactant as compared to test done under water without any surfactant added. Surf1 which has the most water-wet condition shown in the figure having an almost perfect spherical oil bubble shape, showing that the rock surface strongly repelled the oil bubble.

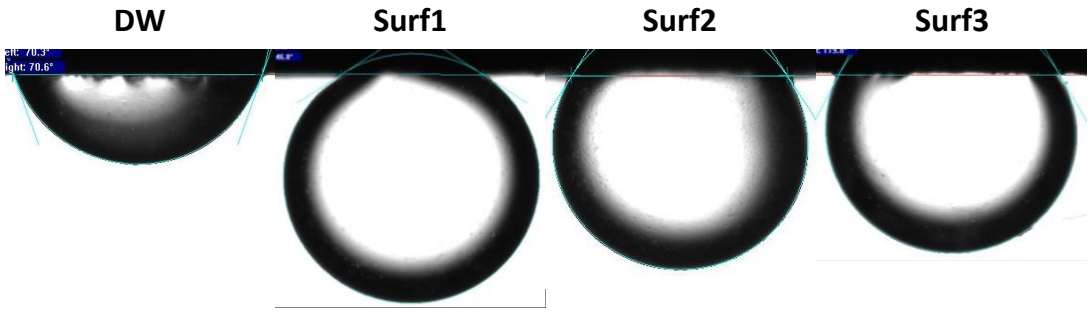

Fig. 30 - Comparison of oil bubble interaction with rock surface of all tested fluid systems

Surf1 was observed to show the strongest wettability alteration performance followed by Surf2 then Surf3. The combination of relatively higher IFT as compared to other fluid systems and premium wettability alteration performance would ideally make Surf1 as the best candidate for enhancing SASI in the Eagle Ford oil and rock system. However, when applied to the field, no

accurate prediction could be made at this point of the work since production of hydrocarbon in the field also includes viscous force by pressure drawdown in addition to the capillary action that grounds the SASI mechanism. Having high IFT could mean lower relative permeability properties that could hinder the viscous force-based flow process.

4.5 Zeta Potential

Fig. 31 - NanoBrook ZetaPALS for zeta potential measurement

Measurement of zeta potential gives out another gauge on the wettability of the rock under different fluid system. High zeta potential would mean a stronger water layer forming around the rock surface, implicating a water-wet surface. Zeta potential in this work was measured utilizing the NanoBrook ZetaPALS device shown in Fig. 31. Electrophoretic mobility of rock particle in the aqueous-phase was measured by the machine which then converted to zeta potential since a

direct measurement of zeta potential is not possible to be done. Mixture of powdered rock and aqueous-phase was poured into a cuvette which also contains two electrodes. Voltage difference then was applied to the two electrode which would cause the rock particle to move from one electrode to the other. The speed of the particle is the important variable that is needed to calculate the zeta potential. Phase Analysis Light Scattering (PALS) was the method used to measure the speed of the rock particle which works by measuring the time needed for light particle that is scattered by the moving rock particle to reach light sensor around the cuvette as explained in the manual supplied with the equipment.

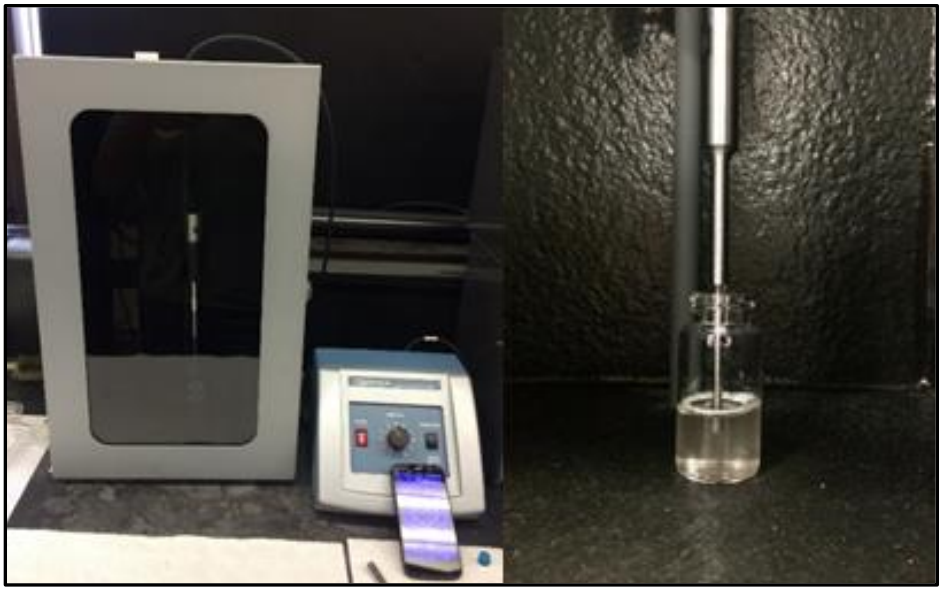

Fig. 32 - Sonicator for zeta potential measurement sample preparation

Powdered rock sample was prepared for the zeta potential measurement by pulverizing rock sample from either broken core plugs or end-trims. Rock particle of size smaller than 45 micron was needed, sieve number 350 was used to ensure the size specification. Then rock-surfactant suspension was prepared by mixing a small amount of rock powder with each of the

fluid system using the sonicator, shown in Fig. 32, for approximately one minute. Since zeta potential measurement is highly sensitive to other particulate, all of the aqueous-phase were filtered three times first before mixed with the rock. Built-in software was used to run the zeta potential measurement. One measurement consists of five replications with 30 cycle of measurement on each replication with the zeta potential result is the average value from all five replications.

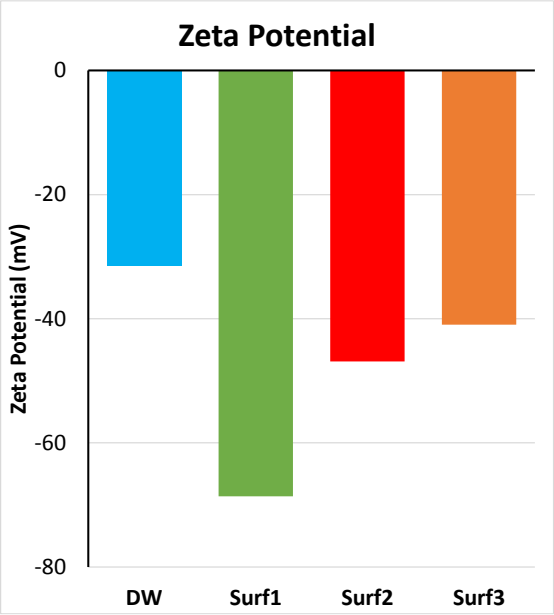

Fig. 33 - Zeta potential for the four tested fluid systems

Fig. 33 contains all the zeta potential measurement data from all four fluid systems. Zeta potential of rock particle in fluid system DW had the lowest value of -31.5 mV followed by Surf3 with -40.95 mV, Surf2 with -46.88 mV, and Surf1 with -68.63 mV. The sign of the zeta potential value reflects the surface charge of the rock surface and the molecule contained in the fluid system. Zeta potential measurement was found to be in-line with wettability given from contact angle

measurement as strongest water-wet condition by Surf1 was observed to have the strongest zeta potential as well and the least water-wet condition of fluid system DW was observed to have the weakest zeta potential. In addition, based on the zeta potential result, it can also be concluded that all surfactants used in this study were anionic surfactants.

4.6 Surfactant Adsorption Isotherm

Fig. 34 - Hitachi U-4100 UV-Vis Spectrophotomter for surfactant adsorption measurement

The measurement of surfactant adsorption isotherm is important for modelling the spontaneous imbibition mechanism that incorporates surfactant molecule. As explained in the previous section, the amount of surfactant adsorbed will be used as the weighting factor for the extent of alteration on the flow properties as caused by surfactant. Surfactant adsorption in this work was measured by utilizing a spectrophotometer, a Hitachi U-4100 UV-Vis

Spectrophotometer, shown in Fig. 34, to be exact. This device has the capability of producing light with wavelength ranging from 190nm to 3000nm allowing a complete wavelength scan for the construction of the calibration curve. Light adsorption on sample solution is compared with the adsorption on reference solution as light coming from a single light source is divided into two, shined through the two solutions to a light sensor as shown in Fig. 39 More detailed information regarding the concept of the spectrometry-based adsorption measurement incorporated in this study can be found in the study done by Alvarez et al. (2017) (AlvarezSaputra et al. 2017a, 2017b)

Procedure for measuring surfactant adsorption was started by building the calibration curve correlating the magnitude of light adsorbed on a specific wavelength to the surfactant concentration in the sample. In order to build the curve, the characteristic wavelength of each surfactant system must be determined first. For each surfactant used in each fluid system, solutions with different concentration, 0.5, 1.0, 1.5, 2.0, 2.5, 3.0, and 4.0 gpt, were made. Then solutions were filtered and wavelength scan from 190-300nm was done on each of them. By analyzing the generated data of different light adsorbance value on different wavelength with different surfactant concentration, the wavelength characteristic of each surfactant was determined by analyzing peaks on the data. Taking the adsorbance of light on the wavelength that was chosen as the wavelength characteristic of the surfactant and the concentration that caused the amount of adsorbance, the calibration curve then was constructed.

After the calibration curve had been constructed, the adsorption measurement then took place. Rock sample preparation for adsorption measurement was done by first, cleaning the rock by soaking chips in toluene for 3 days then methanol for 2 days then vacuum-dried for 2 days. After the cleaning process, rock was pulverized and filtered using the mesh number 50, removing any particulate larger than 300 micron in size.

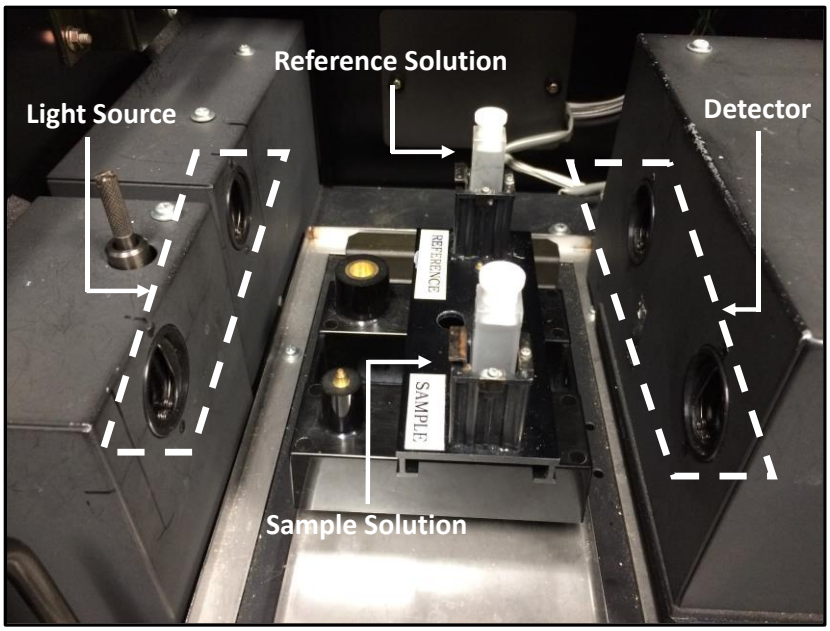

Fig. 35 - Configuration for light adsorbance measurement

Surfactant adsorption measurement curve consists of the amount of surfactant adsorbed on the rock on different surfactant concentration. Therefore solutions with different concentrations of surfactant were prepared for all of the surfactant used in the study. Then the surfactant solutions were filtered to remove any unwanted particle and then finally mixed with the powdered rock on 1:20 weight ratio. Rock-surfactant solution contact was done for 24 hours under room temperature before finally filtered to stop the reaction for the adsorption measurement.

Finally, under the same set-up as shown in Fig. 35, light adsorbance of each corresponding light wavelength characteristic of each fluid system tested on each of the solutions prepared was measured and concentration of surfactant left in the fluid system after contact with rock is calculated using the calibration curve. The concentration then is converted to the adsorption unit in weight unit through Eq. 8. In total, surfactant adsorption measurement required light adsorbance measurement of 55 samples and all the result can be seen on Fig. 36 - Fig. 42.

$$\boldsymbol{\theta_A} = \frac{\left(\boldsymbol{\phi^i_{surf}} - \boldsymbol{\phi^f_{surf}}\right) * \boldsymbol{V_{surf}} * \boldsymbol{\rho_{surf}} * \mathbf{10^5}}{\boldsymbol{w_{rock}}} \ldots\ldots \text{Eq. 8}$$

Wavelength scan of Surf1, Surf2, and Surf3 can be seen in Fig. 36 - Fig. 38. By analyzing the data on each wavelength scan, light wavelength characteristic of each surfactant was determined. Wavelength of 223nm for Surf1, 227nm for Surf2, and 206nm for Surf3 were assigned as the characteristic light wavelength of each surfactant. Taking the value of light adsorbance on each specified wavelength, calibration curve was constructed by plotting the surfactant concentration on the x-axis and adsorbance of each corresponding concentration on the y-axis. Calibration curves for Surf1, Surf2, and Surf3 are shown in Fig. 39 - Fig. 41. Deflection points are observed on all calibration curves, giving two linear correlations between adsorbance and surfactant concentration. The presence of the deflection point could be explained by the surfactant molecule reaching the CMC, forming micelles that no longer follow the Beer-Lambert law that the spectrophotometer-based adsorption measurement based on. However, this phenomenon should not be any problem as the deflection occurred above the concentration of 2gpt. Whereas in this study all measurements were done under 2gpt. From the calibration curves, linear equation correlating the data of adsorbance and the concentration below the deflection point was taken to calculate the

Fig. 42 shows the surfactant adsorption of all three surfactants used in this study. Analyzing the adsorption measurement result, an agreement can be seen between the contact angle, zeta potential, and adsorption isotherm. Where water-wet state as observed from the contact angle measurement is also confirmed by the strong zeta potential as well as high surfactant adsorption value as shown by Surf1. Less water-wetness from Surf2 and Surf3 were also reflected by lower adsorption isotherm of surfactant as compared to Surf1.

As mentioned before, the adsorption isotherm will be used in the modelling part of this work to determine the extent of flow properties alteration as a function of surfactant concentration.

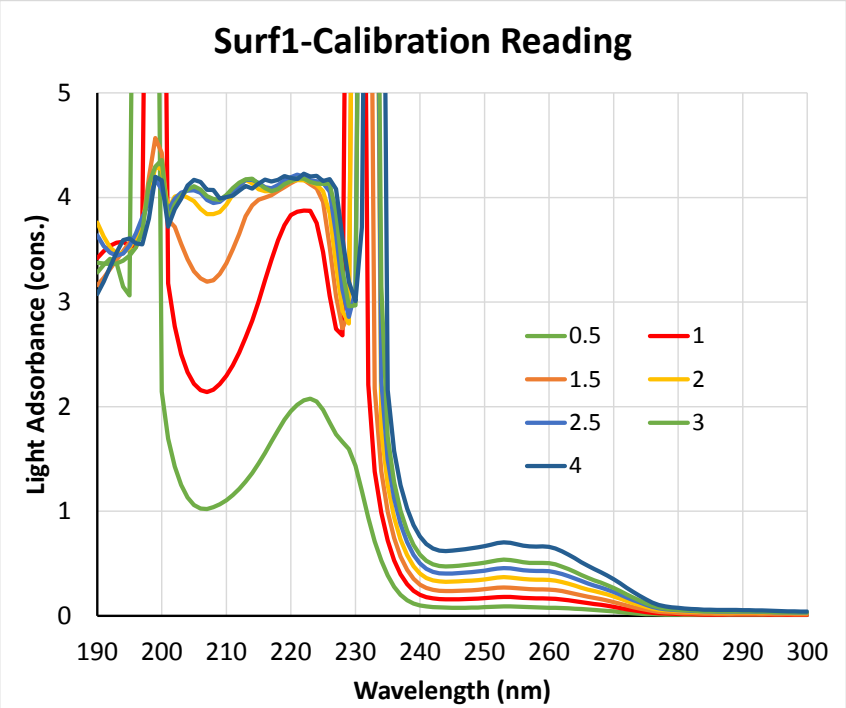

Fig. 36 - UV-Vis spectrometry wavelength scan for Surf1

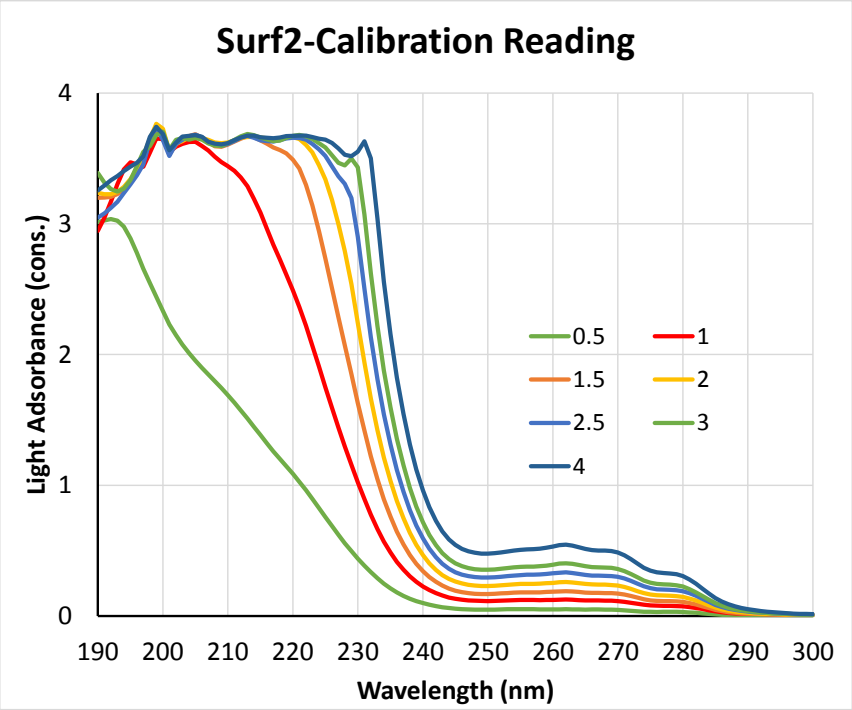

Fig. 37 - UV-Vis spectrometry wavelength scan for Surf2

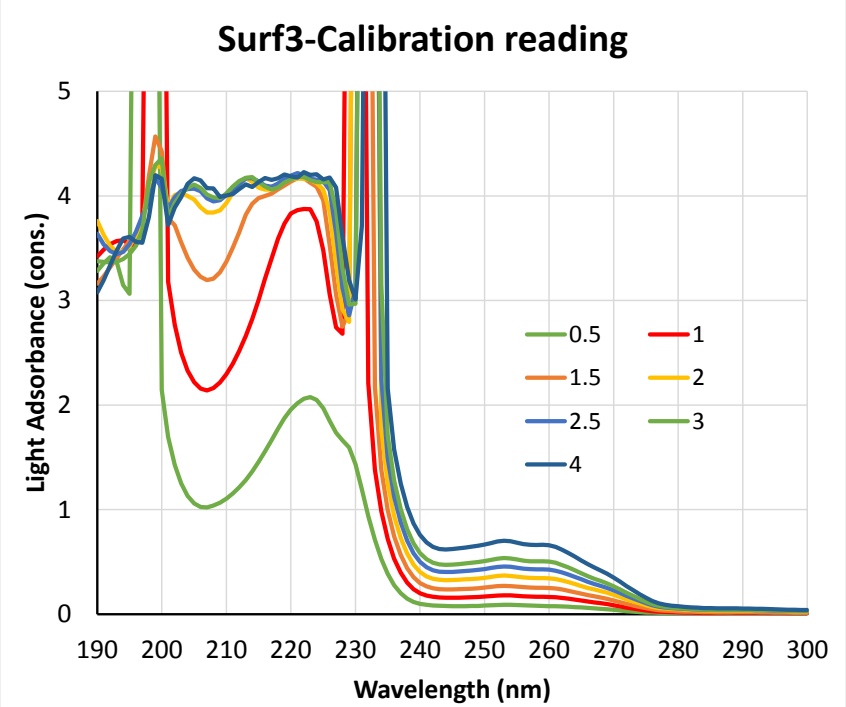

Fig. 38 - UV-Vis spectrometry wavelength scan for Surf3

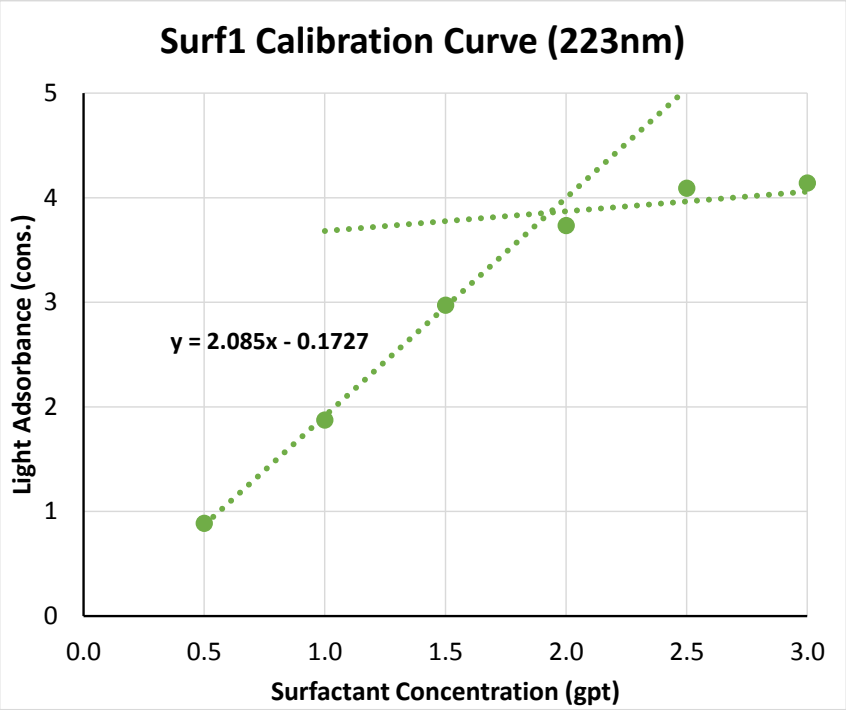

Fig. 39 - Calibration curve of light adsorbance (223nm) to Surf1 concentration

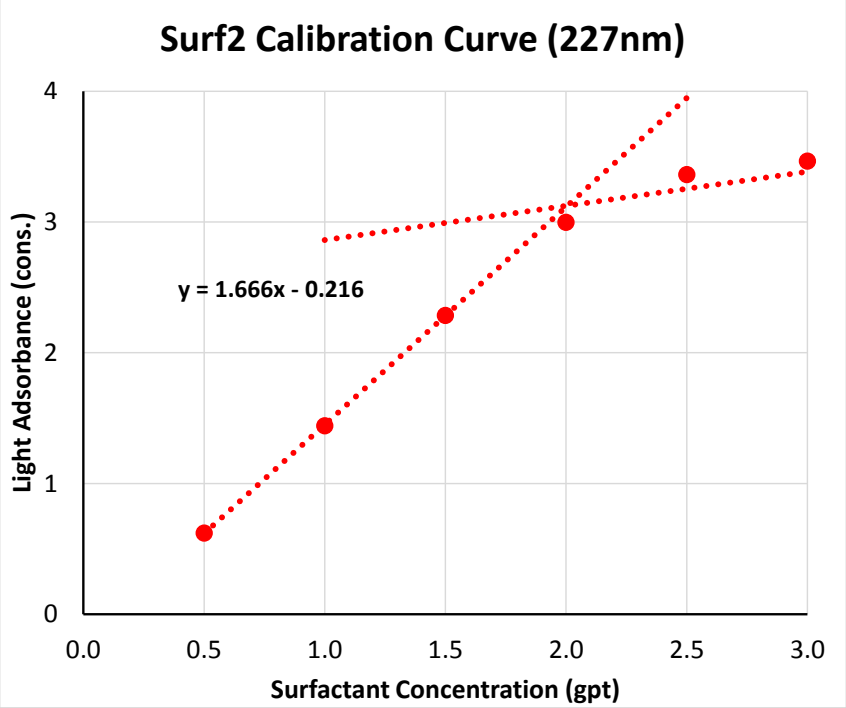

Fig. 40 - Calibration curve of light adsorbance (227nm) to Surf2 concentration

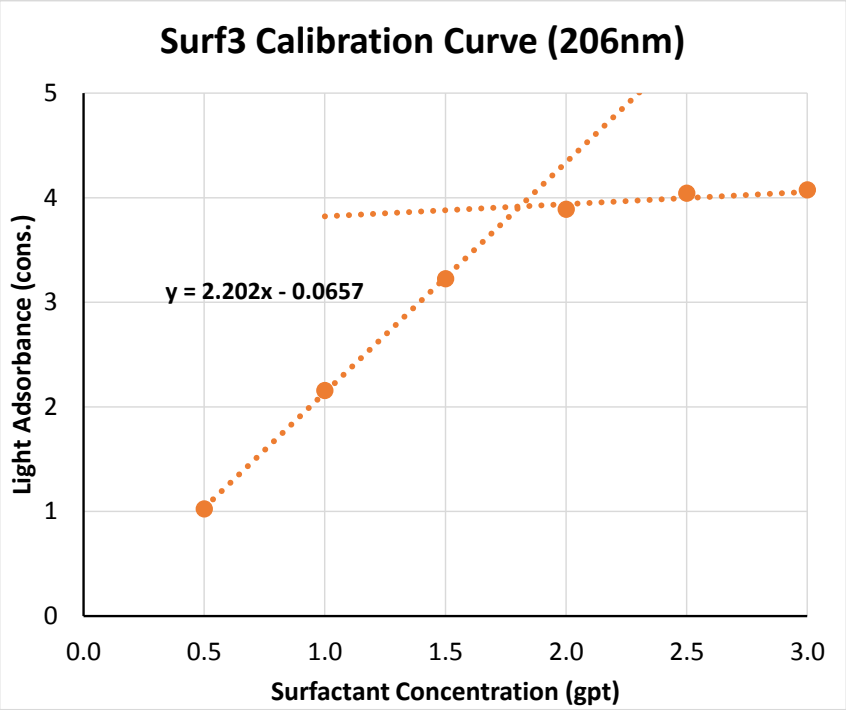

Fig. 41 - Calibration curve of light adsorbance (206nm) to Surf3 concentration

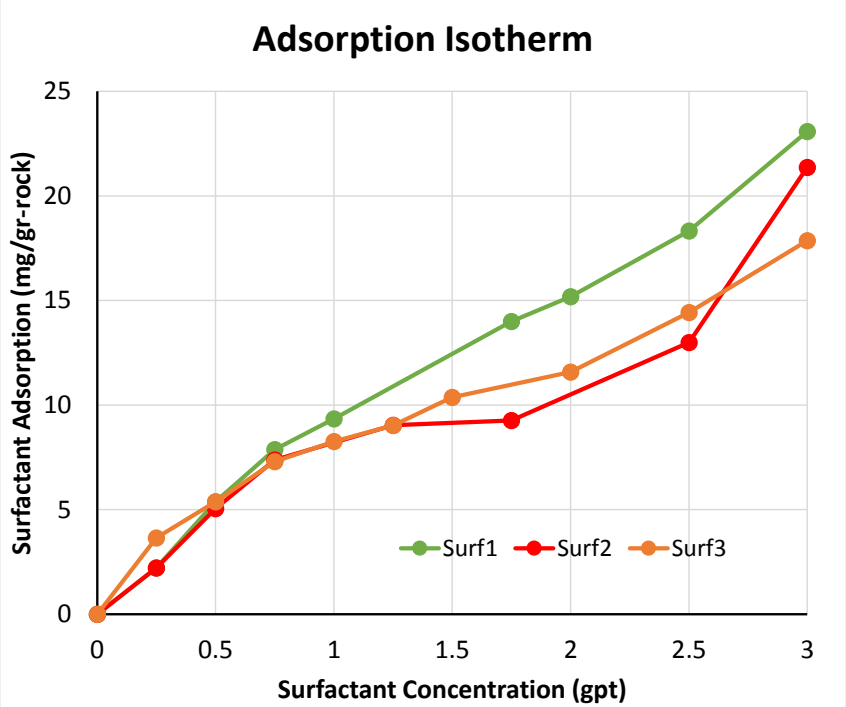

Fig. 42 - Adsorption isotherm of Surf1, Surf2, and Surf3 on Eagle Ford rock sample

4.7 CT-Assisted Spontaneous Imbibition

Fig. 43 - Amott cell configuration for spontaneous imbibition study

Spontaneous imbibition was the final experimental data gathering for the workflow proposed. It is the ultimate test for assessing the surfactant efficacy in improving oil production from surfactant-assisted spontaneous imbibition process as it gave a direct information on the volume of oil produced from the imbibition process. The concept of this experiment is fairly straight-forward, rock sample in the form of core plug was submerged in the fluid system that was going to be tested and the amount of oil produced was recorded with time. No pressure difference should be applied to the set-up as the objective of this experiment is to gauge the capillary-driven performance. However, in opposite to the uncomplicated concept, the experiment was

considerably tedious as constant observation must be done throughout the whole experiment time of 10 days.

In addition to the recording of oil production data through time, CT-Scan image of the rock sample was also recorded in timely manner. Having the ability to incorporate CT-Scan technology into the spontaneous imbibition experiment is a rare luxurious opportunity as it allows the inspection of fluid saturation distribution inside the core plug throughout the imbibition experiment in a non-destructive manner. CT-Scan machine works by emitting X-ray through the scanned sample and also capturing the adsorbed X-ray from the opposite end in a circular motion through the whole length of the sample. A complex algorithm then convert the data obtained from the X-ray emitter and detector to a 3D digital map of a variable named CT-number or Hounsfield Unit (HU) of the scanned sample. Since CT-number is directly related to density as shown by Eq. 9, then it can be safely concluded that high CT-number could be directly interpreted as high density and vice versa. Therefore, CT-Scan image can be used to show the density distribution inside the core plug sample and by having scan images on different time of the experiment would allow the density distribution inside the core sample through time. Aqueous-phase has a higher density than the oleic-phase, therefore a rise in density seen on the CT images can be concluded as a rise in water saturation in that specific part while a decrease in density on the CT images could be concluded as a rise in oil saturation.

$$\mathbf{HU = CT\# = 1000} * \frac{\boldsymbol{\mu - \mu_w}}{\boldsymbol{\mu_w - \mu_a}} \quad \text{.....Eq. 9}$$

Aged core plugs were used as the rock sample in this experiment. The plug was set horizontally on top of a core stand that was positioned at the bottom of a modified Amott cell

shown in Fig. 43. Solution of each fluid system tested then was mixed and poured into the cell, however with an addition of 4 wt% KI which was added as a density dopant to increase the contrast on the CT images by increasing the density difference between the aqueous- and oleic-phase. Then the whole setup was placed in an oven to keep the temperature of the system on $180^{o}\ F$.

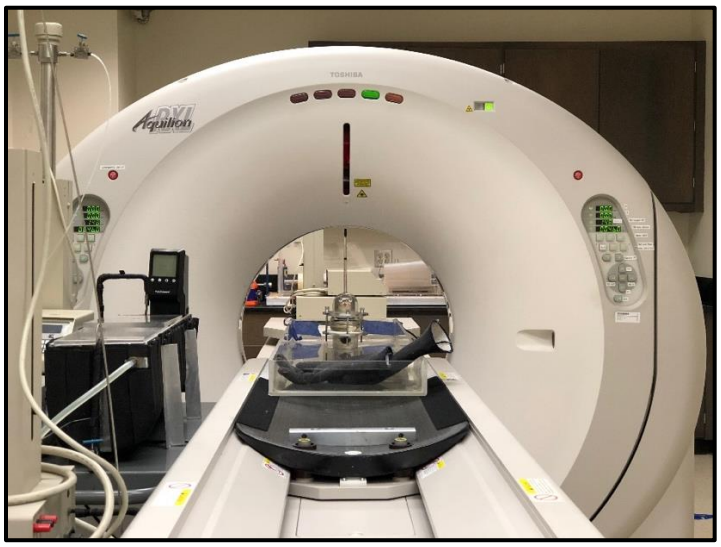

Fig. 44 - Toshiba Aquilion TSX-101A CT-Scan unit

A total of four cells were used as there were four different fluid systems that were incorporated in this study. The experiment was run for 10 days with constant observation on the amount of oil production as it accumulated on the graduated part on the top of the cell. CT-scan was done utilizing the Toshiba Aquilion TSX-101A, shown in Fig. 44, periodically by moving the Amott cell setup back and forth from the oven to the CT machine and back to the oven.

As the ultimate experiment of this work, spontaneous imbibition experiment gave tremendous amount of data to be analyzed. The first and obvious data is the spontaneous imbibition production curve of the four fluid system tested in this study. Production curve was calculated in

the form of recovery factor to accommodate the different size of the core plugs used in the experiment. Recovery factor was calculated by dividing the volume of oil recovered with the initial oil in place of each core plug. Initial oil in place was calculated using the rock dimension data that was listed in Table 2 to calculate the bulk volume of the rock which then multiplied by the porosity to calculate the pore volume and finally an assumption of initial water saturation of 15% was taken to calculate the oil in place of each core plugs.

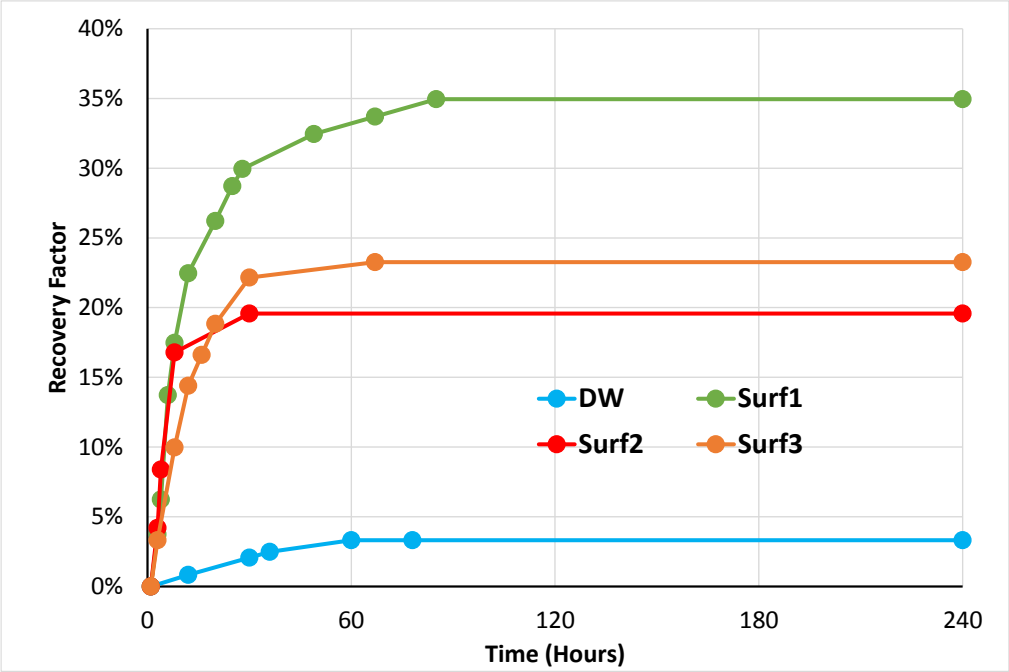

Fig. 45 - Oil recovery from spontaneous imbibition of all four fluid systems tested

Recovery data through spontaneous imbibition of all four fluid system tested is shown on Fig. 45. It was found that oil production through imbibition was still present on the base case fluid system where no surfactant was added to the aqueous-phase. Although that as shown by previous experimental result that the wettability of the system was observed to be in the oil-wet region, production was still possible as the system was not a completely oil-wet system as the contact

angle measurement had shown. Addition of surfactant was proven to be highly advantageous to the oil production in two ways. First, as the most obvious to be seen from the production curve, the recovery factor jumped from 3% on the base case to up to 35% on Surf1, 23% on Surf3, and 19% on Surf2. Second, the production rate was also increased as the time needed to reach half of each corresponding ultimate recovery for Surf1, Surf2, and Surf3 was faster compared to the base case. Therefore, it can be concluded that all surfactant used in this study were able to improve both the rate and the ultimate recovery of oil from the spontaneous imbibition process.

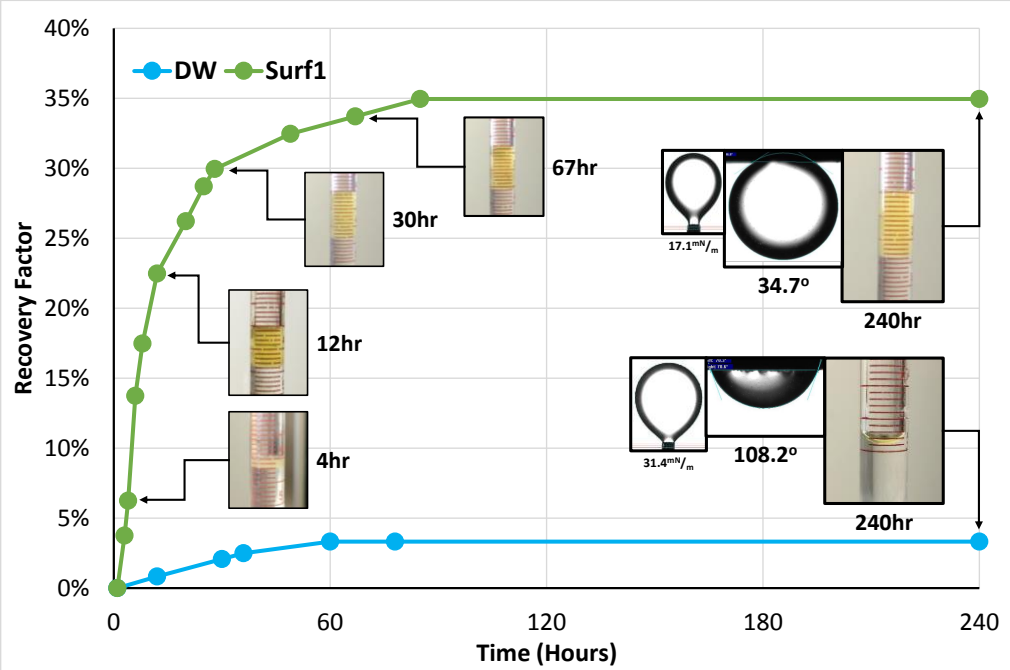

Fig. 46 - Oil recovery, IFT, and contact angle comparison of Surf1 and DW

Comparing the imbibition result of each surfactant, the best recovery improvement was produced by Surf1, followed by Surf3 then Surf2. Compiling the contact angle and IFT data measured on Surf1 as shown in Fig. 46, the extremely effective performance of the surfactant on enhancing the oil production from capillary-driven imbibition was understandable. Magnitude of

capillary force is a function of interfacial tension of oil and water with the orientation of the force is determined by the wettability of the system. Surf1 was observed to have the largest interfacial tension as compared to the other surfactant tested and combined with the strongest water-wetness as shown by the contact angle measurement, Surf1 would have the largest capillary force the oil out of the pore.

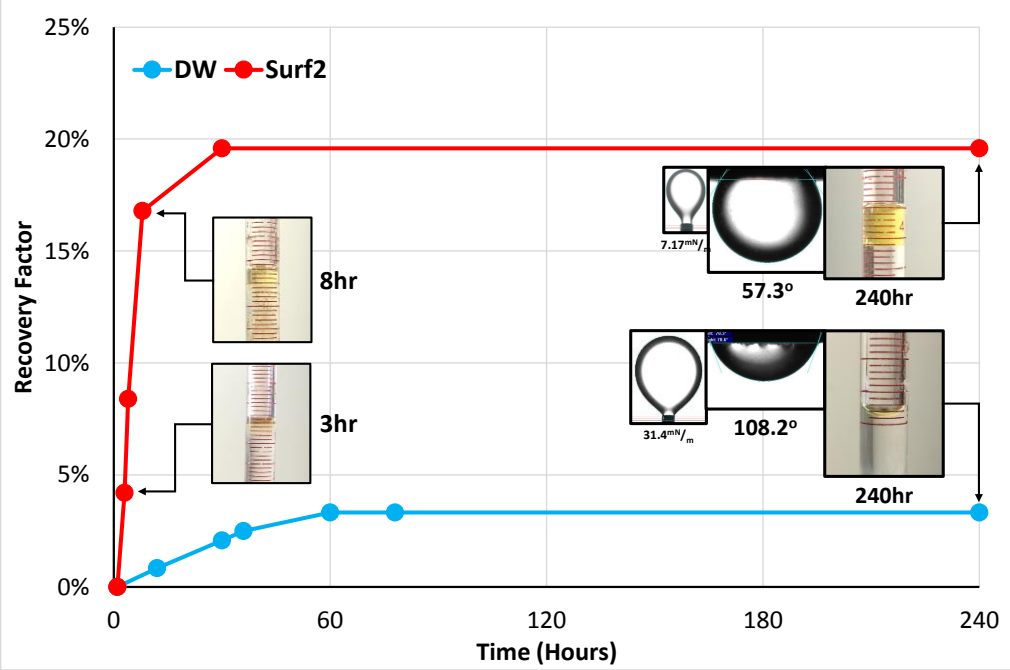

Fig. 47 - Oil recovery, IFT, and contact angle comparison of Surf2 and DW

The same compilation of imbibition, contact angle, and IFT data of Surf2 and Surf3 are shown in Fig. 47 and Fig. 48. If we were going to employ the same concept of analysis as before, Surf2 should have shown a better performance than Surf3 as the capillary force for Surf2 as defined by the IFT and contact angle data was found to be greater than Surf3's. Different result was observed on the imbibition recovery curve, where Surf3 produced more oil compared to Surf2. This discrepancy perhaps can be explained by the heterogeneity of the core plug sample that was

used. A higher content of high permeability region in the form of bedding planes or microfractures were probably present in the core plug used for Surf3, which would cause more oil to be produced even though that the calculated capillary force for Surf3 was lower.

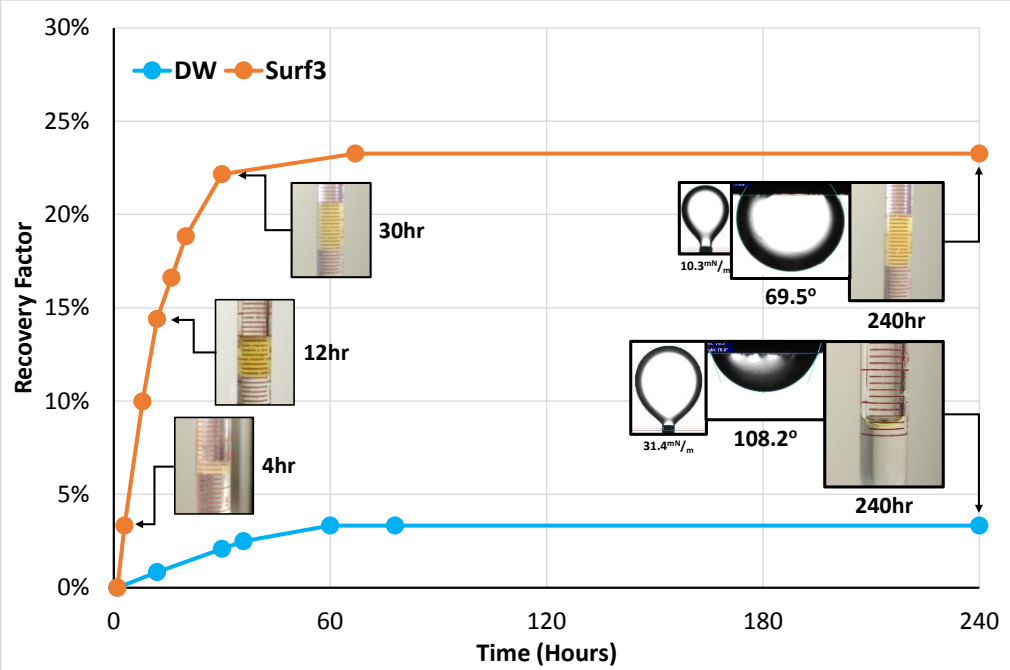

Fig. 48 - Oil recovery, IFT, and contact angle comparison of Surf3 and DW

Images gathered from the CT-Scan were all processed using ImageJ software for compiling and optimizing the image quality purpose. A color table was assigned to each image to provide a better contrast of the different density distributed through the core sample. Brighter color represents higher density while darker color represents lower density as shown by the color legend provided in each figure containing CT images. Noise and area were removed by applying threshold to the images. Different core plug sample used on each of the imbibition experiment were observed to have different thresholding configuration, which could be caused by heterogeneity of rock

density on each sample. However, to ensure the validity of the images, the same constant image threshold parameter was applied for all the scans done in different time of each core plug.

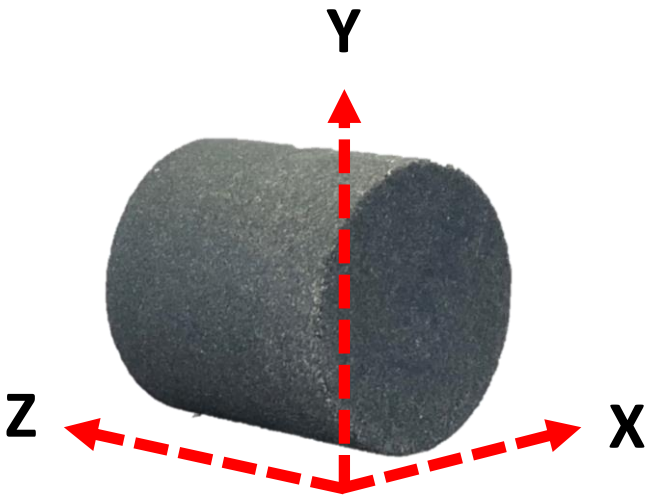

Fig. 49 - X-, Y-, and Z-axis core plug orientation

Configuration of x-, y-, and z- orientation that was used to align the scan result is shown in Fig. 49. As mentioned before, CT-Scan device scanned the sample through the whole length of the rock sample or along the z-axis on the given orientation shown in Fig. 49. Comparing the fluid distribution inside the core plugs of each tested fluid system through the spontaneous imbibition experiment process can be done by observing the XY-plane slices as shown in Fig. 50. The general trend observed on all four cases was that the overall color of the images changed into darker color as time of imbibition experiment progressed, an indication of aqueous-phase as the heavier fluid encroached into the rock sample, replacing the lighter oleic-phase. It can also be seen that on all cases, the bottom-part of the plugs turned into brighter color throughout the time which could be explained as an indication of gravity-driven imbibition. However, the change is insignificant compared to the general color change on the whole area of the core plug. Another interesting trend

that was noticed was the present of heterogeneity in the form of what seems to be a high permeability bedding plane as in the rock sample. Major color change on the bedding plane area was also observed, it was proposed that bedding plane functioned as the passage for exchange of oil and water during the imbibition.

Slice of images on the XY-plane were not the only data recovered from the CT-Scan process. As explained before, a complete 3D map of the scanned core plug was given by the CT machine, meaning that 3D figure of each scan would be available for analysis as well. Since displaying 3D images on a printed document is pointless, slices from two other planes in addition to the XY-plane are given instead.

Slices from three different planes of core plugs tested with fluid system DW are presented in Fig. 51. While no meaningful additional observation was obtained from analyzing the XZ slice, different comment could be given to the YZ slices. YZ slices gave the overview of what was happening on the fluid distribution inside the core plug on the vertical orientation. Significant change of color was observed on this vertical section through the time of the experiment. As capillary force was determined to be insignificant on the base case fluid system, gravitational could be the major force on oil production. Since gravity-driven imbibition is highly dependent on the gravity and gravity works on the vertical plane, activities on the vertical plane as observed on core plugs submerged in the base case fluid system could mean that gravity took control of the imbibition.

The same slices data for the rest of the fluid systems are given in Fig. 52 - Fig. 54. In contrast to the fluid distribution observed on the DW fluid system, major color change was also observed on the XZ slice or the horizontal slices for core plugs submerged in surfactant solution. While gravity-driven imbibition is concentrated on the vertical movement of the fluid system,

capillary-driven imbibition happens regardless of the orientation as it is driven by the physical and chemical interaction of oil/water/rock system. Therefore, fluid distribution variation during the time of the imbibition experiment on the horizontal plane was expected to occur as addition of surfactant into the system enabled the capillary force to significantly drive the spontaneous imbibition.

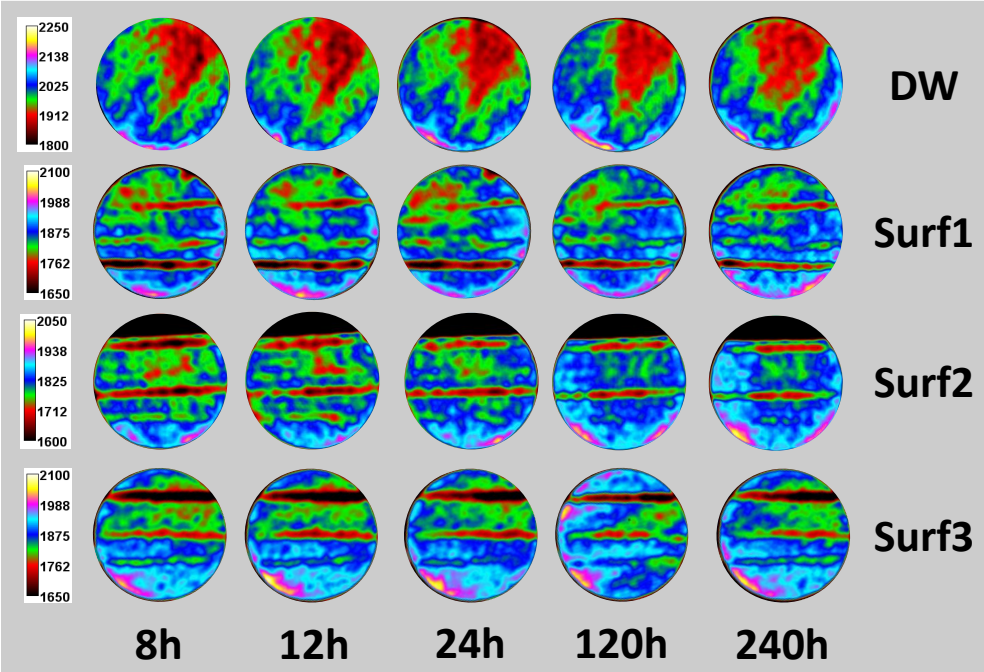

Fig. 50 - XY-slice through time of core plug under spontaneous imbibition in different fluid systems

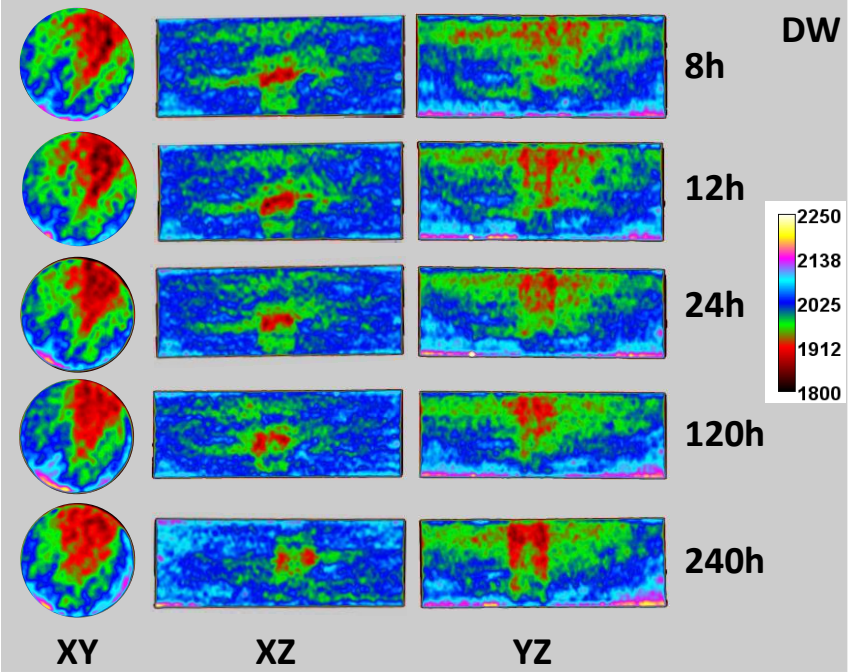

Fig. 51 - XY, XZ, and YZ slice of core plug through time under spontaneous imbibition in fluid system DW

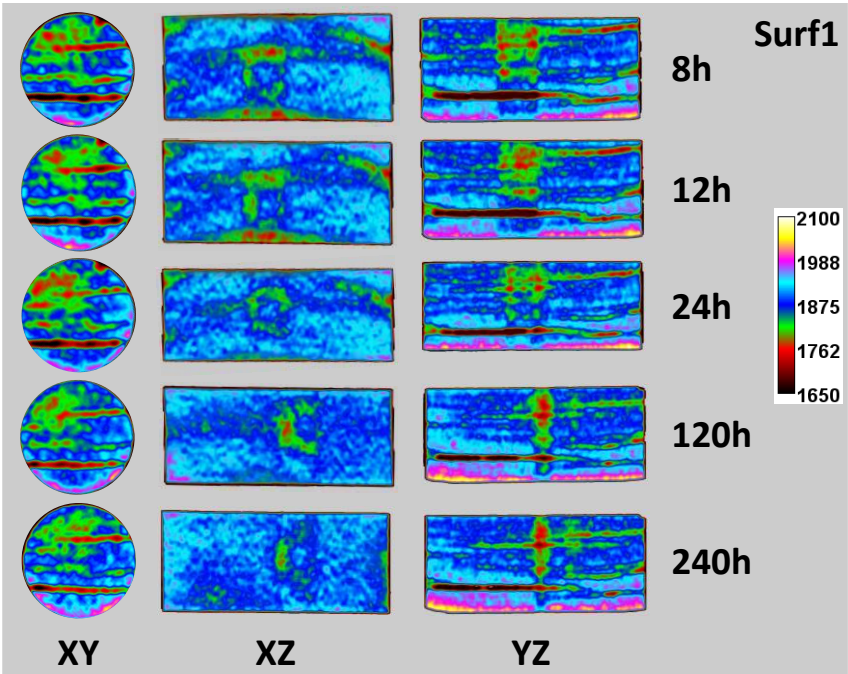

Fig. 52 - XY, XZ, and YZ slice of core plug through time under spontaneous imbibition in fluid system Surf1

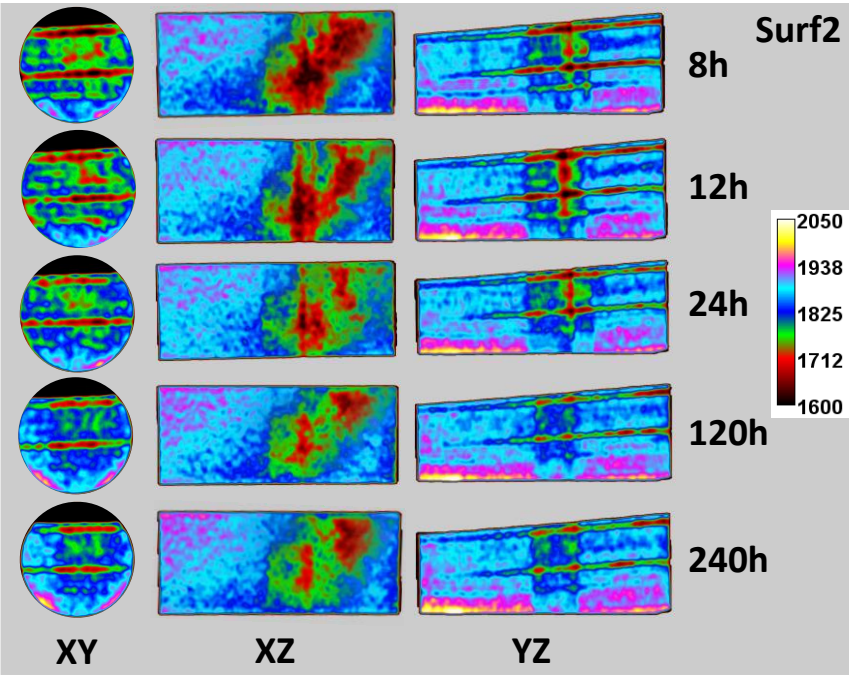

Fig. 53 - XY, XZ, and YZ slice of core plug through time under spontaneous imbibition in fluid system Surf2

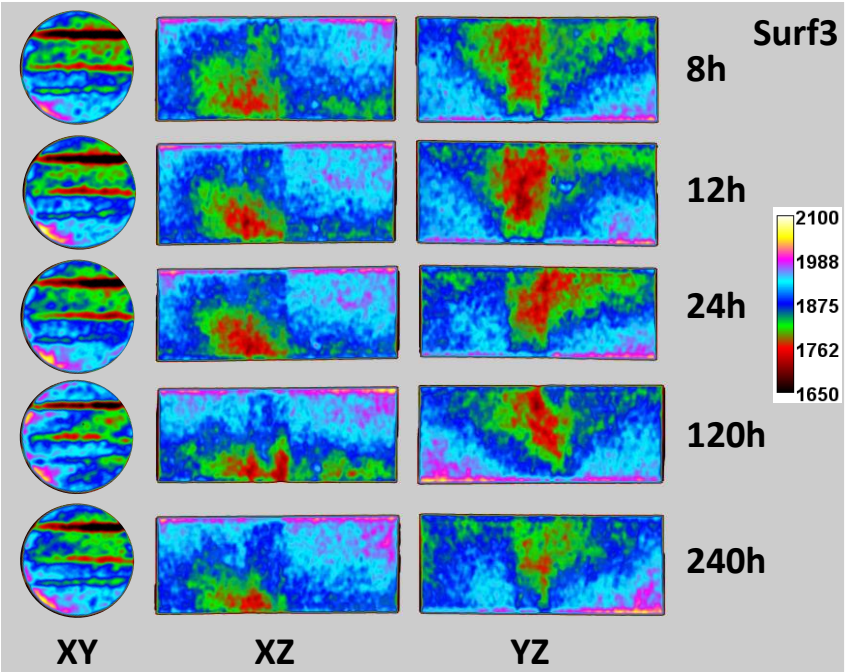

Fig. 54 - XY, XZ, and YZ slice of core plug through time under spontaneous imbibition in fluid system Surf3

5. LABORATORY-SCALE NUMERICAL MODELLING

After all rock and fluid properties, interfacial tension, contact angle, zeta potential, surfactant adsorption, and spontaneous imbibition data were gathered on the laboratory experiment part of the work. The next step of the extensive workflow, which is the laboratory-scale numerical modelling of the surfactant-assisted spontaneous imbibition, will be covered in this section. Lab-scale or core-scale model was built to obtain the capillary pressure, oil relative permeability, and water relative permeability curves of each fluid system which then will be used on the field-scale model to assess the field-scale impact of SASI on a well basis.

Numerical modelling of the surfactant-assisted spontaneous imbibition was constructed as based on all information presented in the literature review section. For spontaneous imbibition without any surfactant involved, the movement of fluid inside the rock sample was caused by capillary force which modeled by the capillary pressure curve that can be fed into a numerical reservoir simulator. In the numerical model, each grid would have each own level of water saturation which then could be transformed to the magnitude of capillary pressure based on the capillary pressure-water saturation curve given. Then, the capillary pressure was used as the pressure that drove fluid in or out of each grid. The process then repeated on each timestep until the equilibrium of where water saturation correlated to zero capillary pressure.

The introduction of surfactant was modeled by introducing a flow properties alteration algorithm. Two set of capillary pressure, oil relative permeability, and water relative permeability curves consisting of the original curves used previously and the surfactant's curves were fed into each grid block. Similar mechanism of fluid movement under no-surfactant spontaneous imbibition as explained previously started the initial oil and water movement in and out of the grid

blocks. However, since surfactant component was added into the water component, the intake of water into the grid block as caused by the initial imbibition also introduced surfactant into the grid block. Surfactant component was used as a marker in the numerical simulation for triggering the flow alteration algorithm. Based on the two sets of curves plugged into each grid block, the flow alteration process generated a new set of curves which was basically a weighted average of the two given sets. Weighted average of the curves was based on the amount of surfactant adsorbed in each grid block which was based on the surfactant adsorption isotherm obtained from experimental work. The weighted average process produced the new set of curves from the original curves, as surfactant was introduced into the grid block and got adsorbed, the new curves set would move closer to the surfactant's set. And with more and more surfactant introduced into the grid as more and more water moved into the grid, the new averaged curves set would get closer and closer into the maximum surfactant's set.

For every time step where fluid and surfactant moved into the grid and new capillary pressure and relative permeability curves were generated, a new equilibrium state was also instated. Introduction of surfactant into the grid improved the capillary force magnitude as shown in the experimental procedure. Therefore, it was expected that the averaged capillary pressure curve would increase the capability of capillary pressure to suck more water inside the grid block, expulsed more oil for production.

Fig. 55 shows a summary of the modelling concept with also information on how to generate the needed data. Based on the explanation given before, there were six curves that were needed in order to model the surfactant-assisted spontaneous imbibition. These six curves were capillary pressure, water relative permeability, and oil relative permeability curves on two different condition, original unaltered condition and maximum surfactant effect condition. None of the

experimental procedure could directly give the curves which mean another way of constructing the curve was needed.

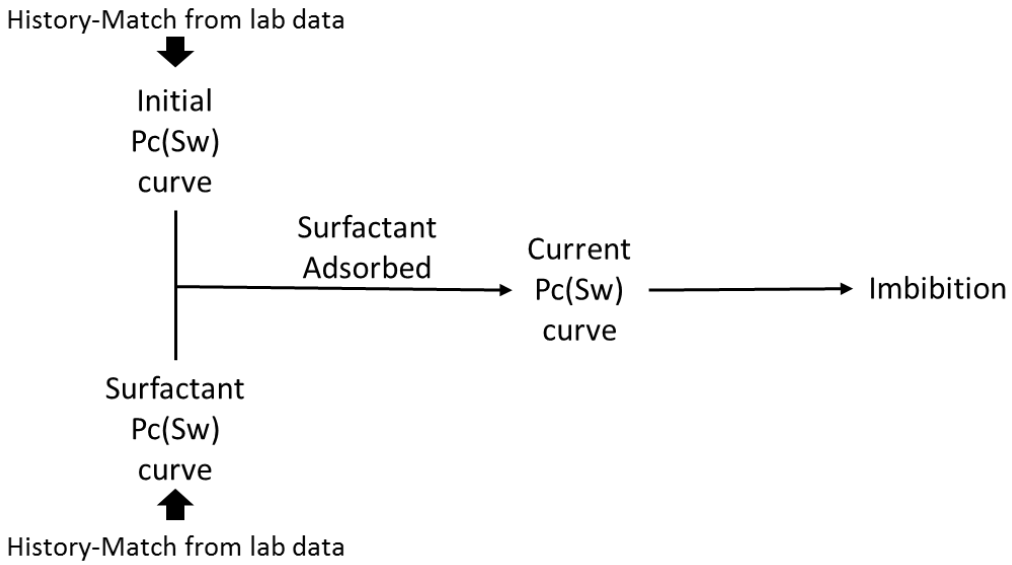

Fig. 55 - Flowchart for modelling surfactant-assisted spontaneous imbibition (SASI)

History-matching process was chosen as the method to construct all curves. Spontaneous imbibition production profile of each fluid system tested were obtained from the spontaneous imbibition experiment done on the experimental part of this work. By building an exact replica of the rock sample used and also the condition of which the tests were under, the six curves could be constructed by trial and error process of plugging different curves and running the simulation model until oil production profile from the numerical model matched the production profile from the laboratory experiment. The original curves set was obtained by modelling and matching the production profile of the imbibition test that was done on the base case fluid system. Then using the same original curve, the maximum surfactant effect curves set was constructed by modelling

and matching the production profile of the experiment done on each corresponding surfactant-included fluid system.

The drawback of utilizing history-matching method as a data gathering method was whether the solution obtained would be unique or not as multiple matched scenario is a possibility. This was where all the experimental data gathered came into use by providing basis for making a data-based analysis to remove any curves produced from the history-matching process that deemed to be unphysical. Another extra measure was also done to ensure the comparability of the curve set between base case and surfactant cases by following the same procedure on matching the laboratory production data.

As explained in the previous section, the advantage of utilizing numerical model-based upscaling method is the ability to remove sample heterogeneity, which is also heterogeneous among different core plugs used for different fluid system tested, from the upscaling result. This ability was found to be extremely useful for upscaling surfactant-assisted spontaneous imbibition on shale sample as heterogeneity is what shale rocks are well-known about. However, in order to eliminate the heterogeneity factor from the upscaling process, sample heterogeneity itself must be included into the lab-scale model. In this work, rock digitalization based on CT-Scan technology was incorporated to tackle this problem. CT-Scan images of the exact core plug used on the imbibition experiment were converted to grid model of the rock with all the heterogeneity in the form of bedding plane, microfracture, etc included and modeled.

In this section, the construction of the digital rock model utilizing CT-Scan technology will be covered followed by the history-matching process and the analysis of data acquired from the history-match process to the data obtained from the lab.

5.1 Digital Rock Grid Model

Generally, CT-Scan is used to visualize what is happening in the interior of an object without the need to destroy the object. This is possible due to the ability of CT-Scan machine to construct a digital 3D map of the density distribution of a sample. CT-scan images can also be looked as a process of creating a digital approximation of the rock sample, digital format of the rock sample is presented in pixel format where each pixel has different CT-number, reflecting the density of the rock part that is represented by the pixel. Resolution of the machine affects the accuracy of the digital approximation, higher resolution results in smaller pixel size and also larger pixel number. Since each pixel is an averaged value of the area of the scanned sample represented by the pixel, this means that a more detail image of the scanned sample would be produced. Since pixel is just a 2D representation, the 3D form is constructed by running another sampling method where multiple 2D slices are gathered by moving the sample along the direction of the normal of the plane where the 2D slices are created.

In the end, multiple 2D slices of scanned core plugs are obtained. Each pixel in this huge number of images contain a CT-number that can be converted to density, providing a density map of the core plugs. With some assumption, this density map can be converted to a porosity map which can be plugged in to a numerical simulator and used as the grid model of the core plug. In addition to porosity data, permeability data is also another essential variable that is required by numerical simulator and can be calculated using a cross-plot correlation between porosity and permeability. Based on this concept, a representative numerical grid model of each core plugs that also incorporates heterogeneity, physical defects, or any specific physical detail of the sample can be constructed.

In this work, the explained concept was applied to construct core plugs grid model from each core plugs used in the spontaneous imbibition experiment. A total of four core plugs from four imbibition tests were cleaned under the cleaning procedure explained in the previous section. Cleaning process was highly essential to ensure that no other material other than the rock matrix would be detected and scanned by the CT machine. Vacuum dry process incorporated at the end of the cleaning process was also found to be important as this process would only left either air or vacuum in the pore space of the system, the importance of this condition will be covered later.

All four cleaned core plugs were scanned using the same Toshiba Aquilion TSX-101A machine used in the previous part. Scanner setting was set to 135kV and 350mA configuration for all the sample. Images from each core plugs then were processed using an in-house image processor which was built on MATLAB® platform. The main job of the image processor program was to convert the CT images to distribution of porosity and permeability in a reservoir numerical simulator-friendly format. In summary, procedure that was included in the program are as follow:

1. Importing and converting the original DICOM format obtained from the CT machine,
2. Removal of excess area by predefined threshold,
3. Resizing procedure to downscale the image data for a more computing power-friendly resolution,
4. Conversion of CT number to density through the following equation,

$$\boldsymbol{\rho = 1.017 + \frac{0.592 * CT\#}{1000}} \quad \text{……Eq. 10 (Massicano et al. 2009)}$$

5. Conversion of density to porosity through the following equation,

$$\boldsymbol{\phi = \frac{\rho_r - \rho}{\rho - \rho_f}} \text{ ……Eq. 11}$$

6. Addition of 5 grids around the core plug model to be used as the model of imbibition cell,
7. Duplicating the porosity distribution array eight times for eight property distribution arrays,
8. Conversion of porosity to permeability through the following equation for one of the arrays,

$$\boldsymbol{k(md) = (1.417E-4)e^{0.2755*\phi}} \text{ ……Eq. 12 (Cho et al. 2016)}$$

9. Assigning initial oil saturation, water saturation, surfactant concentration, water concentration, sector marker, and set curve marker on the other six arrays.

Total pixel number of each 2D slice produced by the CT machine was 262,144 number of pixels. With each core plugs scan having more than 200 of the 2D slices, plugging in unprocessed CT image data would result in running simulation with more than 50 million gridblocks. Downsizing procedure was done by utilizing the built-in image resizing algorithm on MATLAB. Different grid number can be inputted to the program, in this work, gird size of 20x20x20 was chosen which then was founded to result in usual running time of 2-3 hours for each case done on a 3.07GHz processor.

Conversion from CT-number to porosity was done first by converting the CT to density data which was done by utilizing a correlation (Massicano et al. 2009). Then density was converted to porosity by utilizing Eq. 11 under the assumption of only either vacuum or air filled the pore space, which would simplify the porosity measurement, leaving only one variable to be determined, ρ_r, which is the rock matrix density. Trial and error of rock matrix density number

was done by matching the calculated pore space of the grid model with the calculated pore space from measurement data presented in Table 2.

Permeability then was calculated from the porosity data utilizing the equation shown on step 8. Another important assumption was taken in this step. Bedding planes with better flow capacity were observed to be present in the core plugs as shown on the result analysis part of the spontaneous imbibition experiment. In order to incorporate the observed phenomenon, the better flow capacity of this section was modeled by applying a two order of magnitude multiplier to the permeability calculated from the porosity. The high permeability bedding plane zone was also detected by applying porosity threshold which was obtained by comparing the porosity distribution and CT images of the core plug.

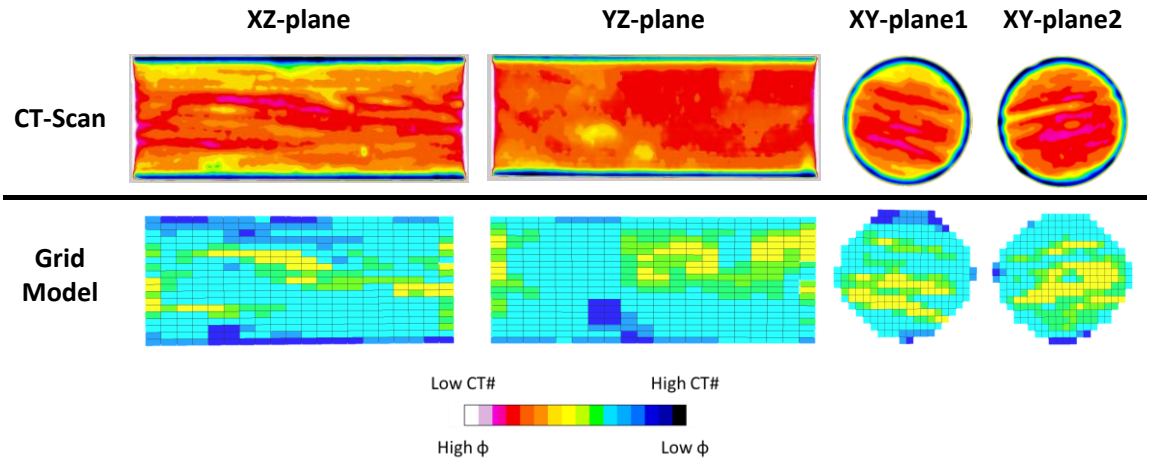

Fig. 56 - Comparison of real and grid model rock used in spontaneous imbibition with DW

Initial fluid saturation of the core plug was assumed on the same number that was used to calculate the original oil in place on the experimental part of the work. Two markers, one for sector

and set curve assignment along with surfactant concentration and water concentration will be explained in the next section of the work

The result of the rock digitalization method utilized in this work are presented in Fig. 56 - Fig. 59. With CT-Scan images of the corresponding core plugs are also presented as a comparison. It is important to note that different color table than the one used to build Fig. 50 - Fig. 54was implemented on these figures in order to match the color table used on the porosity model. Brighter color represents low CT-number and also high porosity while darker color represents high CT-number and also low porosity. Higher CT number are caused by higher density, where an area of the rock with lower porosity would cause the average density of the area to be high as well as there will be more rock matrix and less empty pore space present. Therefore it was logical to use an inversed color table on the CT-number so that a constant color trend would be used to present CT-number and porosity data.

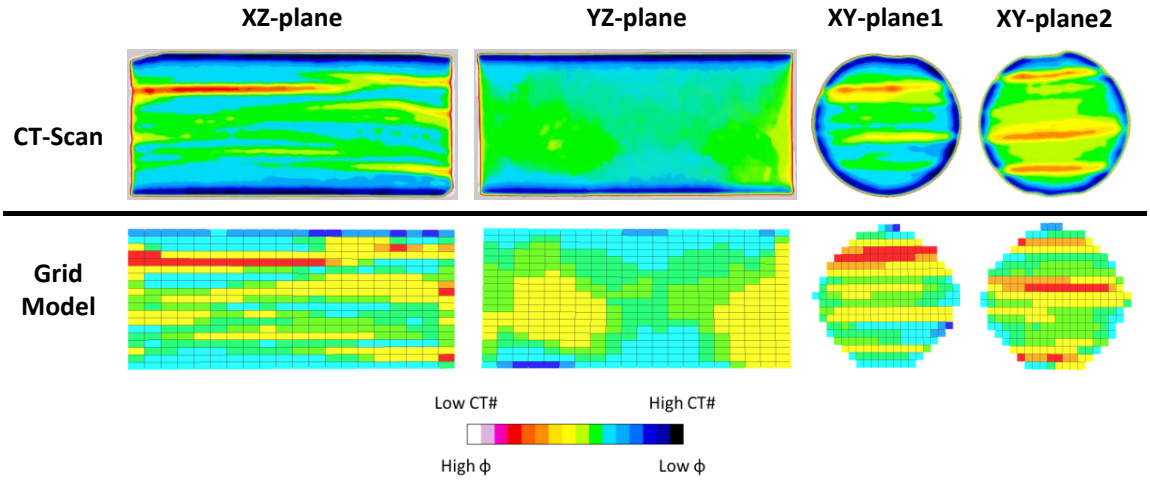

Fig. 57 - Comparison of real and model rock used in spontaneous imbibition with Surf1

The most notable observation that can be done is that every heterogeneity observed on the real core plug as observed in the CT images were modeled in the grid model. Achieving the objective of the rock digitalization method and also enabling the removal of rock sample heterogeneity from the different set curves that would be obtained from history-matching process that will be covered on the next part.

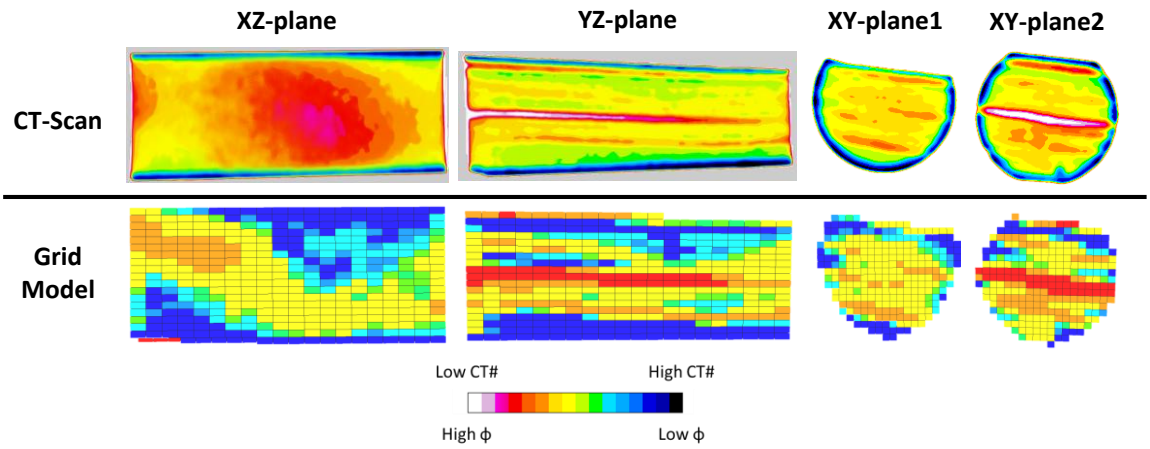

Fig. 58 - Comparison of real and model rock used in spontaneous imbibition with Surf2

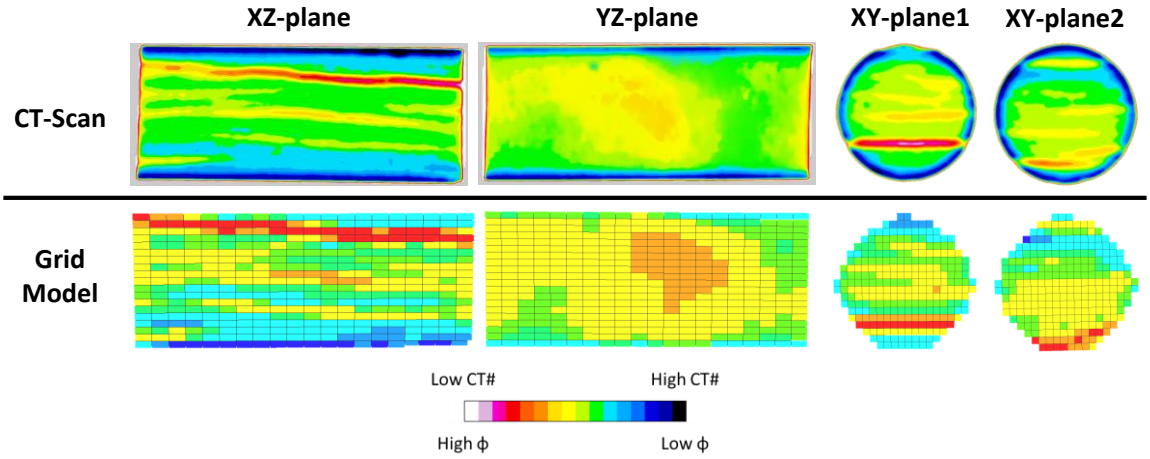

Fig. 59 - Comparison of real and model rock used in spontaneous imbibition with Surf3

5.2 Spontaneous Imbibition History Matching

Four digitalized rock in the form of four set of eight rock property distributions constructed through steps mentioned in the previous section were plugged into a commercial reservoir numerical simulator. In this work, the 2015.10 version of CMG STARS was used to run the numerical model. The choice of CMG as the simulator was based on the more customizable nature of the simulator as compared to other commercially available reservoir simulator. For a start, CMG STARS allows the application of the flow properties alteration modelling mechanism explained before. Another trivial reason was that CMG allows the simulation to be run without any well defined in the grid model, which enabled the model to exactly mimic the spontaneous imbibition laboratory experiment.

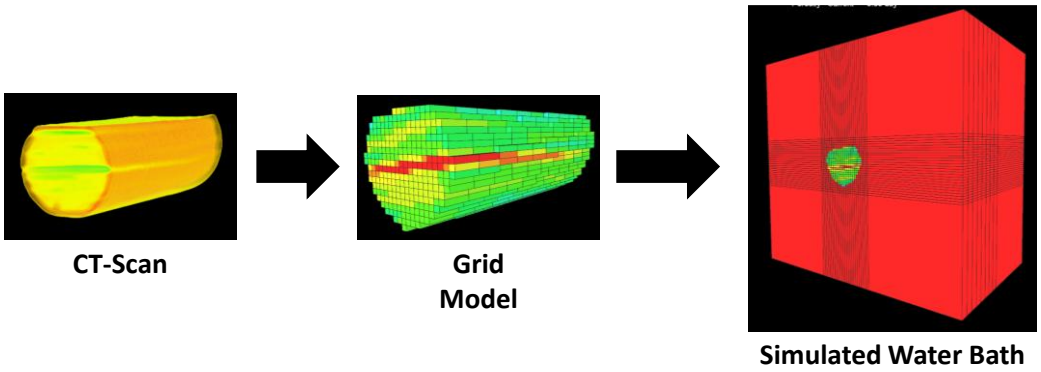

Fig. 60 - Grid model configuration of spontaneous imbibition experiment

The starting condition of the model was initiated as follows. Digital rock model was positioned in the middle of a simulated water bath to model the Amott cell used in the laboratory experiment as shown by Fig. 60. Different sector marker then applied to distinguish the core grid and the cell grid. Water saturation for cell grid was set to 100% as the cell functioned as a water

bath while the core grid initial water saturation was set to 15% as mentioned in the earlier section. For the simulation case of fluid system DW, no surfactant component was added to the model as no surfactant was involved in the laboratory experiment as well. While for the simulation cases that modeled imbibition experiment using fluid system Surf1, Surf2, or Surf3, surfactant component was added into the model. The initial condition for surfactant component was set by assigning surfactant concentration of each corresponding concentration on the aqueous-phase on the cell grid just as it was in the laboratory experiment where surfactant molecule located only in the water-phase that surrounded the core plug sample. There were a total of four lab-scale model that were constructed in this study as there were four imbibition experiments done with four different fluid systems.

History-matching process was done on the base case of fluid system DW first as capillary pressure and relative permeability curves obtained from this case were required for the other cases with surfactant involvement. Procedure of matching the oil production from lab experiment was started by modifying the capillary pressure curve first. It was found that the amount of oil produced from the imbibition model run was determined by the intersection point of capillary pressure curve with the water-saturation axis or in a simplifier form, $\boldsymbol{S_w(Pc = 0)}$. Production rate or the time needed to reach the production plateau was observed as a function of the maximum capillary pressure, $\boldsymbol{Pc_{max}}$, which is the capillary pressure at the initial water saturation. Hundreds of different capillary pressure curve was tried on the model until the best production match from the model and from the experimental data was observed. After the best-possible match from adjusting the capillary pressure curve was achieved, relative permeability curves of both oil and water was done next. It was found that relative permeability did not affect the ultimate production of oil from the imbibition run but rather affected the shape of the oil production curve. Another hundreds sets

of relative permeability curves for both oil and water were tried until the best-possible match was found. It was also important in constructing the relative permeability curves to put into consideration the IFT and wettability state as measured in the laboratory. Incorporating those data into the history-matching process expedited the matching process as physically impossible relative permeability curves could be removed from the trial.

Capillary pressure and relative permeability curves set obtained from the base case history-matching then was plugged into the three model of surfactant-assisted spontaneous imbibition along with the adsorption isotherm of each surfactant. Exact procedure was followed to construct capillary pressure and relative permeability curves of each surfactant that would provide the best-possible match of oil production.

In the process of obtaining the capillary pressure and relative permeability curves that would provide the best-match between oil production from numerical model and laboratory experiment of all four cases, around 4000 simulation cases were run. Fluid distribution through the model run time taken from the best case of each model are presented in Fig. 61. As can be seen, incorporating heterogeneity was found to affect the production pattern on the core grid model. Area with better flow capacity was produced first which was shown by the faster change of fluid saturation in those section of the grid model.

Simulation result of the best case of each fluid system along with the production as observed from their laboratory experiments are shown in Fig. 62. It is also important to notice that the y-axis of the graph was no longer recovery factor but a real volume instead which was because of oil volume on the cell grid was the given result from the numerical simulator. A good agreement between observed oil production in the lab and oil production from the numerical model can be

observed on the curve. Although that there was some deviation observed on early part of the production, a good level of match was observed on the total final production volume.

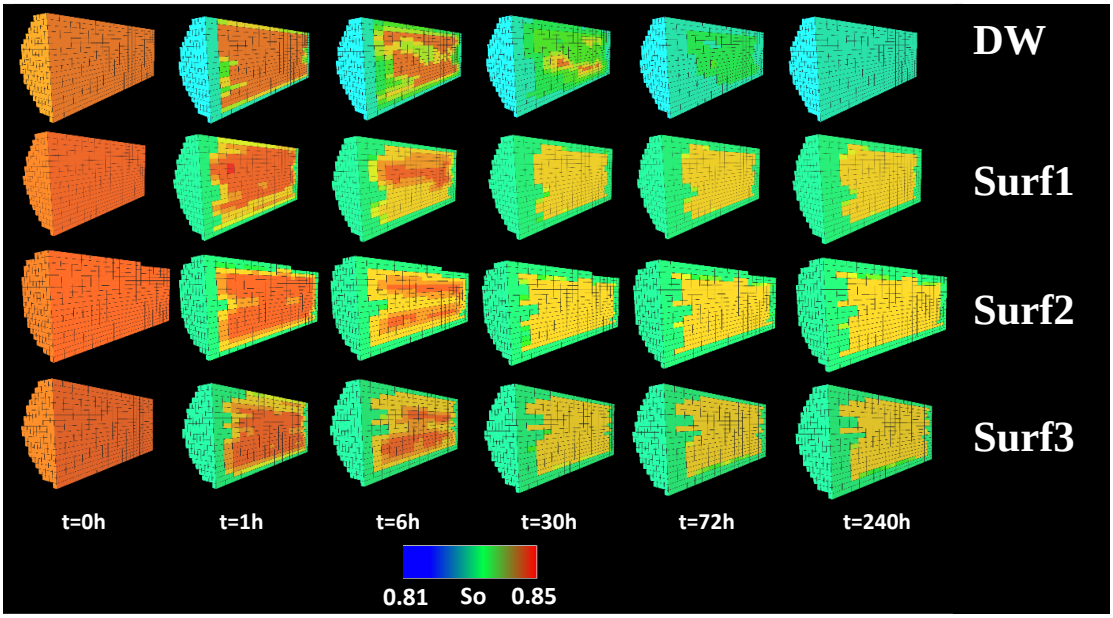

Fig. 61 - Oil saturation distribution inside the core plug grid model during spontaneous imbibition

Capillary pressure that was used to run the best-match case can be seen in Fig. 63. Fluid system DW was observed to have the highest Pc_{max} which could be caused by the highest IFT of what was measured on the experimental procedure. However, the capillary pressure curve intersected the x-axis at a comparably lower saturation, as mentioned before, the intersection point or $S_w(Pc = 0)$ was a function of the volume of oil produced from the core plug during imbibition mechanism. Since production from fluid system DW was the smallest oil production observed, it was expected and confirmed that the $S_w(Pc = 0)$ fluid system DW was the smallest.

Comparing the capillary pressure for the three fluid system containing surfactant, it can be seen that Surf1 had the largest area under the curve which was logical as the largest oil production

was observed from this fluid system. Surf3 was observed to have lower $S_w(Pc = 0)$ compared to Surf2, although that the volume of oil production from Surf3 was higher than Surf2. Going back to the dimension of core plugs used in the two imbibition experiments of Surf2 and Surf3, bigger core plug was used on the Surf3 imbibition experiment, providing an explanation on higher $S_w(Pc = 0)$ on lower volume of oil produced, as the capillary pressure curve is independent to the dimension of the core plug used.

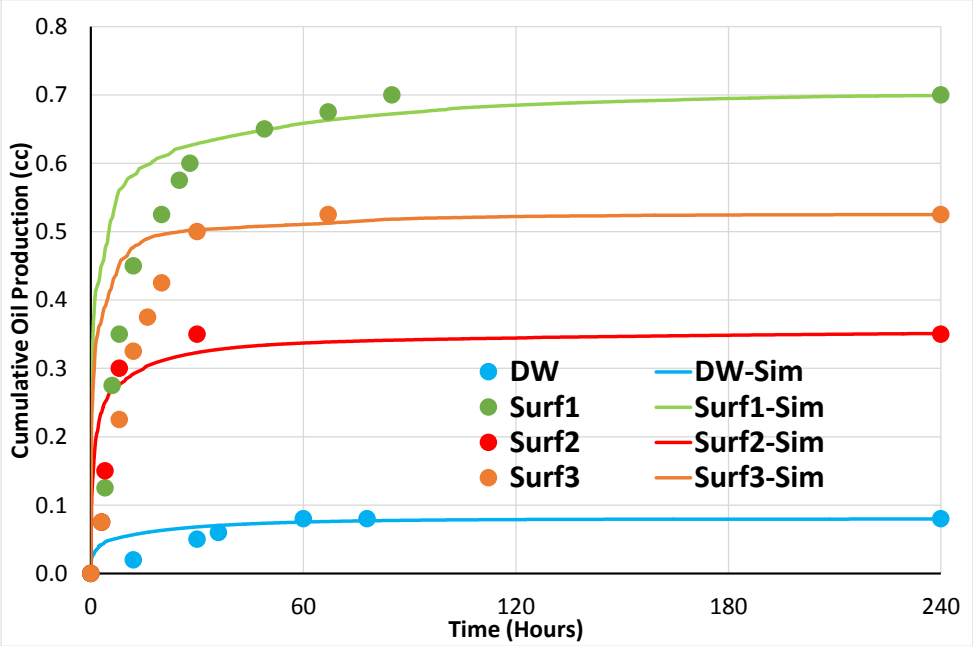

Fig. 62 - Comparison of oil recovery from lab. and history-match of spontaneous imbibition

Moving to the relative permeability curve, shown in Fig. 64, it can be seen that end-points of relative permeability curves were not modified for all three surfactant fluid systems. As IFT measurement showed, the IFT of surfactants used in this study did not fall into ultra-low category which then it could be safely assumed that the end-points did not change (Kathel and Mohanty 2013). Water relative permeability of fluid system DW was observed to be higher than all

surfactant's which could be caused by the water-wetness condition caused by surfactant which hindered the flow of water. The opposite effect can be seen where oil relative permeability for surfactant's cases are higher than those belong to the base case DW.

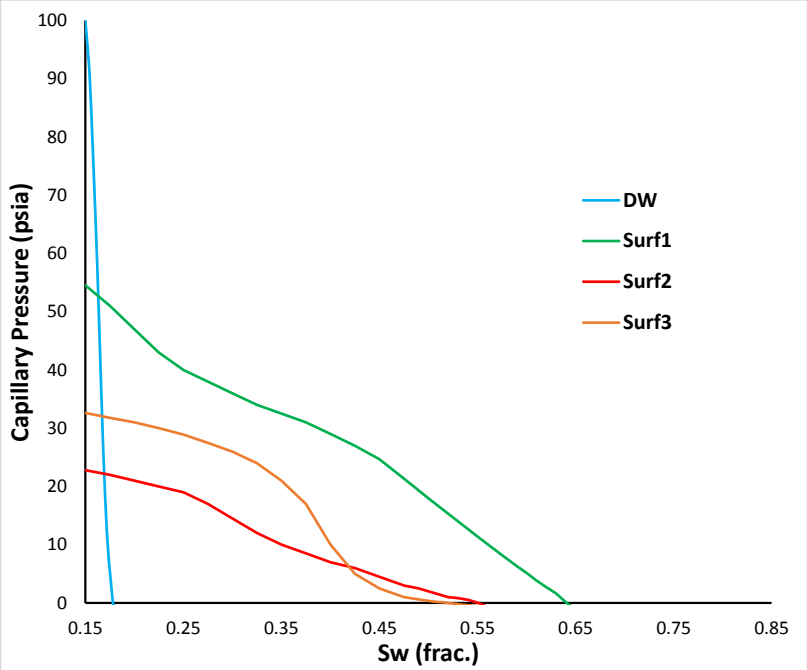

Fig. 63 - Capillary pressure curve for the best-matched case of each fluid system

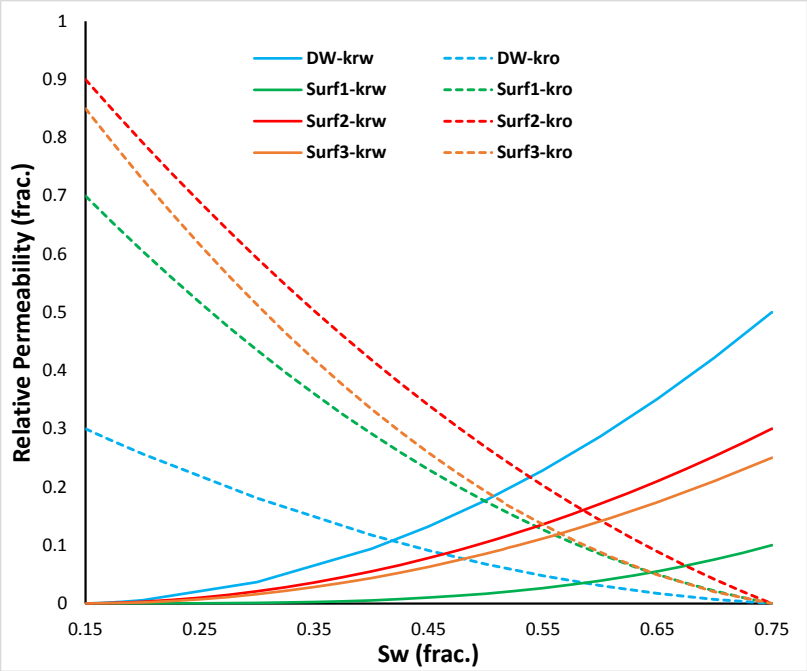

Fig. 64 - Relative permeability curves for the best-matched case of each fluid system

5.3 Result Analysis

In this section, a comparison on several key variables observed on the capillary pressure and relative permeability curves to several data observed in the laboratory measurement is presented. The first comparison is shown in Fig. 65, comparing the relative maximum relative permeability (kr_{max}) of both oil and water phase to the observed interfacial-tension data. A clear correlation was observed between the kr_{max} of oil and the measured IFT where higher IFT would cause lower kr_{max} value. However, for the kr_{max} of water, no clear correlation was observed as the kr_{max} from fluid system DW deviated from the trend shown by the other three cases. Wettability alteration as caused by the surfactant introduction could explain this finding as a possibility of weak water-rock interaction on the base case increased the flow capacity of water.

Correlation between contact angle data observed in the lab and kr_{max} is presented in Fig. 66. Strong connection between kr_{max} of water to contact angle data was observed while none was observed for kr_{max} of oil. As wettability progressed to oil-wet region or to the right direction on the x-axis, higher kr_{max} of water was observed. Oil-wet condition would lower the strength of water-rock interaction which could lead to better flow of water through the pore. Based on the two comparison, a clear correlation between kr_{max} of oil to IFT with no clear connection to contact angle was observed, as well as correlation between kr_{max} of water to contact angle with no trend observed when correlated to IFT.

On the capillary curve side, a comparison of the $S_w(Pc = 0)$ as well as $S_w(k_{ro} = k_{rw})$ to the contact angle is presented in Fig. 67. Both comparison showed that as wettability moves to the oil-wet region, both $S_w(Pc = 0)$ and $S_w(k_{ro} = k_{rw})$ responded in reduction of value. As shown before, $S_w(Pc = 0)$ was found to have a direct control to the amount of oil produced by capillary-driven imbibition. Oil-wet sample would produce less oil compared to water-wet sample as oil would be trapped more in the pores of oil-wet rock samples. Therefore the negative trend between $S_w(Pc = 0)$ and contact angle that was observed from Fig. 67 was expected. As for the $S_w(k_{ro} = k_{rw})$, the intersection between k_{ro} and k_{rw} is often used as another measure to determine permeability where intersection occurring at water saturation below 0.5 would correlated to oil-wet wettability and vice versa (Amyx et al. 1960). Similar trend was observed in Fig. 67, where intersection of relative permeability curves of surfactants cases were all above water saturation of 0.5 while for the base case was below 0.5. It was also observed that the stronger the surfactant altered wettability to water-wet region, the higher intersection point between the two relative permeability curves.

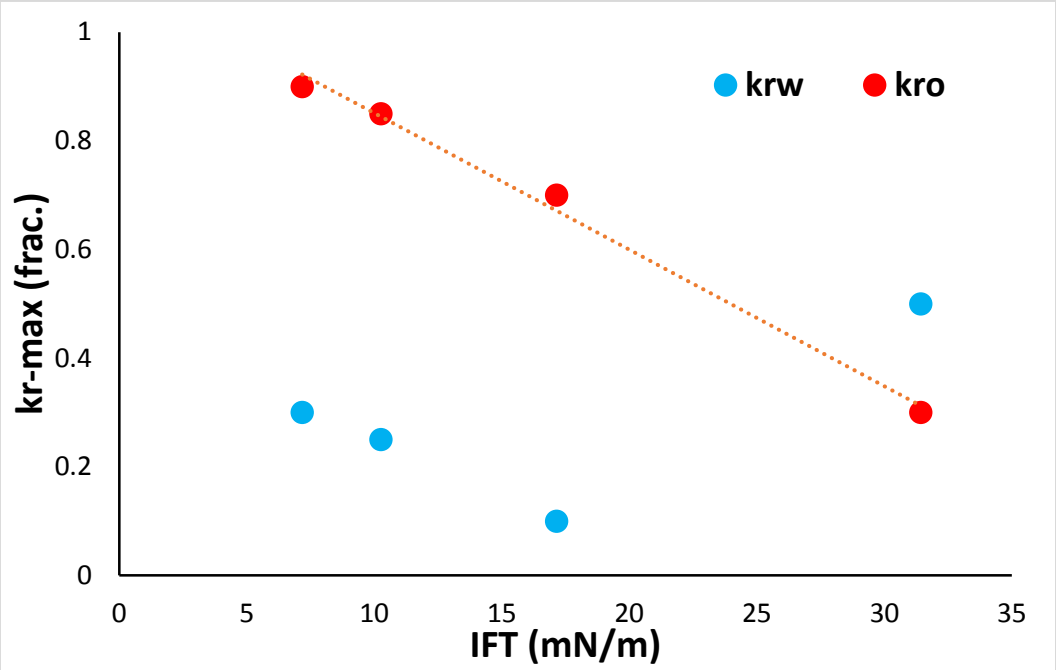

Fig. 65 - Correlation of IFT and maximum relative permeability

Going back to Fig. 63 and Fig. 64 before moving on to the field-scale modelling, it was observed that although that capillary pressure curve of Surf1 was the highest, its relative permeability curves were the lowers out of all surfactant cases. In the lab-scale model where capillary force was the sole driving force on the oil production, this property was found to be not significantly affect the production as Surf1 produced the most oil as compared to other surfactant cases. However, on the field-scale model, viscous force as caused by pressure drawdown would also exist which could affect the performance of Surf1 due to its low relative permeability property compared to the other surfactant cases.

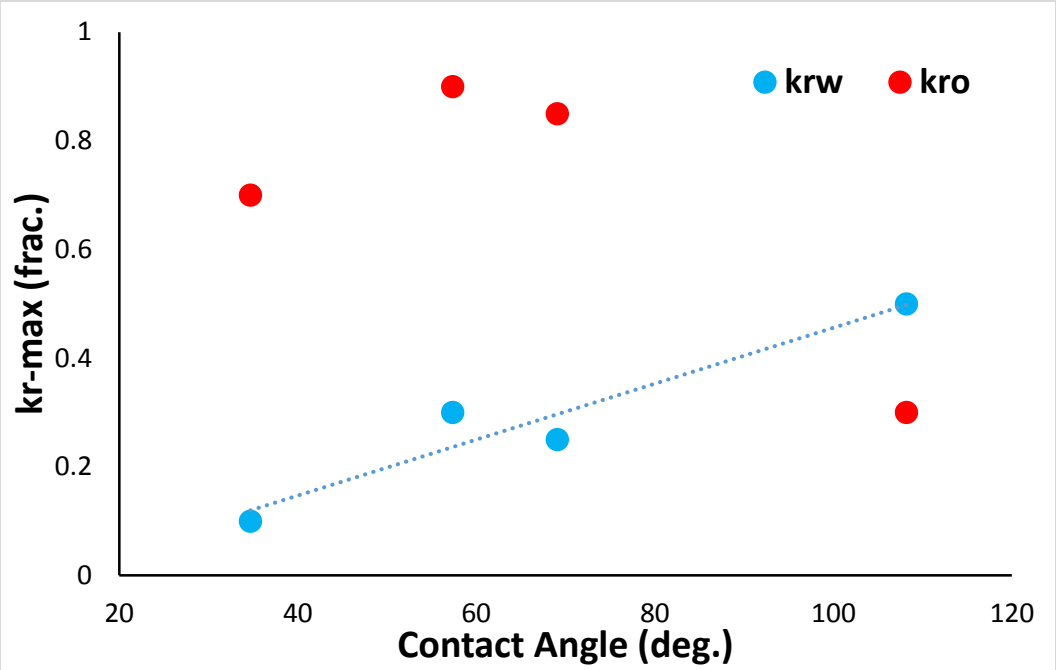

Fig. 66 - Correlation of CA and maximum relative permeability

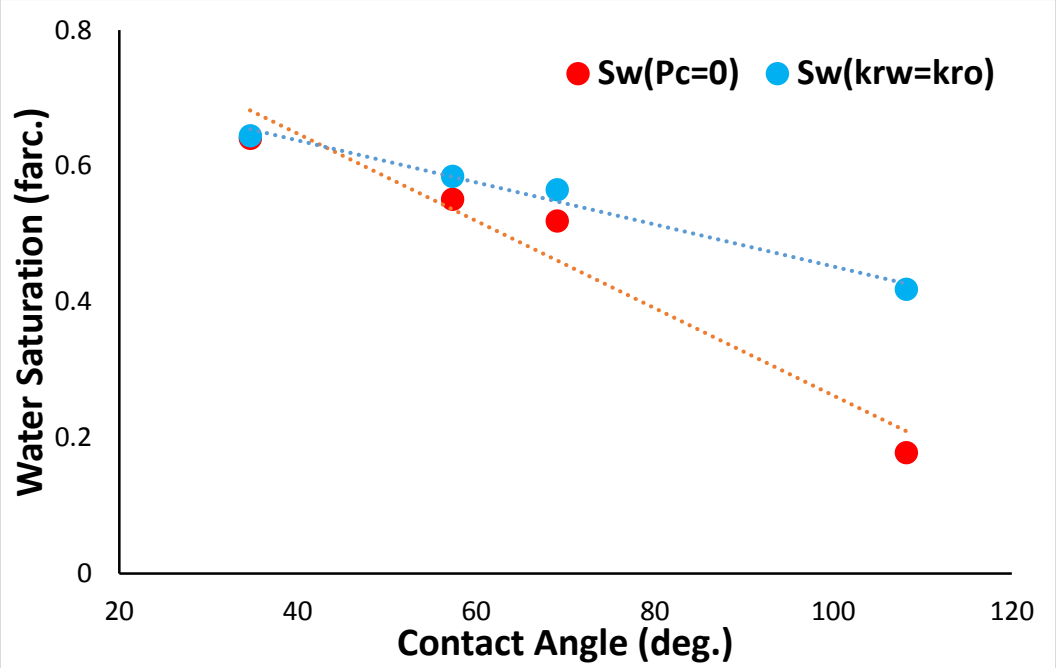

Fig. 67 - Correlation of CA to $\boldsymbol{S_w(P_c = 0)}$ and $\boldsymbol{S_w(k_{rw} = k_{ro})}$

6. FIELD-SCALE NUMERICAL MODELLING

Field-scale impact of surfactant-assisted spontaneous imbibition was studied by applying the flow properties alteration concept explained before in the lab-scale modelling section on a generic mechanistic field model. Three data gathered from laboratory experiment and lab-scale modelling were used in the field-scale model, adsorption isotherm, capillary pressure, and relative permeability curves. Imbibition and surfactant effects were modeled utilizing the concept and algorithm that was used on the lab-scale model with some modification to improve the accuracy of the model to mimic a field-scale production mechanism.

Dual porosity numerical model was employed to construct the field-scale model to include the fracture network that shale oil reservoir is widely known for. In a dual porosity model, each grid contains two kind of properties, matrix and fracture. Each grid contains smaller block which represents matrix and between each block, a high flow capacity channel is present which represents the fracture network. Dual porosity model is often implemented to construct a shale oil reservoir model as it is believed that oil production in this type of reservoir is possible, despite the ultra-low permeability nature of the matrix, through a transfer mechanism between the matrix and fracture. Matrix to matrix flow alone for oil production in shale oil reservoir is highly uneconomical, by transferring oil to the fracture network, a more economical production of oil would be achieved. Dual porosity modeled this concept by configure fracture network in each block to serve as the only part where fluid transfer is possible and matrix block to serve only as the storage of the hydrocarbon but naturally with a transfer function between matrix and fracture put in place.

Since the lab-scale model was built under a single porosity model, different initiation configuration for introducing surfactant component into the reservoir was installed on the field-

scale model. An assumption was taken that the surfactant was introduced into the reservoir by mixing the surfactant into the fracturing fluid. Fracturing fluid would filled the whole fracture system after the hydraulic fracturing process causing the water saturation of the fracture system to be 100% on the starting condition of the numerical model which was set to be the exact time when the hydraulic fracturing job finished. Surfactant component then would be present only in the fracture system in the whole reservoir on the initial condition. It was learned that on a real-life field scenario, a typical 10 days of shut-in time is usually implemented. The 10 days shut-in was first started due to the delay of production after hydraulic fracturing and tie-back to the production line but then was assigned deliberately as it was found that shut-in of well could result to better well performance (Gupta et al. 2017; Makhanov et al. 2013). In the numerical model, surfactant was expected to imbibe into the matrix from the fracture during this shut-in period. In other words, the oil-water fluid exchange between core grid and cell grid that was observed on the lab-scale model would also work here but instead of core and cell, the exchange would occur between matrix and fracture inside the dual-porosity grid as shown in Fig. 68.

To summarize, the field-scale model was constructed by initiating the surfactant component to present only in the fracture network which then oil-water-surfactant fluid movement as caused by spontaneous imbibition would occur between matrix block and fracture system. Shut-in time of 10 days and production for a period of 3 years was assigned to the model where initial oil production rate, cumulative oil production, and cumulative water production from the simulation run were studied and compared to understand the field-scale impact of the surfactant-assisted spontaneous imbibition (SASI). In addition, more detailed effect of surfactant on grid-basis as oil saturation, capillary pressure, and surfactant content progressed through the simulation

run-time was also investigated. Several sensitivity analysis of different reservoir geological properties to the well performance improvement as caused by SASI were also ran.

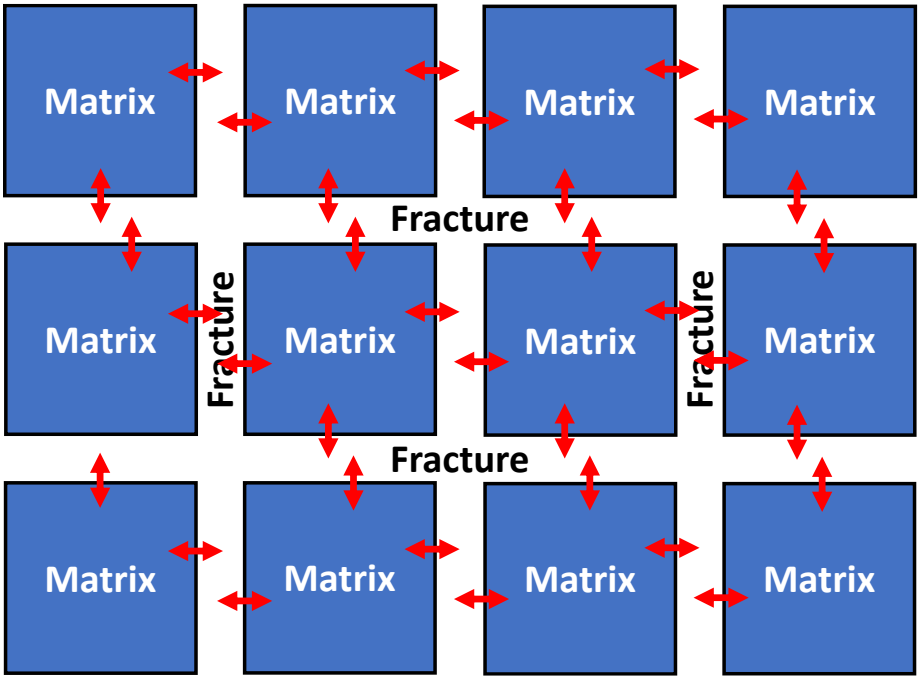

Fig. 68 - Fluid interchange during spontaneous imbibition on dual-porosity numerical model

6.1 Reservoir Model Description

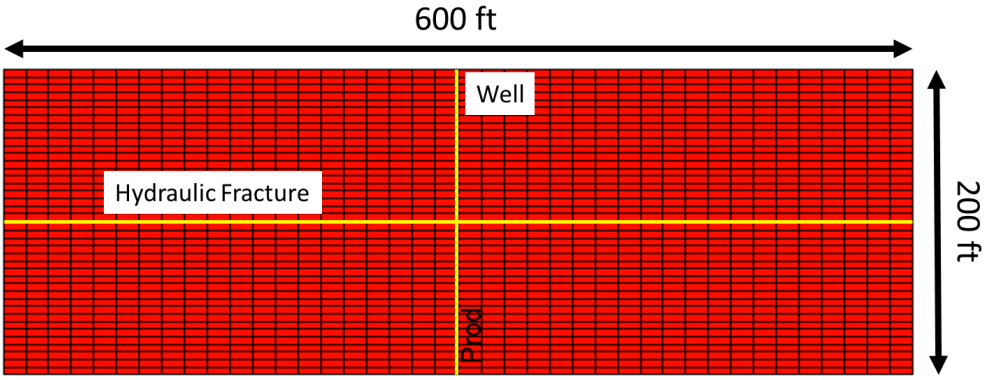

Fig. 69 - Reservoir grid model configuration and dimension

Table 5 - Properties of field-scale model

Property	Value	Property	Value
Thickness (ft)	100	k_{HF} (md)	25
ϕ_m (frac.)	.0867	Fracture spacing (ft)	0.2
ϕ_F (frac.)	0.006	S_{wi} (frac.)	0.15
ϕ_{HF} (frac.)	0.2	P_i (psia)	9000
k_m (nd)	145	Stage spacing (ft)	200
k_F (nd)	300	x_{HF} (ft)	300

Synthetic model with reservoir properties representing the Eagle Ford reservoir was constructed, the selection of each properties was done combining several data found from other literature and also from different opinion from different operator of the area (Fan et al. 2011; Phi and Schechter 2017; Wang and Liu 2011). Table 5 lists all important grid properties. An assumption of hydraulic fracture stage spacing of 200 ft with half-fracture length assumption of 300 ft was taken and grid model was constructed in the dimension of the stage spacing and double the half-length with thickness of 100 ft as shown in Fig. 69. Horizontal well was placed in the middle of the field model with hydraulic fracture assigned manually by setting matrix porosity to zero and fracture porosity to ϕ_{HF} value listed in Table 5 on grid model colored yellow that as shown in Fig. 69. As mentioned before, the initial condition for the field model was set as fractured filled entirely with fracturing fluid and no fluid imbibition from fracture to matrix occurred before. Based on this assumption then it can be assumed that the total fracture volume on the whole grid would be equal to the total volume of fracturing fluid injected to a single stage. It was found that the fracturing fluid volume was around 350,000 gallon which is close to the amount of fracturing fluid that is commonly used in the field. This founding showed that properties and the initial condition of the field model represented the real-life model although that not directly derived from

real production data, meaning that the result of this upscaling result could be used to investigate the field-scale impact of SASI.

6.2 Upscaling Result Analysis

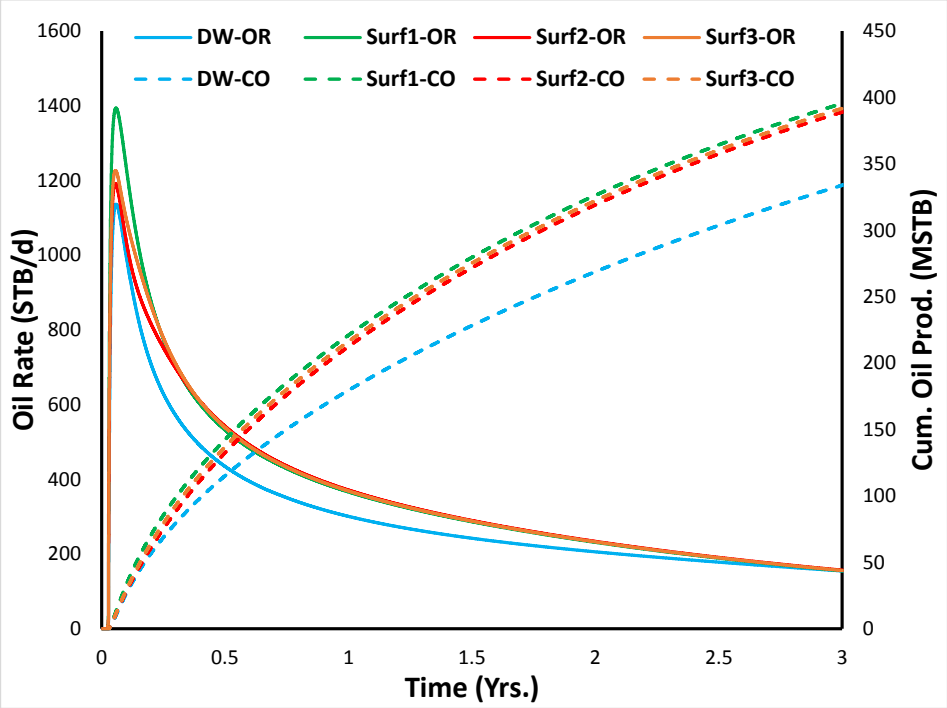

Fig. 70 – SASI Upscaling – oil production rate and cumulative oil production

Upscaling result of the four fluid systems tested in the laboratory is shown in Fig. 70. Introduction of surfactant component into the fracturing fluid was found to be also beneficial on the field-scale case. Since the field-scale numerical model that was run in the previous section was a one hydraulic fracture stage model, all results were multiplied by 20 to convert the result to a well basis as an assumption of 20 hydraulic fracturing stages per well was taken. Where increase of initial peak oil production rate as well as cumulative oil production were observed

from the three surfactant cases when compared to the base case of fluid system DW. Three years oil cumulative production of 335 MSTB was observed from the base case, where Surf1 improved the production the most by 18.4% to 397 MSTB, followed by Surf3 with 17% and Surf2 by 16%. On the initial oil production rate, the initial rate for the base case was 1136 STB/d. Addition of surfactant improved the initial oil rate production by 23% to 1393 STB/d on Surf1 field case, by 8% on Surf3 case, and 5% on Surf2 case. In addition to cumulative oil production and initial oil production rate, water cumulative production from the field-case simulation was also investigated and compared as shown in Fig. 71. Introduction of surfactant reduced the water production from the well from 151 MSTB for a three years cumulative ranging from to a little less than a half on the case of Surf2 up to a third of the original cumulative water production as observed on the case of Surf1.

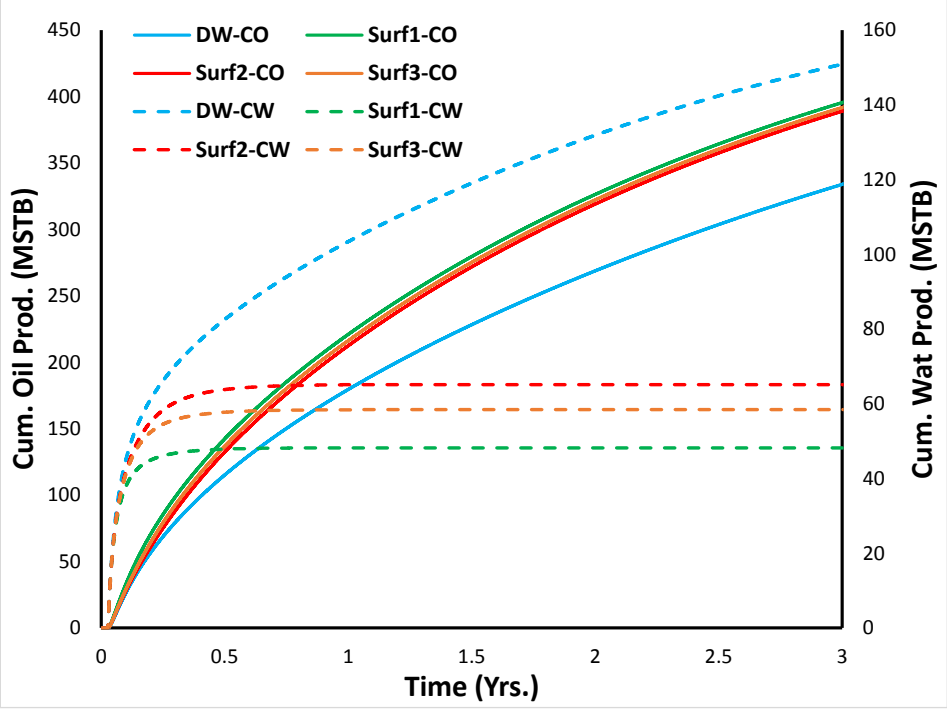

Fig. 71 - SASI Upscaling – cumulative oil production and cumulative water production

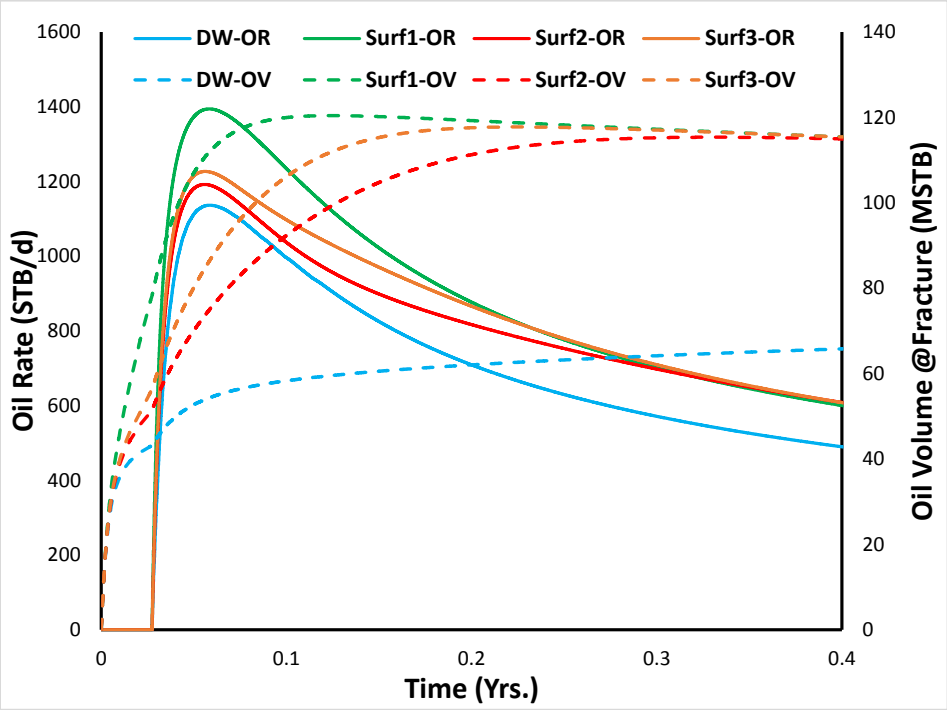

Fig. 72 - SASI Upscaling – oil production rate and fracture oil volume

All surfactant cases improved the initial oil production rate with the best improvement was performed by Surf1 case. A plot between oil rate and oil volume in fracture is given in Fig. 72. Focusing on the shut-in period in the beginning of the simulation as indicated by the zero oil production rate, a positive correlation between the two plotted variable was observed where the higher the fracture oil volume, the higher the initial peak oil rate. During the initial shut-in period, capillary-driven spontaneous imbibition pushed oil out of the matrix system to the fracture system which also accompanied by the intake of water in the reversed direction. Surf1 which performed the best spontaneous imbibition on the lab-scale model also caused the most fluid exchange between the matrix and fracture in the shut-in period. More oil in the fracture would result in higher oil production rate as more oil would be available to be easily produced to the well through the high-permeability fracture system. Two conclusions can be made from

this analysis, that oil volume in the fracture system could be used as an indication of the initial peak oil production rate and that the addition of surfactant component into the fracturing fluid increased the initial peak oil rate by moving larger amount of oil into the fracture system during the shut-in period through the process of enhanced spontaneous imbibition.

Surf3 was observed to have a higher initial oil production rate than Surf2, which should not be the case as $S_w(Pc = 0)$ of Surf2 was larger than Surf3. As it was stated before that initial oil production rate was a function of the amount of oil moved to the fracture through capillary-driven imbibition. It was also stated before that $S_w(Pc = 0)$ determined the amount of oil produced on the imbibition process. Based on the two premises, initial oil production rate on the field-scale of Surf2 should be larger than Surf3. This discrepancy was possibly caused by the short time available for the imbibition process. As it can be seen in Fig. 72. fracture oil volume of Surf2 and Surf3 was getting closer and closer at the end of the shut-in time. Longer shut-in time would allow Surf2 to move more oil to the fracture system than Surf3 and higher initial peak oil rate on Surf2 case would have been higher than Surf3.

On the cumulative oil production side, addition of surfactant also improved the cumulative recovery. However, when compared to the difference in surfactant performance on each surfactant cases in improving oil rate, surfactant performance in increasing cumulative recovery from different surfactant cases was found to be less distinctive to one another especially during the end of the simulation run. It was proposed that during this late-period, the effect of relative permeability alteration was starting to take over the effect of capillary pressure on oil production. As Surf1 was found to have the lowest relative permeability curve compare to Surf2 and Surf3, it was possible that during the late-time, Surf2 and Surf 3 was starting to produce more oil compared to Surf1 due to their better relative permeability properties.

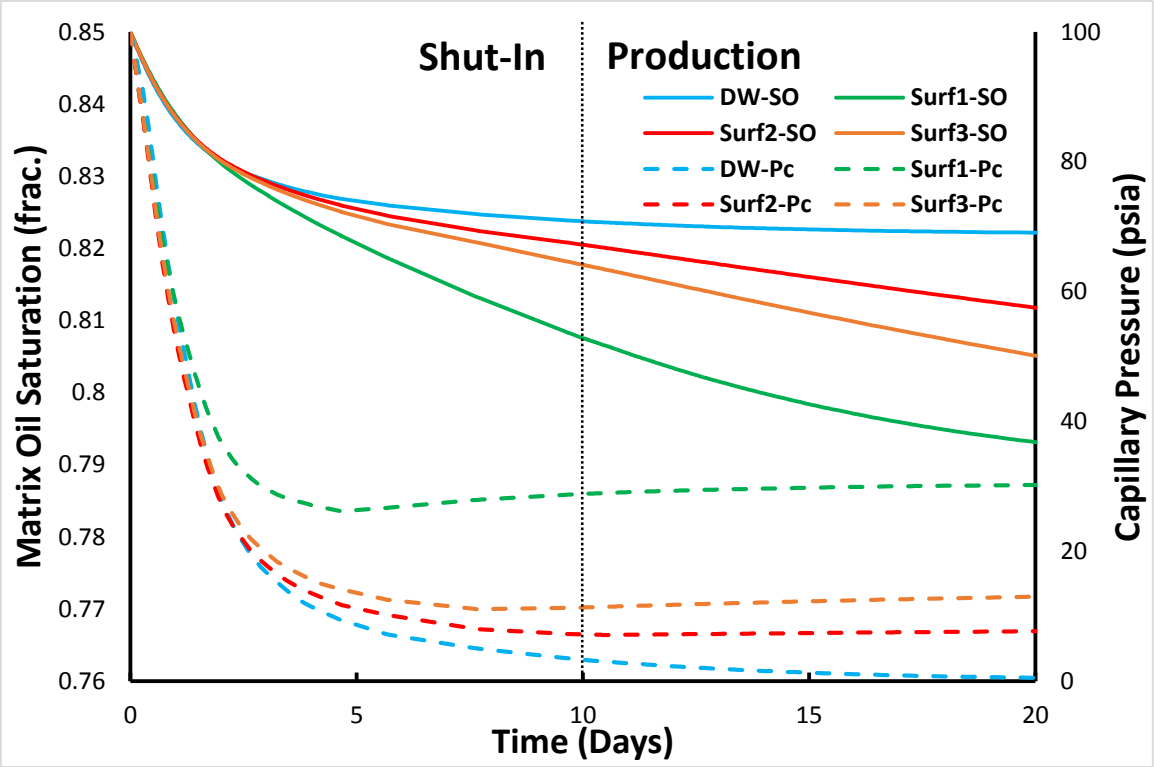

Fig. 73 - SASI Upscaling – matrix oil saturation and capillary pressure during and after shut-in

Grid-based analysis was also done in this work to better understand how surfactant-assisted spontaneous imbibition works on a field-scale. Grid-based analysis done on CMG STARS simulation cases enabled the analysis of surfactant content, oil saturation, and capillary pressure of each grid block through time which are shown in Fig. 73 - Fig. 74. Shut-in and production period were shown and separated by dotted black line. It can be seen that at time zero, oil saturation and capillary pressure of every cases were on the same value. As shut-in time started, imbibition occurred, oil saturation in the matrix decreased as it was moved to the fracture system. Drop of capillary pressure was also observed during the early time but as the amount of surfactant component in each grid increased, capillary pressure of surfactant cases increased and stronger imbibition was observed as a result. The theory was confirmed by Fig. 74, where

surfactant adsorption and capillary pressure are compared. More surfactant adsorbed in each grid block would cause higher capillary pressure to exist as explained in the introduction of the modelling concept in the previous section.

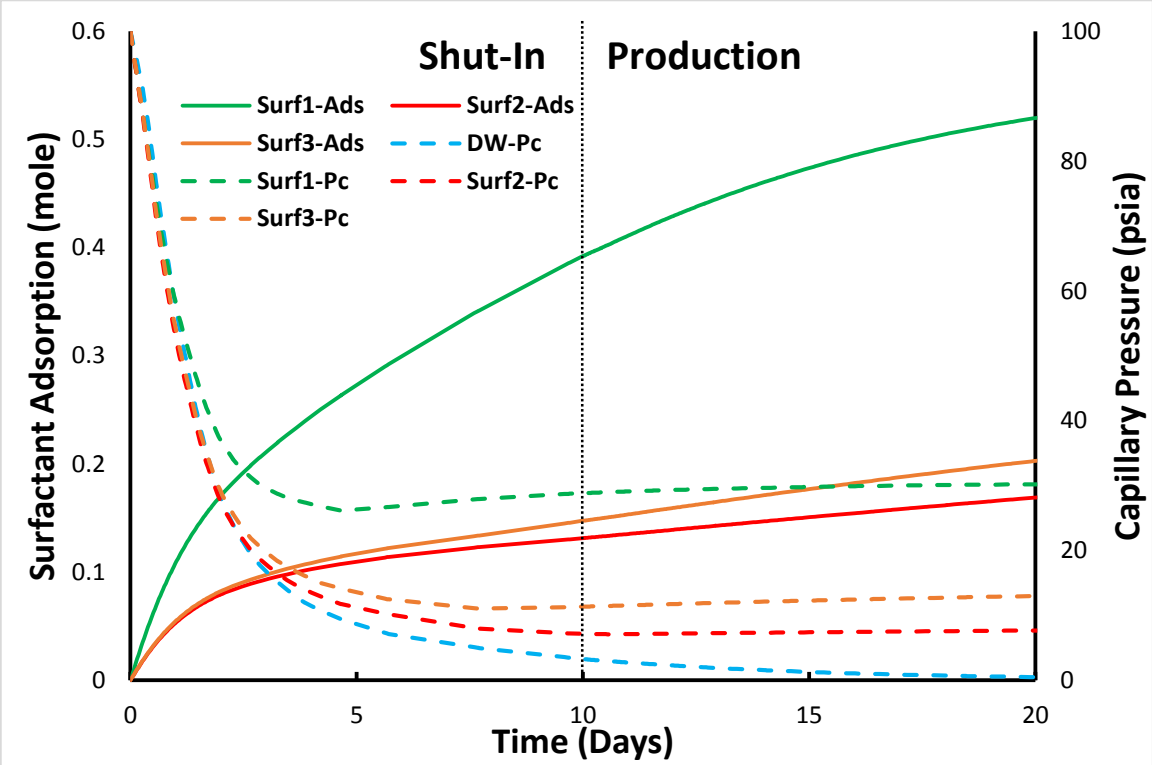

Fig. 74 - SASI Upscaling – surfactant adsorbed and capillary pressure during and after shut-in

6.3 Fracture Properties Sensitivity Analysis

With the result from the upscaling work presented in the previous section, the notion of surfactant-assisted spontaneous imbibition being a beneficial process not only on lab-scale but also on field-scale implementation was proved to be true. Then it would be logical to provide a sensitivity analysis on the performance of SASI as implemented on different reservoir properties.

A deeper insight on what kind of reservoir SASI would perform the best would come in handy when designing the treatment on a real-life field application.

In this work, a total of seven reservoir properties were varied in a most extreme range on both low and high sides. These properties were permeability and porosity of matrix, fracture, and hydraulic fracture with also the spacing of the fracture network in the model. A total of 104 cases for each fluid system were run on this section of the work, making a total of 416 cases with a total running time of ±180 hours with 7 processor cores running in tandem. Results were compiled in percent change of initial oil production rate, cumulative oil production, and cumulative water production using the fluid system DW as the best case. For both oil and water cumulative production, one, two, and three years cumulative production were investigated to observe the change in surfactant performance in different time of production.

Effect of matrix porosity and permeability on peak oil rate and cumulative production are presented in Fig. 75 - Fig. 80. An inverse relationship was observed when comparing matrix porosity and oil rate improvement where lower matrix porosity caused better surfactant performance than higher matrix porosity. The same trend were also observed on both cumulative oil and water production where higher cumulative oil improvement and larger cumulative water reduction was observed on lower matrix porosity.

Correlating matrix permeability on the production enhancement as caused by surfactant addition, a positive correlation was observed. Higher matrix permeability resulted in a more pronounce surfactant effect to oil rate and cumulative production. Higher permeability also resulted in less distinction in performance from all three surfactant tested on improving the oil production rate and cumulative oil production. On oil production rate, the difference in

performance between the three surfactants also decreased when matrix permeability was lowered.

Effect of hydraulic fracture porosity and permeability on the three investigated data are presented in Fig. 81 - Fig. 86. No significant effect of hydraulic fracture porosity to surfactant performance in improving oil production rate and cumulative oil production was observed. While on the cumulative water production, higher hydraulic fracture porosity caused larger cumulative production reduction where after certain value the difference in performance between the three surfactant was not noticeable anymore.

Higher hydraulic fracture permeability resulted in less surfactant-induced improvement of oil production from both initial rate and cumulative production aspects. Peak oil rate between the three surfactants were observed to be similar on low hydraulic fracture permeability cases. While for cumulative oil production, difference in performance between the three surfactants were observed to be unaffected by the change of permeability of the hydraulic fracture.

Effect of fracture porosity, permeability, and spacing to improvement of rate and cumulative production caused by surfactant addition are shown in Fig. 87 - Fig. 95. An interesting relation between fracture porosity and oil rate improvement was observed as shown in Fig. 87. Surf1 which was found as the best performing surfactant on previous section of this work was observed becoming the least effective surfactant on improving the rate of the oil production when lower fracture porosity was tested. In addition, effect of surfactant cumulative oil recovery was also observed to become negative on ultra-low fracture porosity. There was also an optimum point of fracture porosity, where enhancement of cumulative oil was maximum, found. The same trend was observed on the reduction of cumulative water production where another optimal fracture spacing value was found.

Fracture system permeability was observed to have a positive correlation with oil production rate enhancement, where higher fracture permeability resulted in better surfactant performance on increasing the initial oil production rate as shown in Fig. 90. Another infliction point was observed on the magnitude of rate enhancement as fracture permeability was varied. On the cumulative oil recovery, better cumulative oil production enhancement was observed as fracture permeability increased from 0.0001 md to around 0.001 md. However, after this point, increasing fracture permeability resulted in lower surfactant effectivity in increasing the cumulative oil recovery. The same observation was made on the cumulative water production where after 0.001 md, increasing fracture permeability resulted in less reduction of cumulative water production. Nonetheless, this trend was only observed on Surf2 and Surf3. For Surf1 cases, plateau was reached after 0.001 md of fracture permeability.

Fracture spacing and surfactant effectivity for SASI were found to be correlated in negative trend. Larger fracture spacing resulted in lower initial oil production rate enhancement, lower addition of cumulative oil recovery, and lower cumulative water production reduction. Converging data point on all three observed data were noticed on both ends of the tested fracture spacing value range as undistinguishable performance between different surfactant tested was observed on the high-end and also low-end value of fracture spacing.

In summary, variation of result on different reservoir properties tested on this sensitivity analysis could be used as an initial gauge on whether application of SASI would be beneficial or not depending on the properties of the corresponding field.

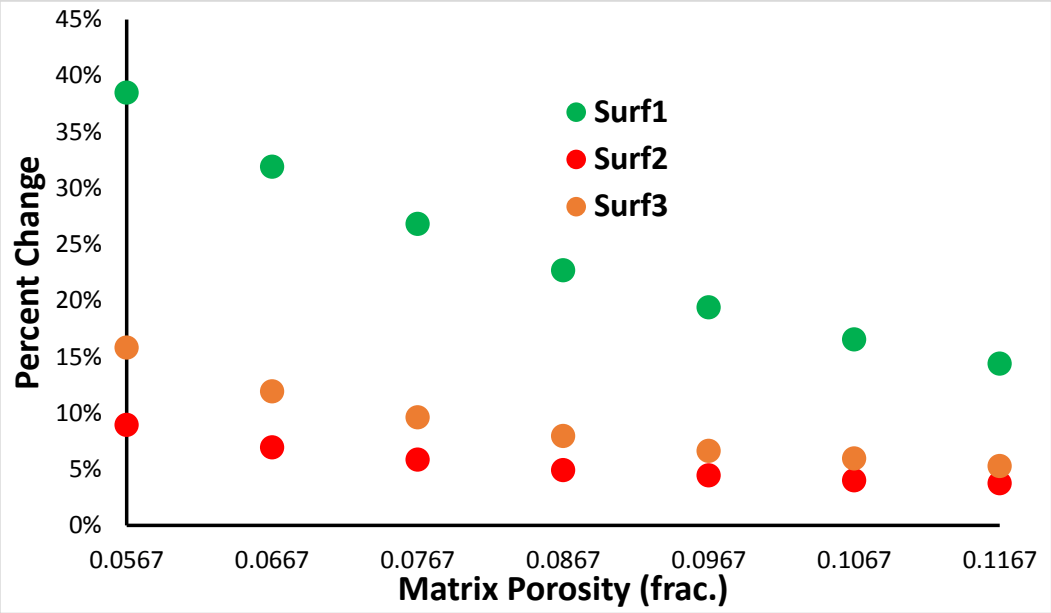

Fig. 75 - Effect of ϕ_m to initial oil production rate

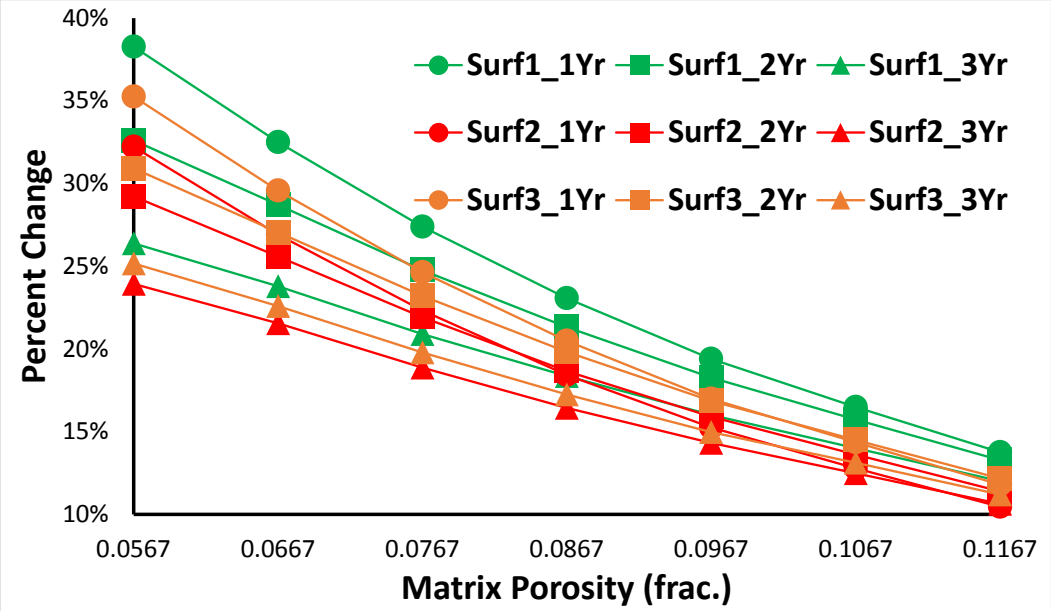

Fig. 76 - Effect of ϕ_m to cumulative oil production

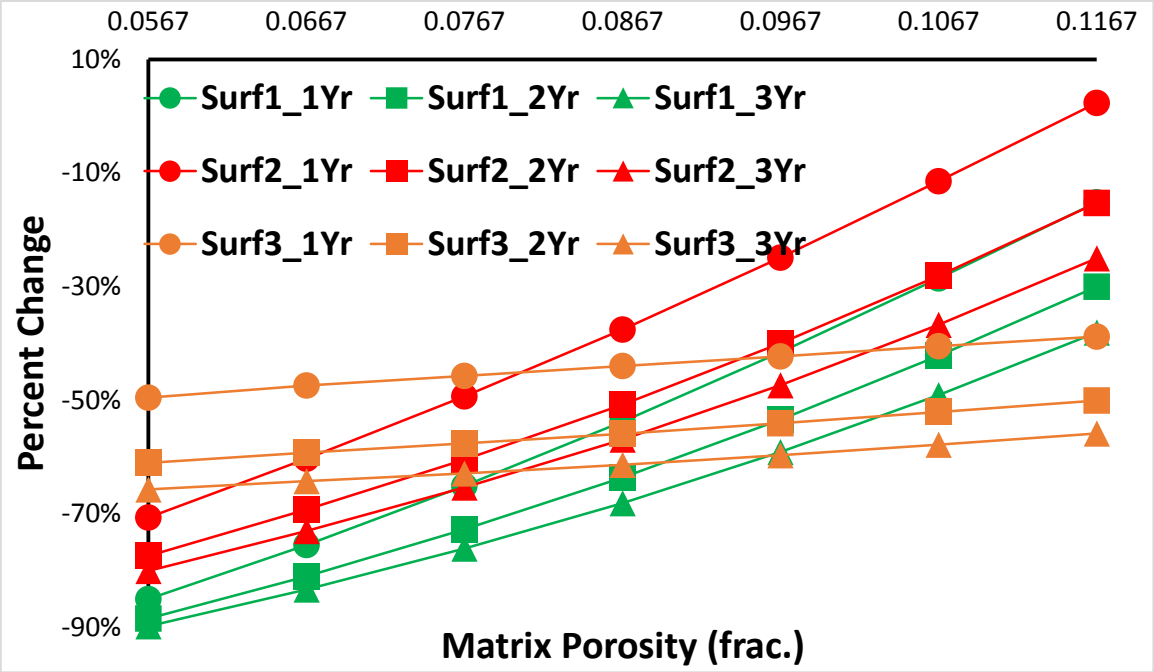

Fig. 77 - Effect of ϕ_m to cumulative water production

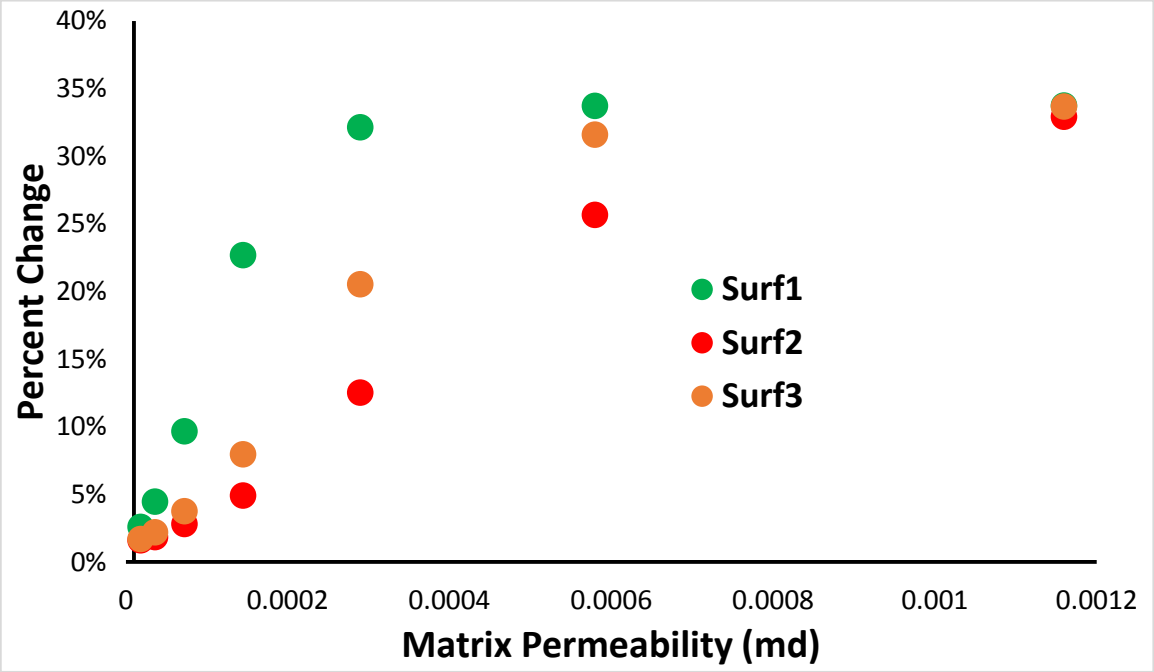

Fig. 78 - Effect of k_m to initial oil production rate

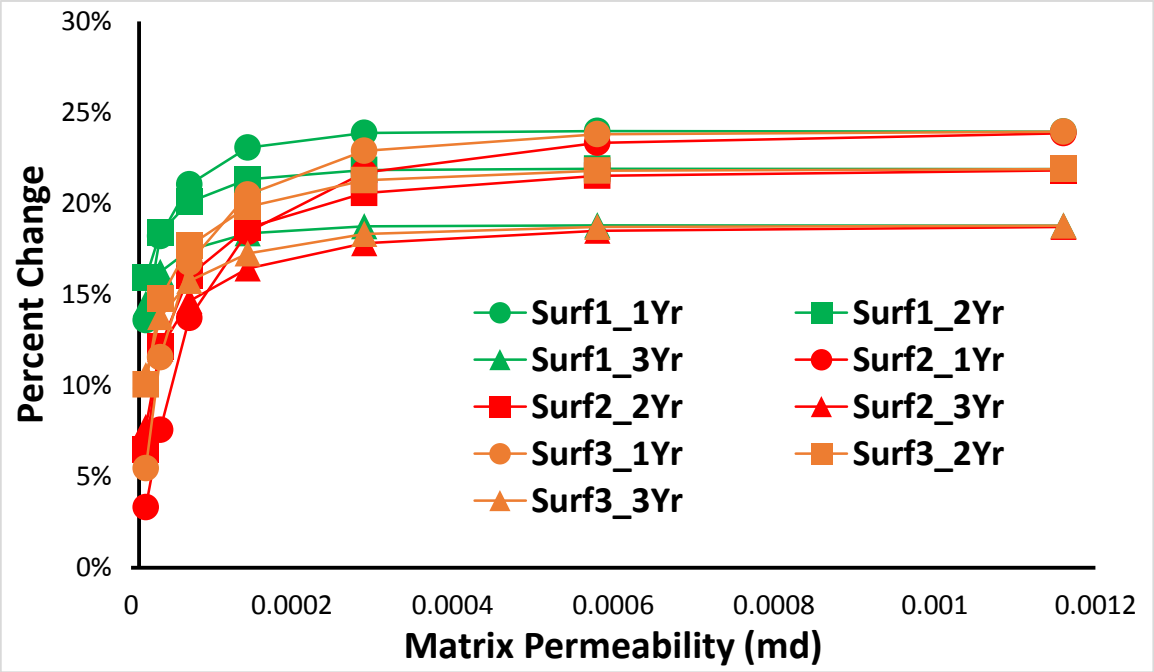

Fig. 79 - Effect of k_m to cumulative oil production

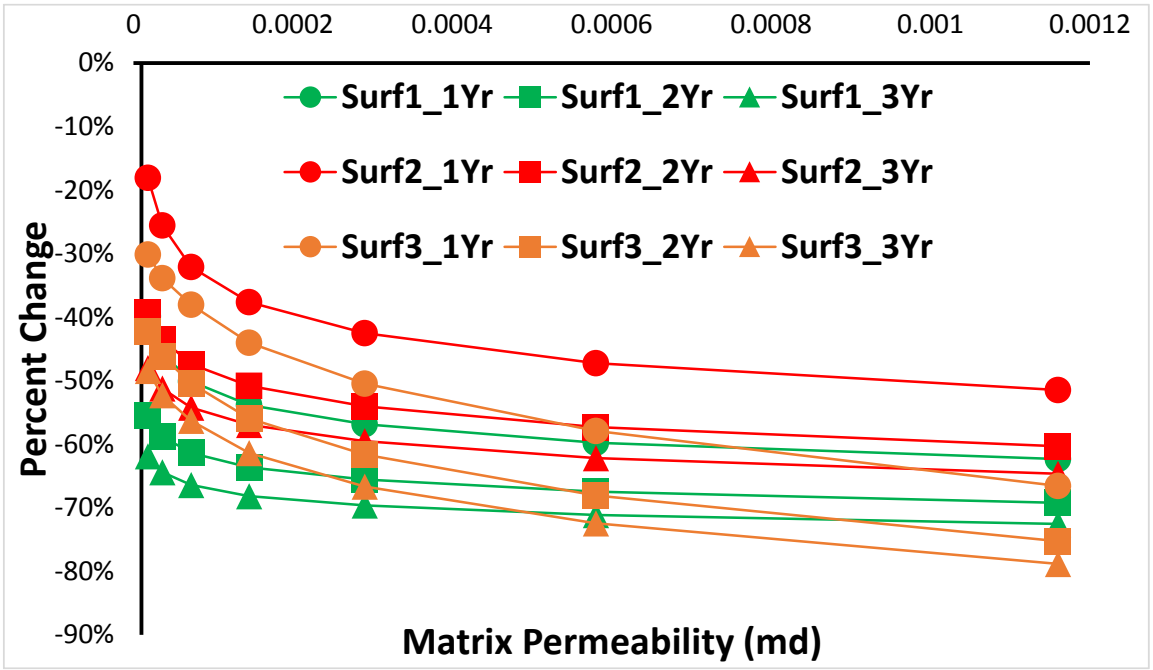

Fig. 80 - Effect of k_m to cumulative water production

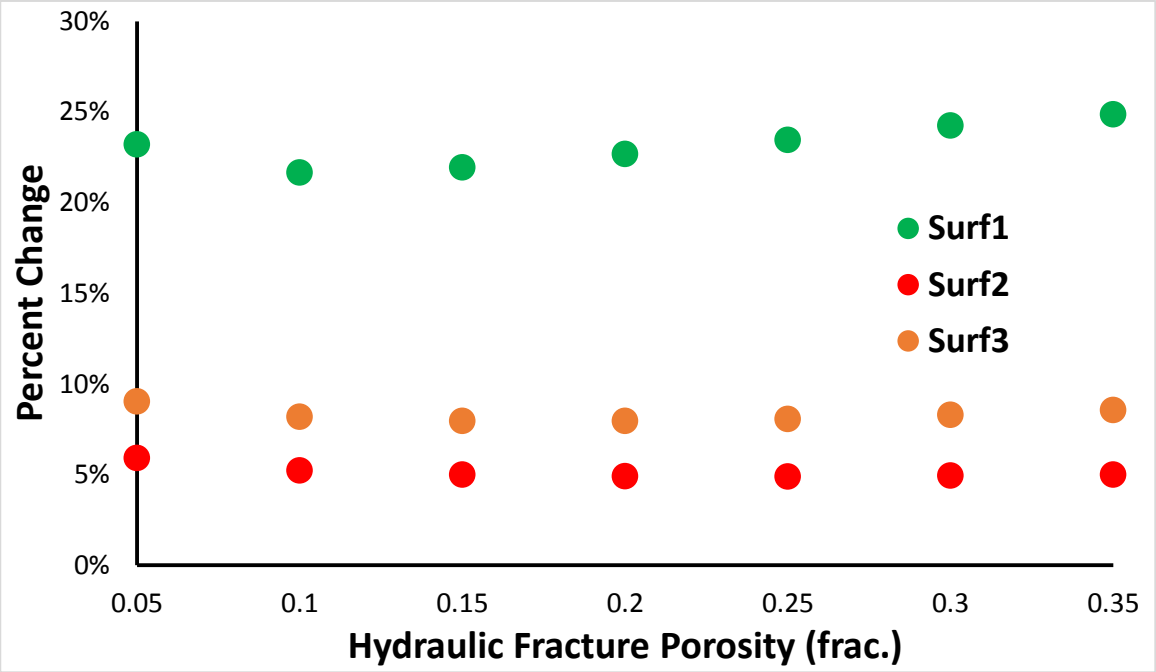

Fig. 81 – Effect of ϕ_{HF} to initial oil production rate

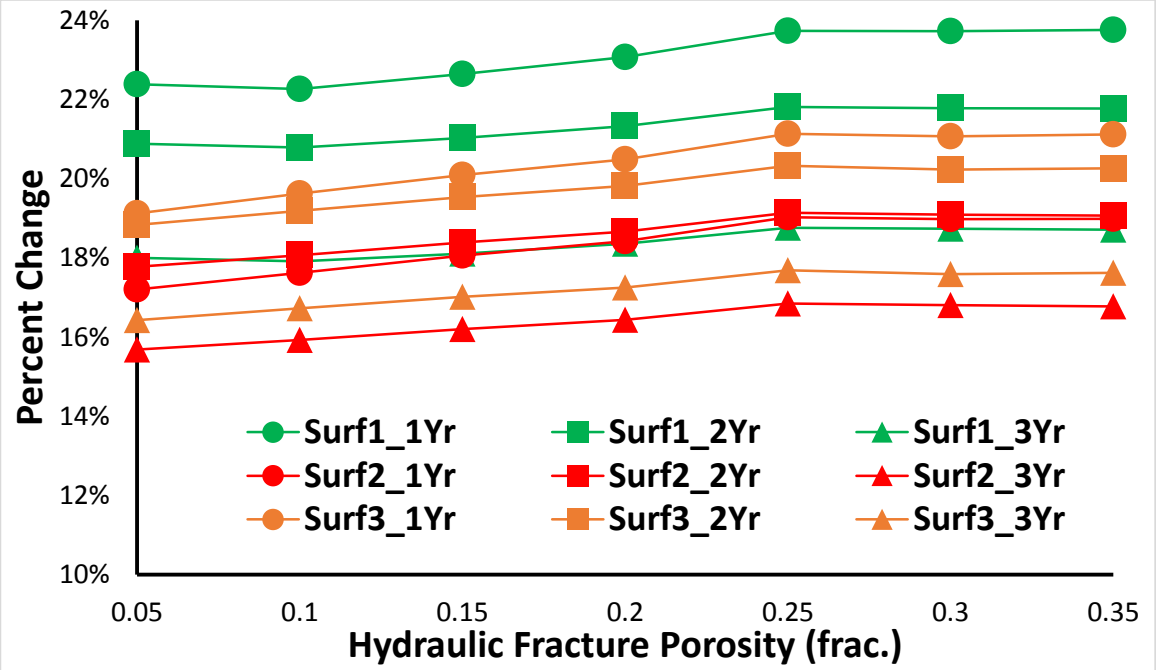

Fig. 82 - Effect of ϕ_{HF} to cumulative oil production

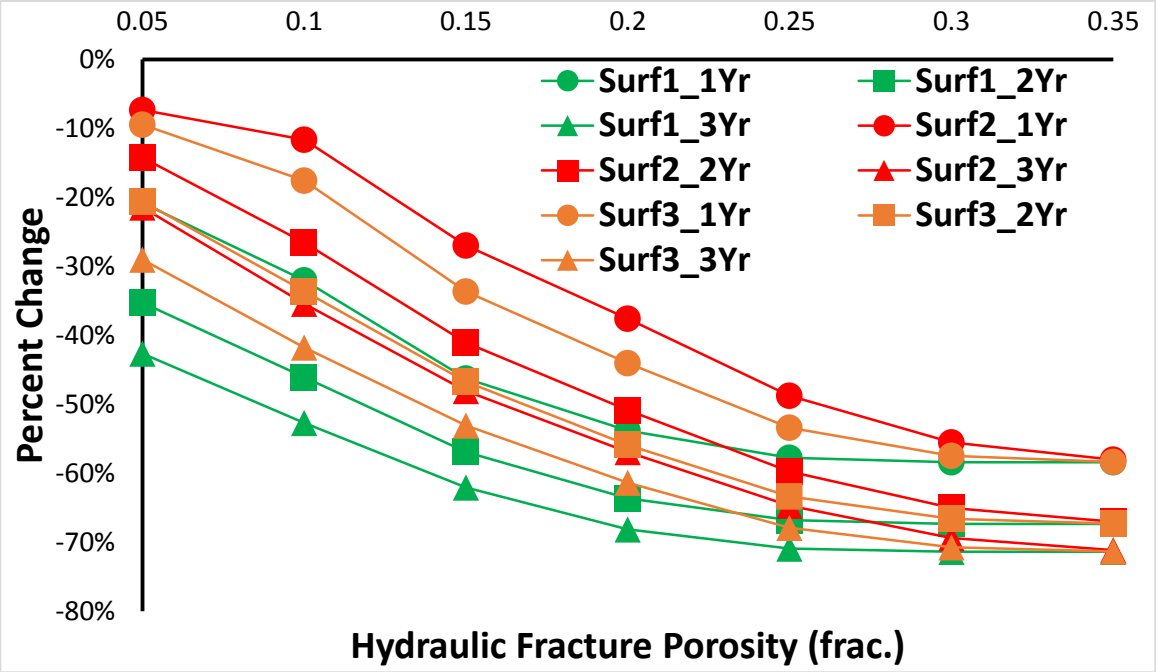

Fig. 83 - Effect of ϕ_{HF} to cumulative water production

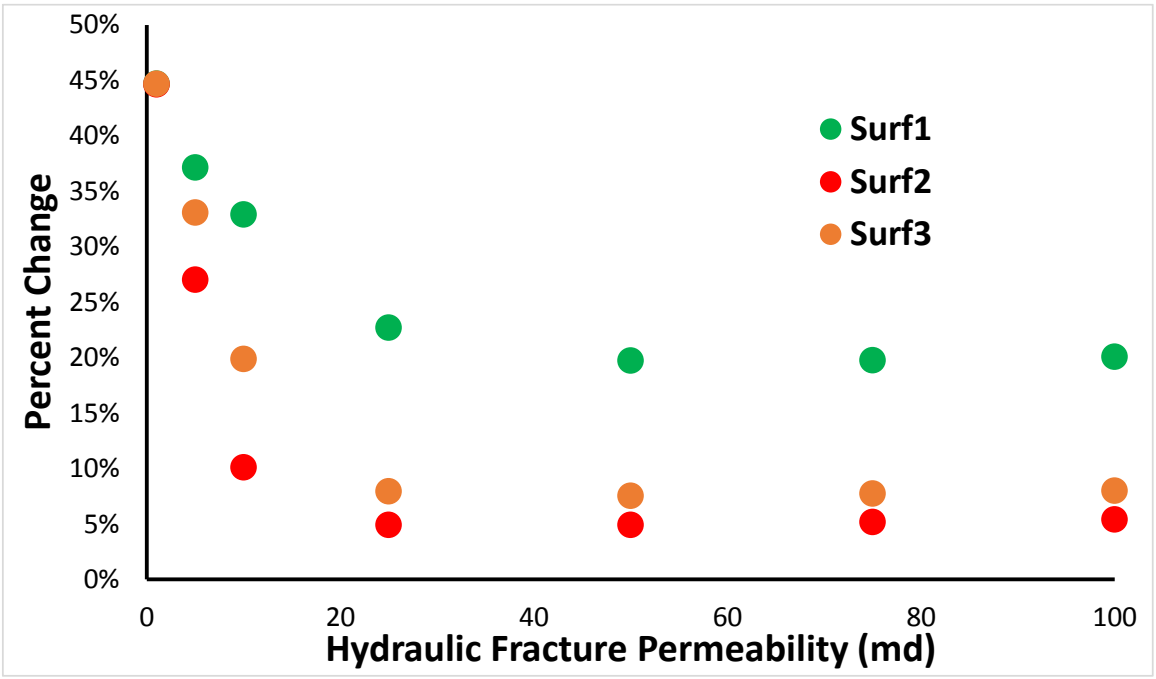

Fig. 84 - Effect of k_{HF} to initial oil production rate

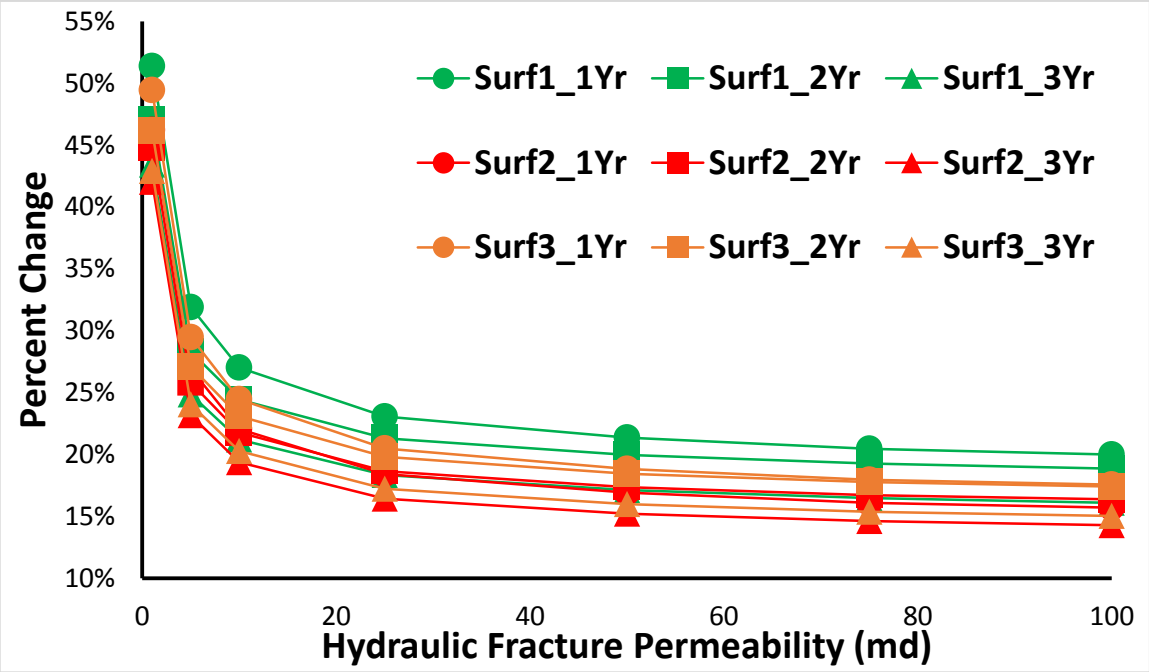

Fig. 85 - Effect of k_{HF} to cumulative oil production

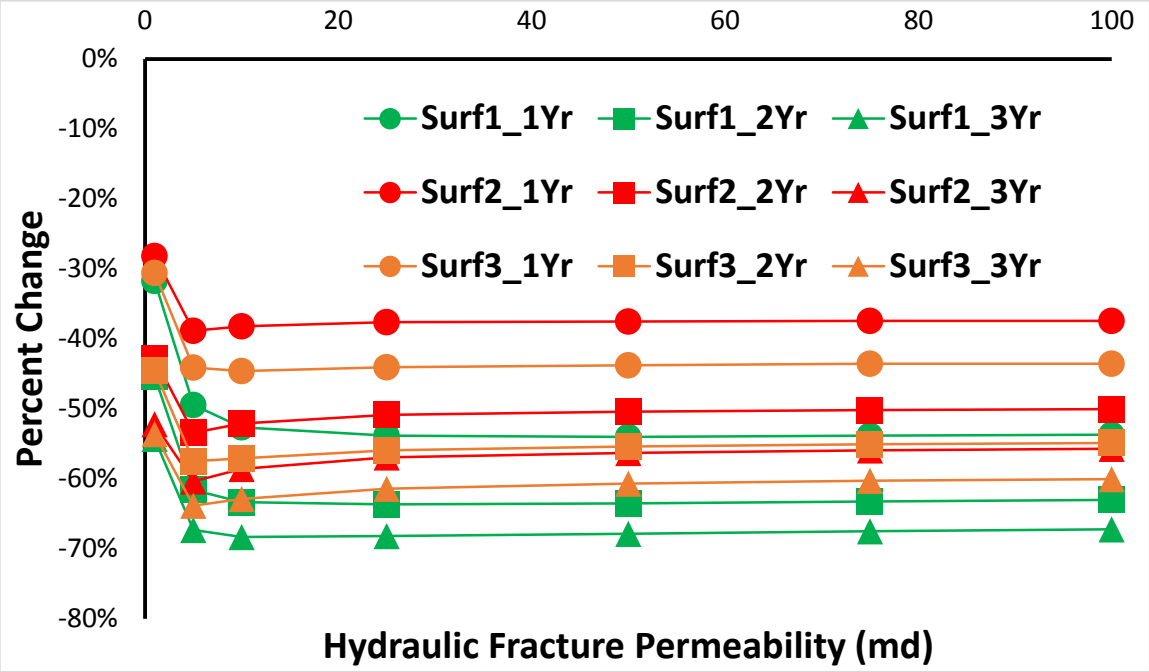

Fig. 86 - Effect of k_{HF} to cumulative water production

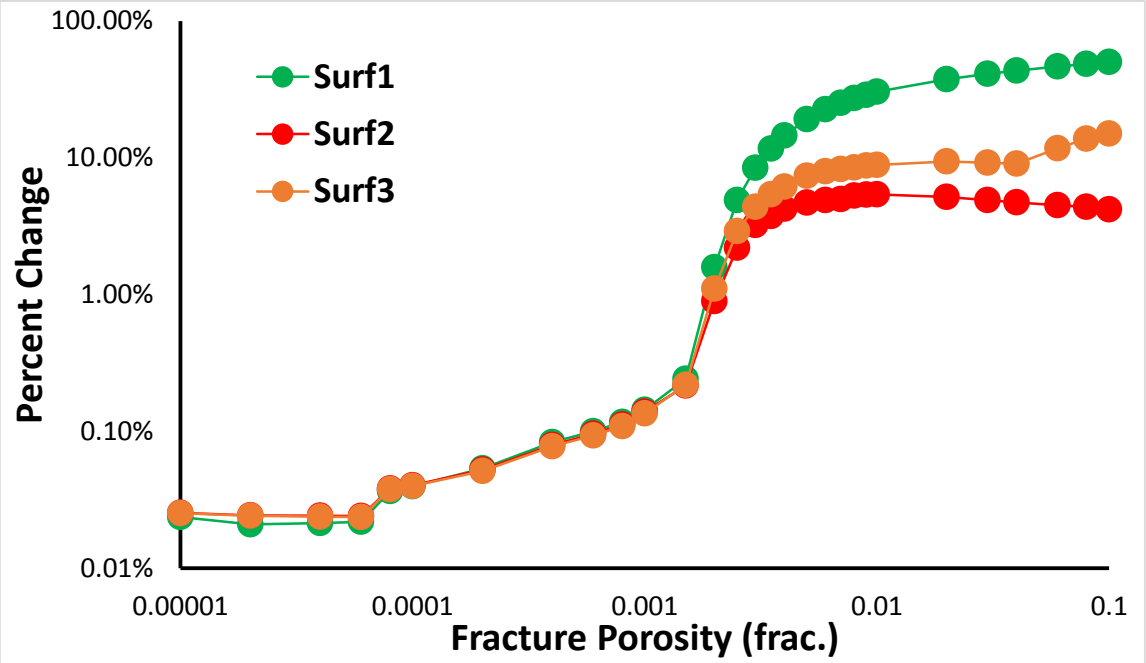

Fig. 87 - Effect of ϕ_F to initial oil production rate

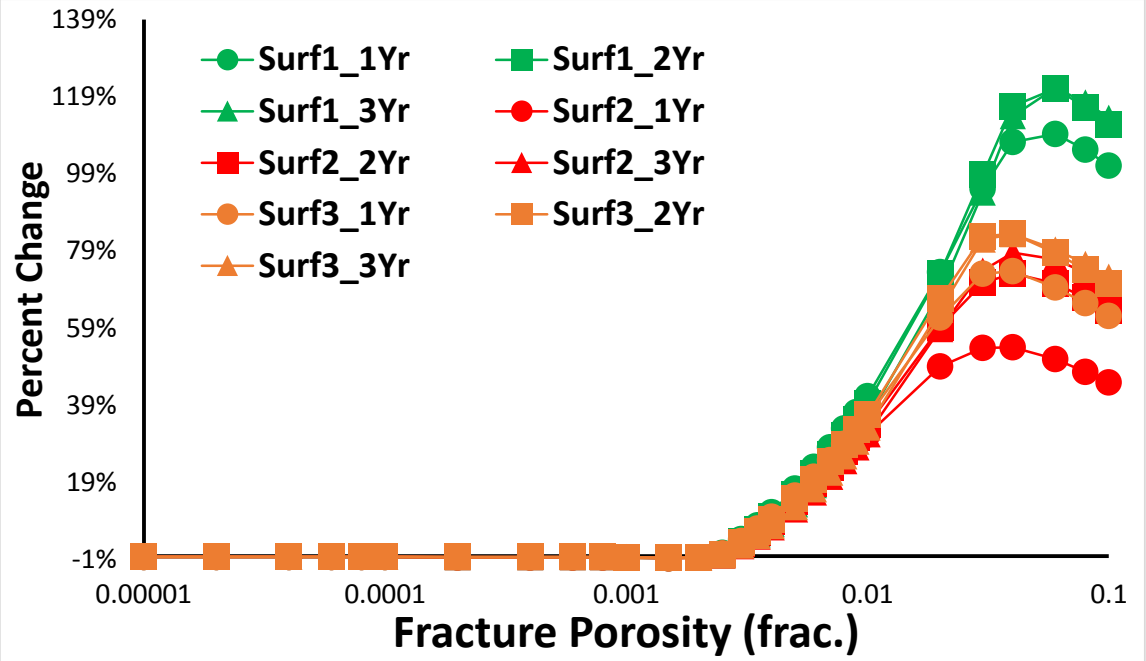

Fig. 88 - Effect of ϕ_F to cumulative oil production

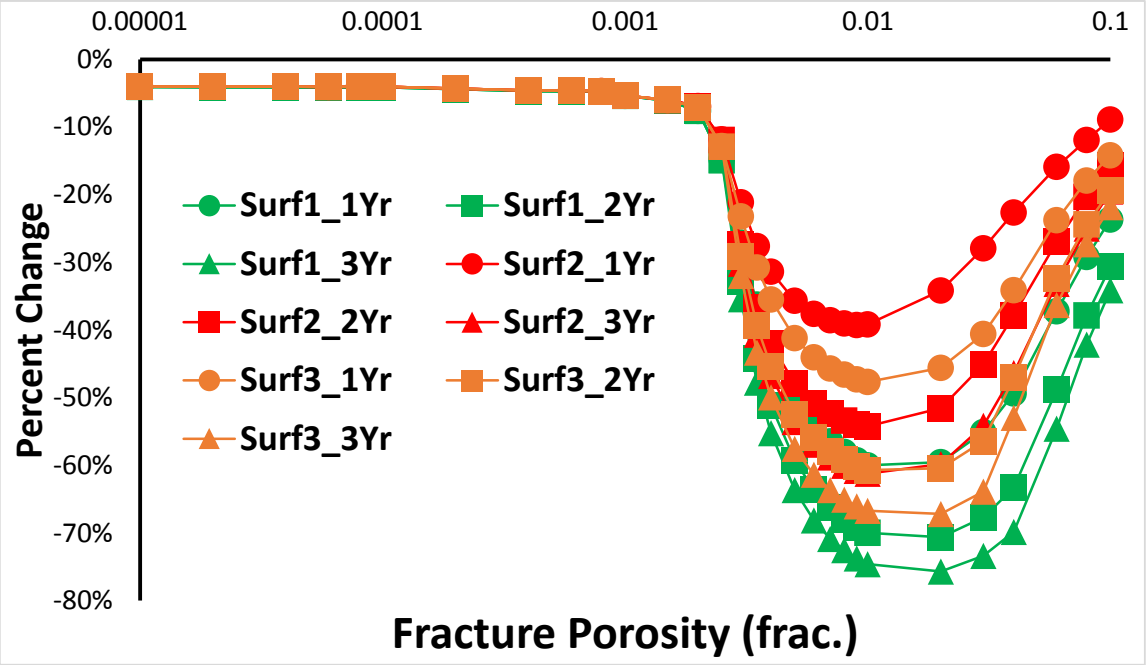

Fig. 89 - Effect of ϕ_F to cumulative water production

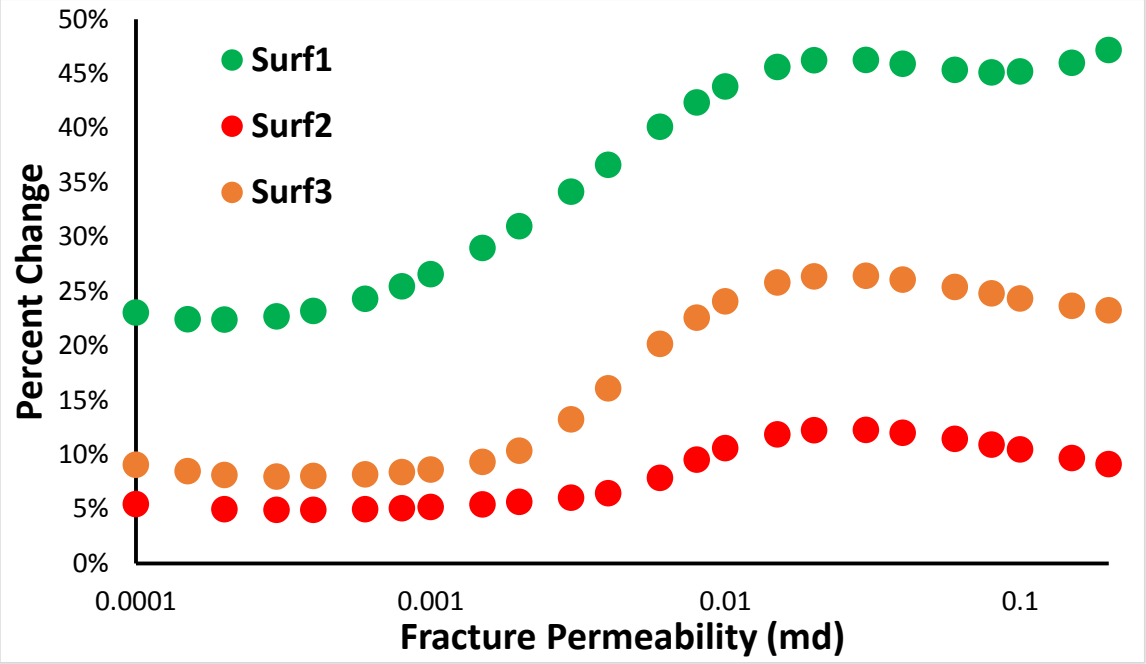

Fig. 90 - Effect of k_F to initial oil production rate

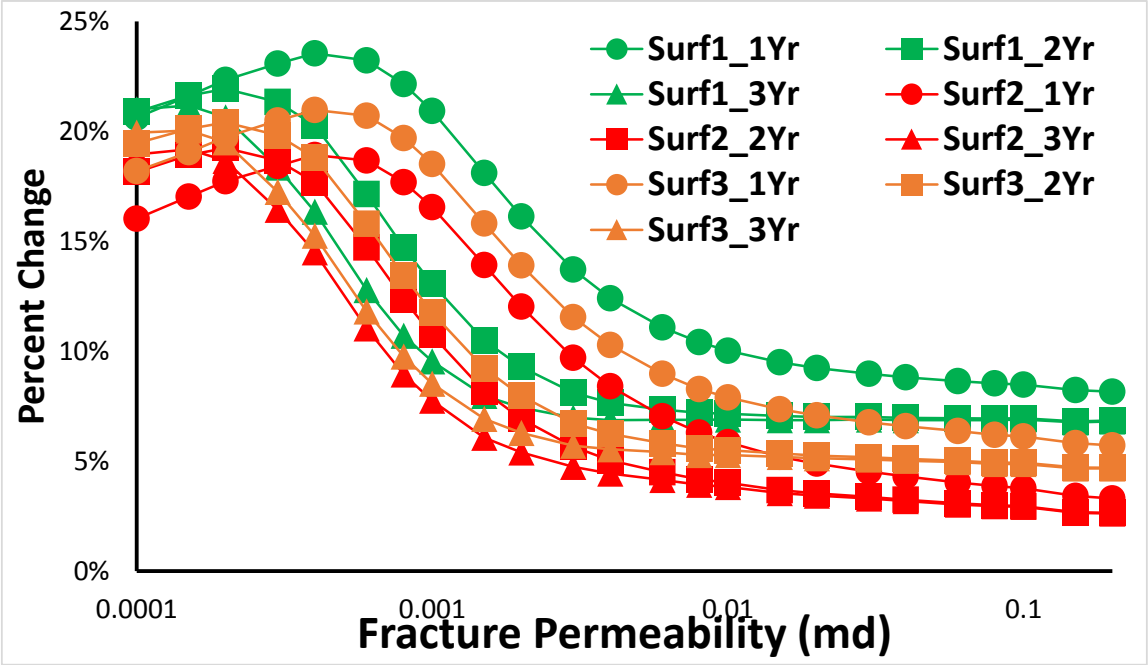

Fig. 91 - Effect of k_F to cumulative oil production

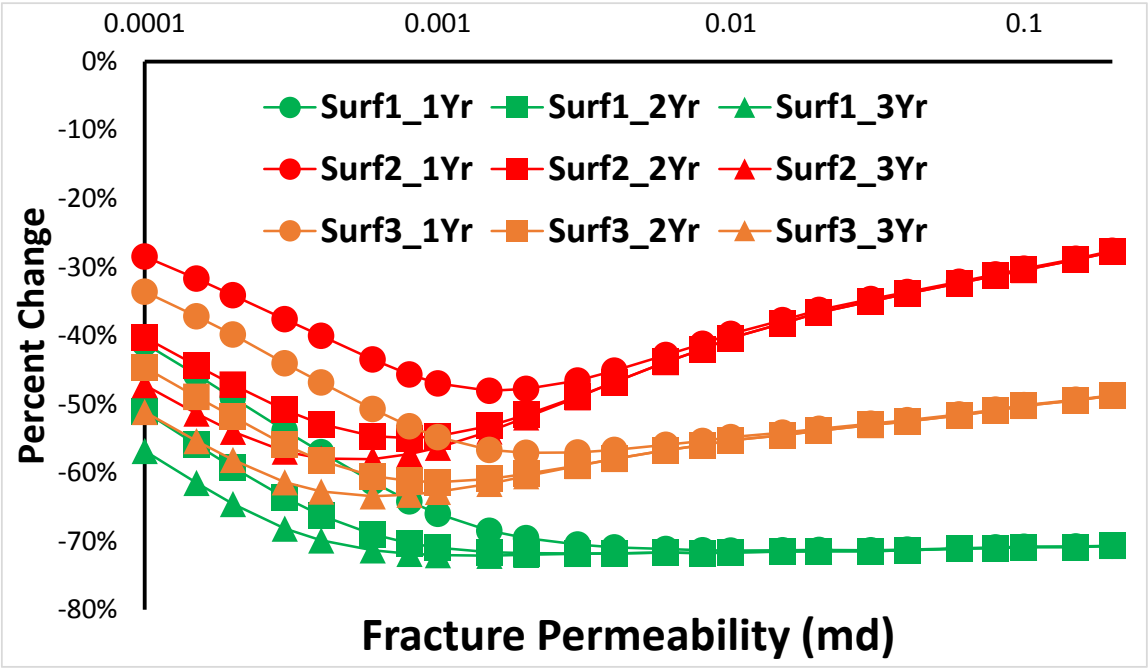

Fig. 92 - Effect of k_F to cumulative water production

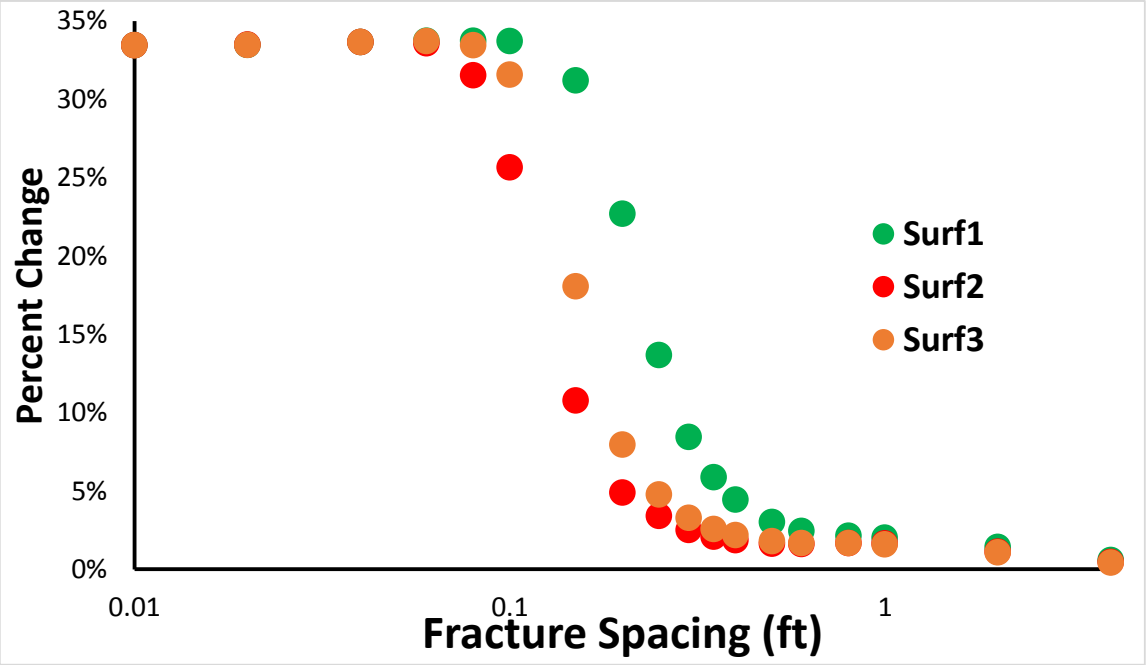

Fig. 93 - Effect of fracture spacing to initial oil production rate

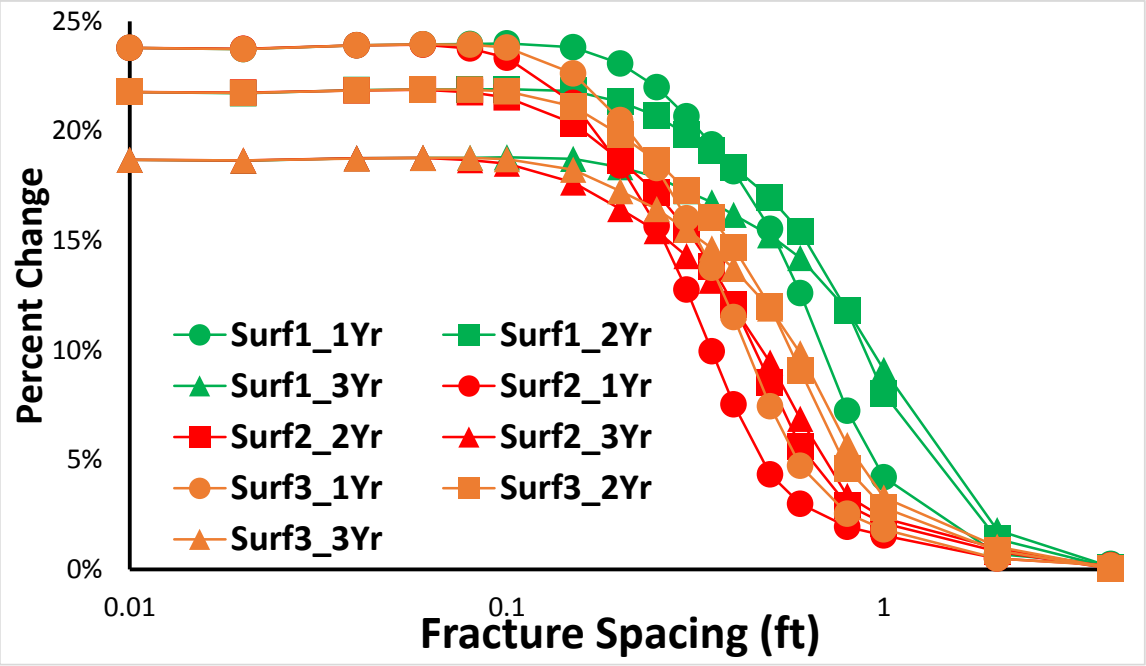

Fig. 94 - Effect of fracture spacing to cumulative oil production

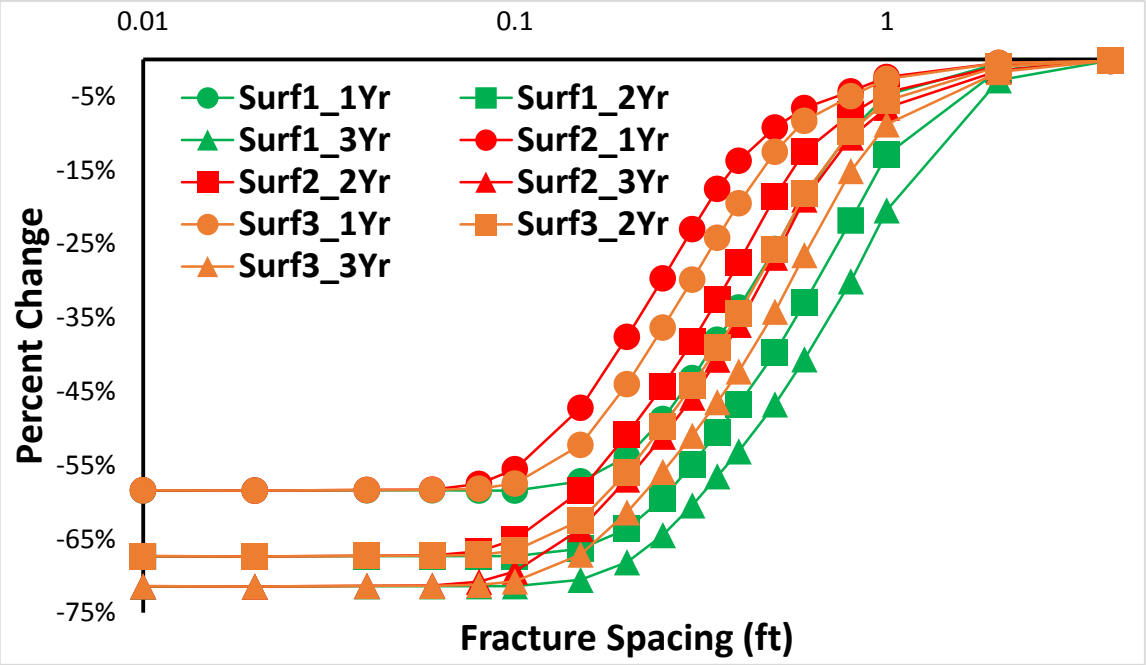

Fig. 95 - Effect of fracture spacing to cumulative water production

7. CONCLUSIONS AND RECOMMENDATIONS

7.1 Conclusions

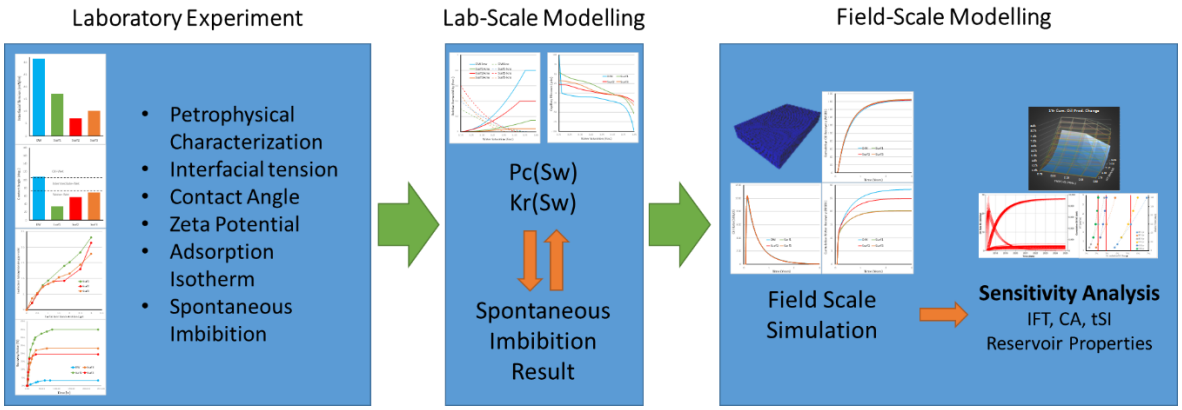

Fig. 96 - Workflow of complete surfactant-assisted spontaneous imbibition (SASI) assessment

This study was conducted with the goal in mind of constructing a complete workflow of assessing surfactant-assisted spontaneous imbibition with the ability of providing a glance of the field-scale impact of the method. The workflow proposed and tested in this work is shown in Fig. 96. The workflow is comprised of three big parts, laboratory experiment, lab-scale modelling, and field-scale modelling. Four fluid systems, three surfactants and one base case, were tested and as shown previously, the concern of water-blockage on SASI field-implementation was dismissed as better well performance in term of both rate and cumulative recovery was observed. To conclude, a list of several conclusions that were made throughout the study is presented below:

1. Addition of surfactant into an oil/water/rock system reduces the IFT of oil and water, however the degree of reduction from surfactants tested in this work is far less than those surfactants designed for conventional water-flooding.

2. Addition of surfactant alters the wettability state of the rock surface where on the contact angle measurement done in this work, the initially oil-wet Eagle Ford rock was transformed to a water-wet surface.
3. Addition of surfactant increases the stability of water layer forming around the rock particle which can be translated to a stronger water-wet state.
4. Surfactant adsorption was observed and measured with the result aligns to the concept of adsorption-induced wettability alteration. Higher surfactant adsorption value correlates to stronger wettability alteration performance.
5. Surfactant addition enhances oil production from capillary-driven spontaneous imbibition in both quantity and rate as higher oil production rate as well as higher cumulative recovery observed on the spontaneous imbibition experiment.
6. Wettability alteration plays a dominant role to the oil production from SASI as surfactant that altered wettability the most also produced the most oil.
7. Modelling of SASI can be done by representing the effect of surfactant as an alteration in flow properties in the form of capillary pressure and relative permeability curves modification. Surfactant adsorption then can be used as the controlling factor that controls the degree of alteration.
8. Lab-scale modelling through the process of history-match combined with CT-based rock digitalization enables the construction of the capillary pressure and relative permeability curves of each fluid system independent to the heterogeneity of rock sample used in the spontaneous imbibition laboratory experiment.
9. Field-scale impact can be assessed by applying the properties obtained from laboratory experiments and laboratory-scale modelling on a field model.

10. SASI improves the initial oil production rate by 22% and three years cumulative oil recovery by 18.4% when compared to the base case of no surfactant.
11. The effectivity of SASI on a field-scale varies on different reservoir properties as shown by the sensitivity analysis section of this work.

7.2 Recommendations

During the execution of this work, there were some possible room of improvement that was found but was not executed due to time and/or equipment constraint. Presented in this section is a list of what could have been done for a future work of improving this workflow:

1. Better resolution on the data acquisition of the volume of oil produced on the spontaneous imbibition experiment should be implemented as the whole workflow presented was virtually based on this data.
2. Porosity measurement on each rock sample used would improve the accuracy of recovery factor calculation and also the accuracy of the digital rock model.
3. Field scale model derived from history-matching process of a real well would improve the accuracy of the field-scale model.
4. More imbibition case should be modeled and upscale, in order to build a correlation between measured surfactant properties, IFT, CA, ZP, adsorption isotherm and the surfactant performance on the spontaneous imbibition.

5. Based on the correlation from previous point, a sensitivity analysis with surfactant properties as the control variable should be done to observe the effect of different surfactant properties to the effectivity of SASI on a field-scale basis.

NOMENCLATURE

Ads	Amount of surfactant adsorbed in one grid block
AFM	Atomic Force Microscopy
C	Pore geometry constant
CA	Contact Angle
CA_m	Measured contact angle
CO	Cumulative oil production
CW	Cumulative water production
CT	Computed Tomography
ΔP	Oil-phase and water-phase pressure difference
$\Delta\rho$	Density difference
g	Gravity
h	Vertical length
HU	Hounsfield Unit
θ	Contact angle
θ_A	Surfactant adsorption value on rock
IFT	Interfacial Tension
k	Permeability
k_F	Fracture permeability
k_{HF}	Hydraulic fracture permeability
k_m	Matrix permeability
k_{ro}	Oil relative permeability

k_{rw}	Water relative permeability
L	Imbibition rock sample length
μ	HU of each pixel
μ_a	HU of air
μ_o	oil viscosity
μ_w	water viscosity
μ_w	HU of water
OOIP	Original Oil In Place
OPEC	Organization of Petroleum Exporting Country
OR	Initial oil production rate
OV	Fracture oil volume
Pc	Capillary pressure
P_i	Initial pressure
r	Pore radius
ρ_f	Fluid density
ρ_r	Rock density
ρ_{surf}	Surfactant density
SASI	Surfactant-Assisted Spontaneous Imbibition
σ	oil-water interfacial tension
SO	Oil saturation in one grid block
S_w	Water saturation
S_{wi}	Initial water saturation

TAN	Total Acid Number
TBN	Total Basic Number
ϕ	Porosity
ϕ_F	Fracture porosity
ϕ_{HF}	Hydraulic fracture porosity
ϕ_m	Matrix porosity
ϕ_{surf}^{i}	Initial surfactant concentration
ϕ_{surf}^{f}	Final Surfactant concentration
US	United States
V_{surf}	Surfactant volume
w_{rock}	Weight of rock sample
x_{HF}	Hydraulic fracture half-length
ZP	Zeta potential

REFERENCES

Adibhatia, B., Sun, X., and Mohanty, K.K. 2005. Numerical Studies of Oil Production from Initially Oil-Wet Fracture Blocks by Surfactant Brine Imbibition. Paper presented at the SPE International Improved Oil Recovery Conference in Asia Pacific, Kuala Lumpur, Malaysia. Society of Petroleum Engineers.

Advani, S.H., Khattab, H., and Lee, J.K. 1985. Hydraulic Fracture Geometry Modeling, Prediction, and Comparisons. Paper presented at the SPE/DOE Low Permeability Gas Reservoirs Symposium, Denver, Colorado. Society of Petroleum Engineers. DOI: 10.2118/13863-MS.

Ahmadi, M.A. and Shadizadeh, S.R. 2013. Experimental Investigation of Adsorption of a New Nonionic Surfactant on Carbonate Minerals. *Fuel* **104**: 462-467. DOI: https://doi.org/10.1016/j.fuel.2012.07.039

Alvarez, J.O., Saputra, I.W.R., and Schechter, D.S. 2017a. The Impact of Surfactant Imbibition and Adsorption for Improving Oil Recovery in the Wolfcamp and Eagle Ford Reservoirs. Paper presented at the SPE Annual Technical Conference and Exhibition, San Antonio, Texas. Society of Petroleum Engineers.

Alvarez, J.O., Saputra, I.W.R., and Schechter, D.S. 2017b. Potential of Improving Oil Recovery with Surfactan Additives to Completion Fluids for the Bakken. *Energy Fuels* **31** (6): 5982-5994.

Alvarez, J.O. and Schechter, D.S. 2016. Altering Wettability in Bakken Shale by Surfactant Additives and Potential of Improving Oil Recovery During Injection of Completion Fluids. Paper presented at the SPE Improved Oil Recovery Conference, Tulsa, Oklahoma. Society of Petroleum Engineers.

Alvarez, J.O. and Schechter, D.S. 2017. Wettability Alteration and Spontaneous Imbibition in Unconventional Liquid Reservoirs by Surfactant Additives. *SPE Reservoir Evaluation & Engineering* **20** (01): 107-117.

Alvarez, J.O., Tovar, F.D., and Schechter, D.S. 2017. Improving Oil Recovery in Unconventional Liquid Reservoirs by Soaking-Flowback Production Schedule with Surfactant Additives. Paper presented at the SPE Liquids-Rich Basins Conference - North America, Midland, Texas. Society of Petroleum Engineers.

Amott, E. 1959. Observations Relating to the Wettability of Porous Rock. In: Society of Petroleum Engineers.

Amyx, J.W., Bass, D.M., and Whiting, R.L. 1960. *Petroleum Reservoir Engineering: Physical Properties*: McGraw-Hill College. Original edition. ISBN.

Andersen, P.O., Evje, S., and Kleppe, H. 2014. A Model for Spontaneous Imbibition as a Mechanism for Oil Recovery in Fractured Reservoirs. *Transport in Porous Media* **101** (2): 299-331.

Anderson, W. 1986. Wettability Literature Survey- Part 2: Wettability Measurement. DOI: 10.2118/13933-PA

Andreas, J.M., Hauser, E.A., and Tucker, W.B. 1937. Boundary Tension by Pendant Drops1. *The Journal of Physical Chemistry* **42** (8): 1001-1019. DOI: 10.1021/j100903a002

Aronofsky, J.S., Masse, L., and Natanson, S.G. 1958. A Model for the Mechanism of Oil Recovery from the Porous Matrix Due to Water Invasion in Fractured Reservoirs. *Petroleum Transactions* **213**: 17-19.

Austad, T. and Standnes, D.C. 2003. Spontaneous Imbibition of Water into Oil-Wet Carbonates. *Journal of Petroleum Science & Engineering* **39** (3-4): 363-376.

Babadagli, T., Al-Bemani, A., and Boukadi, F. 1999. Analysis of Capillary Imbibition Recovery Considering the Simultaneous Effects of Gravity, Low Ift, and Boundary Conditions. Paper presented at the SPE Asia Pacific Improved Oil Recovery Conference, Kuala Lumpur, Malaysia. Society of Petroleum Engineers.

Bashfort, F. and Adams, J.C. 1883. *An Attempt to Test the Theories of Capillary Action: By Comparing the Theoretical and Measured Forms of Drops of Fluid*: University Press. Original edition. ISBN.

Bech, N., Jensen, O.K., and Nielsen, B. 1991. Modeling of Gravity-Imbibition and Gravity-Drainage Processes: Analytic and Numerical Solutions. *SPE Reservoir Engineering* **6** (01): 129-136.

Behbahani, H.S. and Blunt, M.J. 2005. Analysis of Imbibition in Mixed-Wet Rocks Using Pore-Scale Modeling. *Society of Petroleum Engineers Journal* **10** (04): 466-474.

Chahardowli, M. and Bruining, H. 2014. Modeling of Wettability Alteration During Spontanous Imbibition of Mutually Soluble Solvents in Mixed-Wet Fractured Reservoirs. In *COMSOL Conference*. Cambridge, UK.

Chahardowli, M., Zholdybayeva, A., Farajzadeh, R. et al. 2013. Solvent-Enhanced Spontaneous Imbibition in Fractured Reservoirs. Paper presented at the EAGE Annual Conference & Exhibition incorporating SPE Europec, London, UK. Society of Petroleum Engineers.

Cho, Y., Eker, E., Uzun, I. et al. 2016. Rock Characterization in Unconventional Reservoirs: A Comparative Study of Bakken, Eagle Ford, and Niobrara Formations. Paper presented at the SPE Low Perm Symposium, Denver, Colorado, USA. Society of Petroleum Engineers. DOI: 10.2118/180239-MS.

Craig, F.F. 1993. *The Reservoir Engineering Aspects of Waterflooding*: Henry L. Doherty Memorial Fund of AIME. Original edition. ISBN 9780895202024.

Cuiec, L., Bourbiaux, B., and Kalaydjian, F. 1994. Oil Recovery by Imbibition in Low-Permeability Chalk. *SPE Formation Evaluation* **9** (03): 200-208.

Curbelo, F., I. C. Garnica, A., and L. Barros Neto, E. 2013. *Enhanced Oil Recovery and Adsorption of Ionic Surfactant* Original edition. ISBN.

Dąbrowski, A. 2001. Adsorption — from Theory to Practice. *Advances in Colloid and Interface Science* **93** (1): 135-224. DOI: https://doi.org/10.1016/S0001-8686(00)00082-8

Delshad, M., Najafabadi, N.F., Anderson, G. et al. 2009. Modeling Wettability Alteration by Surfactants in Naturally Fractured Reservoirs. *SPE Reservoir Evaluation & Engineering* **12** (03): 361-370.

Dominguez, A., Fernandez, A., Gonzalez, N. et al. 1997. Determination of Critical Micelle Concentration of Some Surfactants by Three Techniques. *Journal of Chemical Education* **74** (10): 1227. DOI: 10.1021/ed074p1227

Drelich, J., Fang, C., and White, C.L. 2002. *Measurement of Interfacial Tension in Fluid-Fluid Systems* Original edition. ISBN.

Energy, D.o. 2014. *Updates to the Eia Eagle Ford Play Maps*, by EIA. EIA.

Energy, D.o. 2017. *Us Tight Oil Production*, by EIA. EIA.

Fan, L., Thompson, J., Atwood, K. et al. 2011. An Integrated Approach for Understanding Oil and Gas Reserves Potential in Eagle Ford Shale Formation. Paper presented at the Canadian Unconventional Resources Conference, Calgary, Alberta, Canada. Society of Petroleum Engineers. DOI: 10.2118/148751-MS.

Gdanski, R.D. and Funkhouser, G.P. 2011. Surfactant Modeling for Insight into Load-Recovery Enhancement for Fracturing Treatment. Paper presented at the SPE International Symposium on Oilfield Chemistry, The Woodlands, Texas. Society of Petroleum Engineers.

Gupta, A., Xu, M., Dehghanpour, H. et al. 2017. Experimental Investigation for Microscale Stimulation of Shales by Water Imbibition During the Shut-in Periods. Paper presented at the SPE Unconventional Resources Conference, Calgary, Alberta, Canada. Society of Petroleum Engineers. DOI: 10.2118/185058-MS.

Hirasaki, G. and Zhang, D.L. 2004. Surface Chemistry of Oil Recovery from Fractured, Oil-Wet, Carbonate Formations. DOI: 10.2118/88365-PA

Ingle, J.D.J. and Crouch, S.R. 1988. *Spectrochemical Analysis*: Old Tappan, NJ (US); Prentice Hall College Book Division. Original edition. ISBN.

Instruments, M. 2011. *Zetasizer Nano Serles Tech. Note. MRK654-01*. **2**: 1-6.

Jadhunandan, P.P. and Morrow, N.R. 1995. Effect of Wettability on Waterflood Recovery for Crude-Oil/Brine/Rock Systems. *SPE Reservoir Engineering*: 40-46. DOI: 10.2118/22597-PA

Kalaei, M.H., Green, D.W., and Willhite, G.P. 2012. A New Dynamic Wettability Alteration Model for Oil-Wet Cores During Surfactant Solution Imbibition. Paper presented at the SPE Improved Oil Recovery Symposium, Tulsa, Oklahoma. Society of Petroleum Engineers.

Kathel, P. and Mohanty, K.K. 2013. Wettability Alteration in a Tight Oil Reservoir. *Energy Fuels* **27** (11): 6460-6468.

Kazemi, H. and Jr., L.S.M. 1979. Numerical Simulation of Water Imbibition in Fractured Cores. *Society of Petroleum Engineers Journal* **19** (03): 175-182.

Kim, J., Zhang, H., Sun, H. et al. 2016. Choosing Surfactants for the Eagle Ford Shale Formation: Guidelines for Maximizing Flowback and Initial Oil Recovery. Paper presented at the SPE Low Perm Symposium, Denver Colorado. Society of Petroleum Engineers.

Kumar, K., Dao, E.K., and Mohanty, K.K. 2005. Atomic Force Microscopy Study of Wettability Alteration. Paper presented at the SPE International Symposium on Oilfield Chemistry, The Woodlands, Texas. Society of Petroleum Engineers.

Li, K. and Horne, R.N. 2002. A General Scaling Method for Spontaneous Imbibition. Paper presented at the SPE Annual Technical Conference and Exhibition, San Antonio, Texas. Society of Petroleum Engineers.

Liang, T., Achour, S.H., Longoria, R.A. et al. 2016. Identifying and Evaluating Surfactant Additives to Reduce Water Blocks after Hydraulic Fracturing for Low Permeability Reservoirs. Paper presented at the SPE Improved Oil Recovery Conference, Tulsa, Oklahoma, USA. Society of Petroleum Engineers. DOI: 10.2118/179601-MS.

Lindsay, G., Miller, G., Xu, T. et al. 2018. Production Performance of Infill Horizontal Wells Vs. Pre-Existing Wells in the Major Us Unconventional Basins. Paper presented at the SPE Hydraulic Fracturing Technology Conference and Exhibition, The Woodlands, Texas, USA. Society of Petroleum Engineers. DOI: 10.2118/189875-MS.

Lord, D.L. and Buckley, J.S. 2002. An Afm Study of the Morphological Features That Affect Wetting at Crude Oil-Water-Mica Interfaces. *Colloids and Surface A: Physicochemical and Engineering Aspects* **206** (1-3): 531-546.

Ma, S., Morrow, N.R., and Zhang, X. 1997. Generalized Scaling of Spontaneous Imbibition Dat for Strongly Water-Wet Systems. *Journal of Petroleum Science & Engineering* **18** (3-4): 165-178.

Makhanov, K., Dehghanpour, H., and Kuru, E. 2013. Measuring Liquid Uptake of Organic Shales: A Workflow to Estimate Water Loss During Shut-in Periods. Paper presented at the SPE Unconventional Resources Conference Canada, Calgary, Alberta, Canada. Society of Petroleum Engineers. DOI: 10.2118/167157-MS.

Massicano, F., Massicano, A.V., da Silva, N.G. et al. 2009. Analysis of Ct and Pet/Spect Images for Dosimetry Calculation. In *International Nuclear Atlantic Conference, Brazil. ASSOCIAÇÃO BRASILEIRA DE ENERGIA NUCLEAR. doi*:978-985.

Mattax, C.C. and Kyte, J.R. 1962. Imbibition Oil Recovery from Fractured, Water-Drive Reservoir. *Society of Petroleum Engineers Journal* **2** (02): 177-184.

Menouar, H. and Knapp, R.M. 1980. Numerical Simulation of the Imbibition Process in Fractured Reservoirs. Paper presented at the SPE Annual Technical Conference and Exhibition, Dallas, Texas. Society of Petroleum Engineers.

Metrohm. 905 Titrando. Accessed 02/24/2018.

Mirchi, V., Saraji, S., Goual, L. et al. 2015. Dynamic Interfacial Tension and Wettability of Shale in the Presence of Surfactants at Reservoir Conditions. *Fuel* **148**: 127-138. DOI: https://doi.org/10.1016/j.fuel.2015.01.077

Morrow, N.R. 1990. Wettability and Its Effect on Oil Recovery. *Journal of Petroleum Technology* **42** (12): 1476-1484.

Morrow, N.R. and Mason, G. 2001. Recovery of Oil by Spontaneous Imbibition. *Current Opinion in Colloid & Interface Science* **6** (4): 321-337.

Morsy, S., Zhou, J., Lant, K. et al. 2014. Optimizing Surfactant Additives for Enhanced Well Stimulation in Bakken Formation. Paper presented at the SPE International Symposium and Exhibition on Formation Damage Control, Lafayette, Louisiana. Society of Petroleum Engineers.

Nelson, P.H. 2009. Pore-Throat Sizes in Sandstones, Tight Sandstones, and Shales. *AAPG Bulletin* **93** (3): 329-340. DOI: 10.1306/10240808059

Neog, A. and Schechter, D.S. 2016. Investigation of Surfactant Induced Wettability Alteration in Wolfcamp Shale for Hydraulic Fracturing and Eor Applications. Paper presented at the SPE Improved Oil Recovery Conference, Tulsa, Oklahoma. Society of Petroleum Engineers.

Nguyen, D., Phan, T., Phan, J. et al. 2017. Investigation of Oil Adhesion to Shale Rocks for Eor. Paper presented at the SPE International Conference on Oilfield Chemistry, Tulsa, Oklahoma. Society of Petroleum Engineers.

Nguyen, D., Wang, D., Oladapo, A. et al. 2014. Evaluation of Surfactants for Oil Recovery Potential in Shale Reservoirs. Paper presented at the SPE Improved Oil Recovery Symposium, Tulsa, Oklahoma. Society of Petroleum Engineers.

O'Brien, R.W., Cannon, D.W., and Rowlands, W.N. 1995. Electroacoustic Determination of Particle Size and Zeta Potential. *Journal of Colloid and Interface Science* **173** (2): 406-418. DOI: https://doi.org/10.1006/jcis.1995.1341

Parsons, R.W. and Chaney, P.R. 1966. Imbibition Model Studies on Water-Wet Carbonate Rocks. *Society of Petroleum Engineers Journal* **6** (01): 26-34.

Patel, K.R., Mehta, M.N., and Patel, T.R. 2013. A Mathematical Model of Imbibition Phenomenon in Heterogeneous Porous Media During Secondary Oil Recovery Process. *Applied Mathematical Modelling* **37** (5): 2933-2942.

Phi, T. and Schechter, D.S. 2017. Co2 Eor Simulation in Unconventional Liquid Reservoirs: An Eagle Ford Case Study. Paper presented at the SPE Unconventional Resources Conference, Calgary, Alberta, Canada. Society of Petroleum Engineers. DOI: 10.2118/185034-MS.

Pooladi-Darvish, M. and Firoozabadi, A. 2000. Cocurrent and Countercurrent Imbibition in a Water-Wet Matrix Block. *Society of Petroleum Engineers Journal* **5** (01): 3-11.

Rassenfoss, S. 2017. Shale Eor Works, but Will It Make a Difference? *Journal of Petroleum Technology* **69** (10): 34-40. DOI: 10.2118/1017-0034-JPT

Reed, R.L. and Healy, R.N. 1984. Contact Angles for Equilibrated Microemulsion Systems. *Society of Petroleum Engineers Journal*. DOI: 10.2118/8262-PA

Rosen, M.J. 2004. *Surfactants and Interfacial Phenomena*: Wiley. Original edition. ISBN 9780471670551.

Salehi, M., Johnson, S.J., and Liang, J.-T. 2008. Mechanistic Study of Wettability Alteration Using Surfactants with Applications in Naturally Fractured Reservoirs. *Langmuir* **24** (24): 14099-14107.

Salopek, B., Krasic, D., and Filipovic, S. 1992. Measurement and Application of Zeta Potential. *Mining-Geological-Petroleum Engineering Bulletin* **4** (1): 147-151.

Schechter, D.S., Zhou, D., and Jr., F.M.O. 1991. Capillary Imbibition and Gravity Segregation in Low Ift Systems. Paper presented at the SPE Annual Technical Conference and Exhibition, Dallas, Texas. Society of Petroleum Engineers.

Schechter, D.S., Zhou, D., and Jr., F.M.O. 1994. Low Ift Drainage and Imbibition. *Journal of Petroleum Science & Engineering* **11** (4): 283-300.

Seiedi, O., Rahbart, M., Nabipour, M. et al. 2011. Atomic Force Microscopy (Afm) Investigation on the Surfactant Wettability Alteration Mechanism of Aged Mica Mineral Surfaces. *Energy Fuels* **25** (1): 183-188.

Somasundaran, P. and Zhang, L. 2006. Adsorption of Surfactants on Minerals for Wettability Control in Improved Oil Recovery Processes. *Journal of Petroleum Science & Engineering* **52** (1-4): 198-212.

Standnes, D.C. and Austad, T. 2000a. Wettability Alteration in Chalk: 1. Preparation of Core Material and Oil Properties. *Journal of Petroleum Science & Engineering* **28** (3): 111-121.

Standnes, D.C. and Austad, T. 2000b. Wettability Alteration in Chalk: 2. Mechanism for Wettability Alteration from Oil-Wet Using Surfactants. *Journal of Petroleum Science & Engineering* **28** (3): 123-143.

Standnes, D.C. and Austad, T. 2003. Wettability Alteration in Carbonates: Interaction between Cationic Surfactant and Carboxylates as a Key Factor in Wettability Alteration from Oil-Wet to Water-Wet Conditions. *Colloids and Surface A: Physicochemical and Engineering Aspects* **216** (1-3): 243-259.

Stauffer, C.E. 1965. The Measurement of Surface Tension by the Pendant Drop Technique. *The Journal of Physical Chemistry* **69** (6): 1933-1938. DOI: 10.1021/j100890a024

Steward, D.B. 2013. George P. Mitchell and the Barnett Shale. DOI: 10.2118/1113-0058-JPT

Teklu, T.W., Li, X., Zhou, Z. et al. 2018. Low-Salinity Water and Surfactants for Hydraulic Fracturing and Eor of Shales. *Journal of Petroleum Science & Engineering* **162**: 367-377.

Thomas, M.M., Clouse, J.A., and Longo, J.M. 1993. Adsorption of Organic Compounds on Carbonate Minerals: 1. Model Compounds and Their Influence on Mineral Wettability. *Chemical Geology* **109** (1): 201-213. DOI: https://doi.org/10.1016/0009-2541(93)90070-Y

Treiber, L.E. and Owens, W.W. 1972. A Laboratory Evaluation of the Wettability of Fifty Oil-Producing Reservoirs. DOI: 10.2118/3526-PA

Vonnegut, B. 1942. Rotating Bubble Method for the Determination of Surface and Interfacial Tensions. *Review of Scientific Instruments* **13** (1): 6-9. DOI: 10.1063/1.1769937

Wang, D., Zhang, J., Butler, R. et al. 2014. Flow Rate Behaviour and Imbibition Comparison between Bakken and Niobrara Formation. Paper presented at the Unconventional Resources Technology Conference, Denver, Colorado. Unconventional Resources Technology Conference.

Wang, D., Zhang, J., Butler, R. et al. 2016. Scaling Laboratory-Data Surfactant-Imbibition Rates to the Field in Fractured-Shale Formations. *SPE Reservoir Evaluation & Engineering* **19** (03): 440-449.

Wang, J., Han, M., Fuseni, A.B. et al. 2015. Surfactant Adsorption in Surfactant-Polymer Flooding for Carbonate Reservoirs. Paper presented at the SPE Middle East Oil & Gas Show and Conference, Manama, Bahrain. Society of Petroleum Engineers. DOI: 10.2118/172700-MS.

Wang, J. and Liu, Y. 2011. Well Performance Modeling of Eagle Ford Shale Oil Reservoirs. Paper presented at the North American Unconventional Gas Conference and Exhibition, The Woodlands, Texas, USA. Society of Petroleum Engineers. DOI: 10.2118/144427-MS.

Weiss, W.W. and Xie, X. 2007. Oilfield Surfactants Improve Recovery Via Imbibition. Paper presented at the International Symposium on Oilfield Chemistry, Houston, Texas. Society of Petroleum Engineers.

Xie, X., Weiss, W.W., Tong, Z.J. et al. 2005. Improved Oil Recovery from Carbonate Reservoirs by Chemical Stimulation. *Society of Petroleum Engineers Journal* **10** (03): 276-285.

Xu, L. and Fu, Q. 2012. Ensuring Better Well Stimulation in Unconventional Oil and Gas Formations by Optimizing Surfactant Additives. Paper presented at the SPE Western Regional Meeting, Bakersfield, California. Society of Petroleum Engineers.

Zhang, J., Nguyen, Q.P., Flaaten, A. et al. 2009. Mechanisms of Enhanced Natural Imbibition with Novel Chemicals. *SPE Reservoir Evaluation & Engineering* **12** (06): 912-920.

Zhang, R. and Somasundaran, P. 2006. Advances in Adsorption of Surfactants and Their Mixtures at Solid/Solution Interfaces. *Advances in Colloid and Interface Science* **123-126**: 213-229.

Ziegler, V.M. and Handy, L.L. 1981. Effect of Temperature on Surfactant Adsorption in Porous Media. DOI: 10.2118/8264-PA